

**VALIDATION/ENHANCEMENT OF THE "JONES-OWENS" TECHNIQUE
FOR THE PREDICTION OF PERMEABILITY
IN LOW PERMEABILITY GAS SANDS**

A Thesis

by

FRANCOIS-ANDRE FLORENCE

Submitted to the Office of Graduate Studies of
Texas A&M University
in partial fulfillment of the requirements for the degree of

MASTER OF SCIENCE

May 2007

Major Subject: Petroleum Engineering

**VALIDATION/ENHANCEMENT OF THE "JONES-OWENS" TECHNIQUE
FOR THE PREDICTION OF PERMEABILITY
IN LOW PERMEABILITY GAS SANDS**

A Thesis

by

FRANCOIS-ANDRE FLORENCE

Submitted to the Office of Graduate Studies of
Texas A&M University
in partial fulfillment of the requirements for the degree of

MASTER OF SCIENCE

Approved by:

Chair of Committee,
Committee Member,

Head of Department,

Thomas A. Blasingame
Peter P. Valko
Richard Gibson
Stephen A. Holditch

May 2007

Major Subject: Petroleum Engineering

ABSTRACT

Validation/Enhancement of the "Jones-Owens" Technique for the Prediction of Permeability in Low Permeability Gas Sands. (May 2007)

François-André Florence

Dipl., Ecole des Mines de Saint Etienne, France

Chair of Advisory Committee: Dr. Thomas A. Blasingame

This work presents the validation and enhancement of existing correlations for estimating and predicting the permeability in low permeability gas sands. The "original" problem of predicting the corrected or "liquid equivalent" permeability has been under investigation since the early 1940s — in particular, using the application of "gas slippage" theory to petrophysics by Klinkenberg.

In the first part of this work, the viability of the Jones-Owens and Sampath-Keighin correlations for estimating the Klinkenberg-corrected (absolute) permeability from single-point, steady-state measurements were investigated. We also provide an update to these correlations using modern petrophysical data.

In the second part of this work we proposed and validated a new "microflow" model for the evaluation of an equivalent liquid permeability from gas flow measurements. This work was based on a more detailed application of similar concepts employed by Klinkenberg. In fact, we obtained the Klinkenberg result as an approximate form of this result. A theoretical "microflow" result was given as a rational polynomial (*i.e.*, a polynomial divided by a polynomial) in terms of the Knudsen number (ratio of the mean free path of the gas molecules to the characteristic flow length (typically the radius of the capillary)), and this result can be applied as an explicit correlation device, or as an implicit prediction model (presuming the model is tuned to a particular data set).

The following contributions are derived from this work:

- Validation and extension of the correlations proposed by Jones-Owens and Sampath-Keighin for low permeability samples.
- Development and validation of a new "microflow" model which correctly represents the flow of gases in low permeability core samples. This model is also applied as a correlation for prediction of the equivalent liquid permeability in much the same fashion as the Klinkenberg model, although the new model is substantially more theoretical (and robust) as compared to the Klinkenberg correction model.

DEDICATION

This thesis is dedicated to my parents and my sisters — for their love and support.

Without technique, a gift is nothing but a bad habit.

— *Georges Brassens*

I am not serious enough to give advices, but I am too serious to receive them.

— *Hugo Pratt*

ACKNOWLEDGEMENTS

I want to express my gratitude and appreciation to:

Dr. Tom Blasingame for his constant support and guidance during my research and graduate studies.

Dr. Peter Valko for serving as a member of my advisory committee.

Dr. Richard Gibson for serving as a member of my advisory committee.

TABLE OF CONTENTS

	Page
ABSTRACT	iii
DEDICATION	iv
ACKNOWLEDGEMENTS.....	v
TABLE OF CONTENTS	vi
LIST OF FIGURES.....	viii
 CHAPTER	
I INTRODUCTION	1
1.1 Research Problem.....	1
1.2 Research Objectives	2
1.3 Previous Work.....	2
1.4 Summary	5
II OVERVIEW OF THE EXISTING CORRELATIONS.....	6
2.1 Inventory of the Existing Correlations	6
2.2 Comparison for Unsteady-State Data.....	9
2.3 Comparison for Steady-State Data	11
III KLINKENBERG MODEL REVISITED.....	17
3.1 Preliminary Discussion.....	17
3.2 The Theory of Rarefied Gases (and Surface Phenomena).....	18
3.3 Unified Flow Model for Gas in Pipes.....	20
3.4 Correlation of the Knudsen Number with Porosity, Permeability and Pressure	21
3.5 Application of the Pseudo-Knudsen Number Using Field Data.....	22
IV SUMMARY, CONCLUSIONS, AND RECOMMENDATIONS FOR FUTURE WORK	26

	Page
4.1 Summary	26
4.2 Conclusions	26
4.3 Recommendations, Comments and Future Work.....	26
NOMENCLATURE.....	27
REFERENCES.....	28
APPENDIX A KLINKENBERG DERIVATION.....	30
APPENDIX B DERIVATION OF A THEORETICAL SQUARE-ROOT CORRELATION	35
APPENDIX C A RIGOROUS MICRO-FLOW MODEL APPLIED TO THE PROBLEM OF GAS FLOW THROUGH POROUS MEDIA.....	43
APPENDIX D CORRELATIONS FOR THE "PSEUDO-KNUDSEN" NUMBER — APPLICA- TION TO A TIGHT GAS EXAMPLE (LOUISIANA, USA).....	48
APPENDIX E COMPARISON OF ALL MODELS FOR STEADY-STATE MEASURE- MENTS	73
VITA.....	85

LIST OF FIGURES

FIGURE	Page
1.1 Plot of the gas slippage factor versus Klinkenberg-corrected permeability for data and correlation from Heid <i>et al</i>	4
1.2 Plot of the gas slippage factor versus Klinkenberg-corrected permeability/porosity ratio for data and correlation from Sampath and Keighin	5
2.1 Comparison of the " b_K vs. k_{∞} " correlations by Heid <i>et al</i> and Jones-Owens with various field and literature data, acquired with unsteady-state or steady-state techniques	6
2.2 Comparison of the " b_K vs. k_{∞}/ϕ " correlations by Sampath and Keighin and this work with various field and literature data, acquired with unsteady-state or steady-state techniques	8
2.3 Comparison of the " b_K vs. k_{∞} " correlations by Heid <i>et al</i> and Jones-Owens with unsteady-state data	9
2.4 Comparison of the " b_K vs. k_{∞}/ϕ " correlations by Sampath and Keighin and this work with unsteady-state data	10
2.5 Comparison of the Cotton Valley steady-state data with the Jones-Owens and Heid <i>et al</i> correlations	11
2.6 Comparison of the Cotton Valley steady-state data with the Sampath-Keighin and proposed square-root correlations	12
2.7 Computed equivalent liquid permeability versus Klinkenberg-corrected permeability, for the Lower Cotton Valley Sample No.1	14
2.8 Computed equivalent liquid permeability versus Klinkenberg-corrected permeability, for the Lower Cotton Valley Sample No.2	15
2.9 Average absolute relative errors for equivalent liquid permeability versus Klinkenberg-corrected permeability, for Lower Cotton Valley Sample No.1	16
2.10 Average absolute relative errors for equivalent liquid permeability versus Klinkenberg-corrected permeability, for Lower Cotton Valley Sample No.2	16
3.1 Initial correlation plot of Klinkenberg-corrected permeability plotted against the measured gas permeability [log-log coordinates].	18
3.2 Limits of the different flow regimes, as a function of the characteristic length of the geometry (l_{char}), and the reciprocal mean free path normalized (1 atm, 300 K).....	20

FIGURE	Page
3.3 Computed equivalent liquid permeability versus Klinkenberg-corrected permeability (theoretical Knudsen number and pseudo-Knudsen number approaches, implicit and explicit relations for K_{np}).....	23
3.4 Computed equivalent liquid permeability versus Klinkenberg-corrected permeability (fully implicit formulation for the pseudo-Knudsen number).....	25

CHAPTER I

INTRODUCTION

1.1 Research Problem

In the last decades, the interest for low permeability reservoirs has grown substantially. Although costly and time-consuming, the coring of a well and the analysis of the extracted sample remains the best way to assess the formation, prior to any treatment and economic decision. Permeability measurements in the laboratory can be performed by either steady-state or unsteady-state methods — our work will focus on data acquired by steady-state methods. Steady-state measurements are considered by some to be more reliable than unsteady-state measurements, especially for low permeability cores, but these also have a major drawback — liquid is used as the flowing fluid, but the lower the permeability of the sample, the longer the time to required to achieve steady-state flow. To reduce this effect, the use of gas as the flowing fluid is preferred. However, the use of gas as the flowing fluid raises a fundamental issue: *the permeability measured with gas is not the same than the permeability measured with liquid*. More problematically, the permeability measured with gas changes with the flowing pressure — this conclusion is in conflict with the definition of the permeability as being a property of the porous medium only.

This discrepancy is explained by the *gas slippage effect*, a phenomenon occurring at relatively low flowing pressure (typically the range of pressures reached in the laboratory experiments) and yielding an overestimation of the measured permeability to gas. Klinkenberg¹ proposed a correction for this effect and later works (Heid *et al.*,² Jones and Owens³ and Sampath and Keighin⁴) developed correlations based on the Klinkenberg model allowing, with various successes, to estimate/predict the true permeability of the porous medium using a single measure of permeability to gas. These single point steady-state measurements provide a time-saving and cost-effective method to assess the true permeability of the sample. This study presents the most promising of the correlations found in the petroleum engineering literature.

From the theoretical point of view, Klinkenberg developed a first-order slippage correction based on the results of the theory of rarefied gases developed by Kundt and Warburg.⁵ Recent developments in this area of study allowed us to develop a new model for gas slippage in porous medium, based on the concept of the study of flow regimes.

This thesis follows the style and format of the *SPE Journal*.

1.2. Research Objectives

The overall objectives of this work are:

- To validate the correlation proposed by Jones and Owens for individual and mixed sample cases of core data obtained from the literature and the industry.
- To provide enhancements to the Jones-Owens correlation — based on new data, as well as on the possibility of employing other correlation models.
- To consider other mechanisms, correlations or conversions to estimate the absolute (liquid) permeability from gas permeability reservoir samples evaluated at various average pressures.

1.3. Previous Work

Our overall objective is to develop a method based on theoretical equations and/or empirical correlations to determine with the maximum accuracy the true liquid permeability of tight sandstone core samples at the lowest possible cost. To achieve this goal, we investigate the theoretical and empirical studies documented in the literature to date.

The problem of the flow of gases through tubes and porous media has been under investigation since the last quarter of the nineteenth century — in particular by Kundt and Warburg⁵ who developed the fundamentals of the theory of gas slippage — based on the work of Maxwell⁶ (not discussed here) on the modeling of the motion of gases molecules. Klinkenberg¹ was the first to apply the results for the theory of slippage to the petrophysical domain, addressing the issue of discrepancies between permeabilities to air and to water (*i.e.*, the wetting phase liquid). Such discrepancies are usually more important for lower permeability sands.

For reference, the Klinkenberg formulation is derived in complete detail in **Appendix A**. Klinkenberg derived an approximate linear relationship between the apparent gas permeability (k_a) and the reciprocal mean pressure (\bar{p}), which is given as:

$$k_a = k_\infty \left[1 + \frac{b_K}{\bar{p}} \right] \dots\dots\dots (1.1)$$

Where b_K is the "gas slippage factor" — which is a "constant" (for a given sample) that relates the mean free path ($\bar{\lambda}$) of the molecules at the mean pressure (\bar{p}) and the effective pore radius (r). The *definition* of the b_K/\bar{p} -term is given by:

$$\frac{b_K}{\bar{p}} = \frac{4c\bar{\lambda}}{r}, \text{ where } c \approx 1 \text{ (see ref. 5)} \dots\dots\dots (1.2)$$

In Eq. 1.1, k_∞ is the "equivalent liquid permeability" (or *Klinkenberg-corrected permeability*), which is the true permeability of the porous medium.

From Eqs. 1.1 and 1.2, Klinkenberg drew the following conclusions:

- The gas permeability can be approximated as a linear function of the reciprocal mean pressure — in particular, the apparent permeability (k_a) can be extrapolated to infinite pressure (using the k_a versus $1/\bar{p}$ plot, such a plot is known as a *Klinkenberg plot*) (i.e., as $\bar{p} \rightarrow \infty$ or $1/\bar{p} \rightarrow 0$), which should yield the true permeability (k_∞).
- The *gas permeability is independent of the pressure drop along the core* — provided that the mean pressure along the core is constant.
- The gas slippage factor (b_K) is inversely proportional to the radius of the capillaries.

Klinkenberg confirmed his theoretical work with a series of experiments on glass filters and rock samples. The steady-state measurement methods consist of collecting several data points ($k_a, 1/\bar{p}$) and obtaining the Klinkenberg plot from which the Klinkenberg-corrected permeability (k_∞) and from which the Klinkenberg gas slippage factor (b_K) can be extracted.

Taking the Klinkenberg equation as fact, later work in this area focused on the determination of the gas slippage (b_K) factor. In the late 1940s Heid *et al*² conducted a study including the effect of pressure, pore size, and type of porous medium on permeability. Heid *et al* determined the gas slippage factor and the (extrapolated) true permeability of 11 synthetic cores and 164 natural core samples of representative sands from different producing areas of the United States. Based on the results of their core sample experiments shown in **Fig. 1.1**, Heid *et al* developed a relationship between the Klinkenberg gas slippage factor (b_K) and the corresponding equivalent liquid permeability (k_∞):

$$b_K = 11.419(k_\infty)^{-0.39} \dots\dots\dots(1.3)$$

With the development of the interest in unconventional resources, and particularly tight gas sands (which typically exhibit permeabilities much lower than that of the core samples Heid *et al.* studied), further investigations were conducted in the late 1970s to respond the need for reliable permeability assessments. In a paper focused on core analysis for tight gas (or low permeability) sands, Jones and Owens³ studied the effects of several phenomena for more than one hundred samples from tight gas sands. The phenomena by Jones and Owens considered are:

- Confining pressure
- Gas slippage
- Pore Volume Compressibility
- Effect of water on core permeability
- Effect of partial water saturation on gas permeability

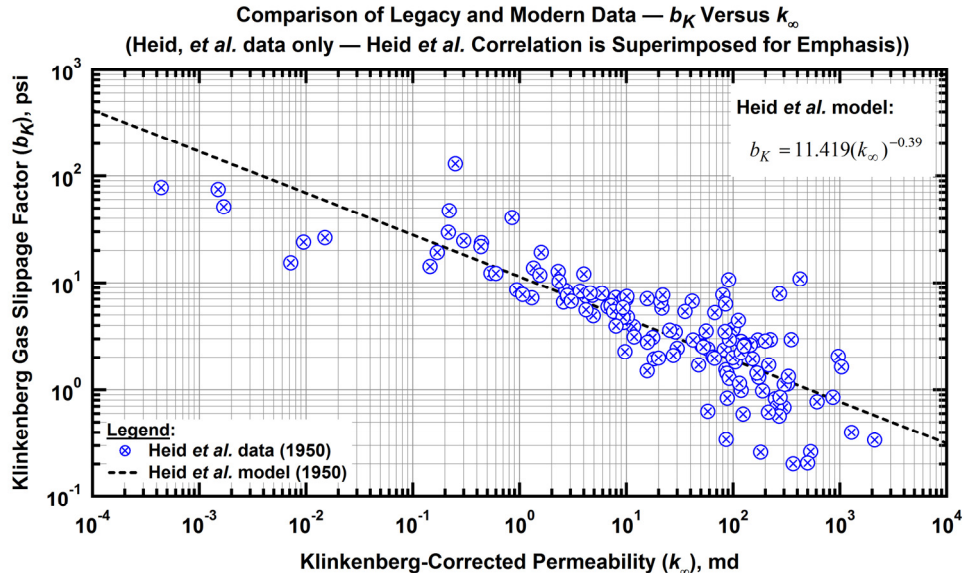


Figure 1.1 — Plot of the gas slippage factor (b_K) versus Klinkenberg-corrected permeability for data and correlation from Heid *et al.* (ref. 2). The correlation is acceptable (*i.e.*, reasonably well-defined) for values of permeability greater than 1 md.

Unfortunately, the database that Jones and Owens developed for their article is not available (or, more aptly, cannot be found). Jones and Owens provide a formula similar in form to the one presented by Heid *et al.* for the relationship between the gas slippage factor (b_K) and the equivalent liquid permeability (k_{∞}). This formula also confirms that the gas slippage effect is more significant for lower permeability rocks:

$$b_K = 12.639(k_{\infty})^{-0.33} \dots\dots\dots (1.4)$$

Jones and Owens propose the application of Eq. 1.4 to estimate the Klinkenberg-corrected permeability (Eq. 1.1) using ordinary, steady-state, gas permeability data: Jones and Owens also developed a correlation of the Klinkenberg-corrected permeability as a function of the *gas permeability* (k_a) *estimated at 100 psig*. This correlation is given as: (recall that $1\mu\text{d} = 10^{-3}$ md)

$$k_{\infty} = 10^{(-0.398 \log^2 k_a + 1.067 \log k_a - 0.0825)}, \text{ for } 0.0001 \text{ md} < k_a < 1 \text{ md} \dots\dots\dots (1.5)$$

In 1981 (two years after Jones and Owens), Sampath and Keighin⁴ studied 10 core samples from the Uinta County, Utah, and published a formula relating the gas slippage factor (b_K) to the ratio of Klinkenberg-corrected permeability to porosity (*i.e.*, k_{∞}/ϕ). The Sampath-Keighin relation is given by:

$$b_K = 13.851 \left[\frac{k_{\infty}}{\phi} \right]^{-0.53} \dots\dots\dots (1.6)$$

The data and correlation developed by Sampath-Keighin are shown on **Figure 1.2**.

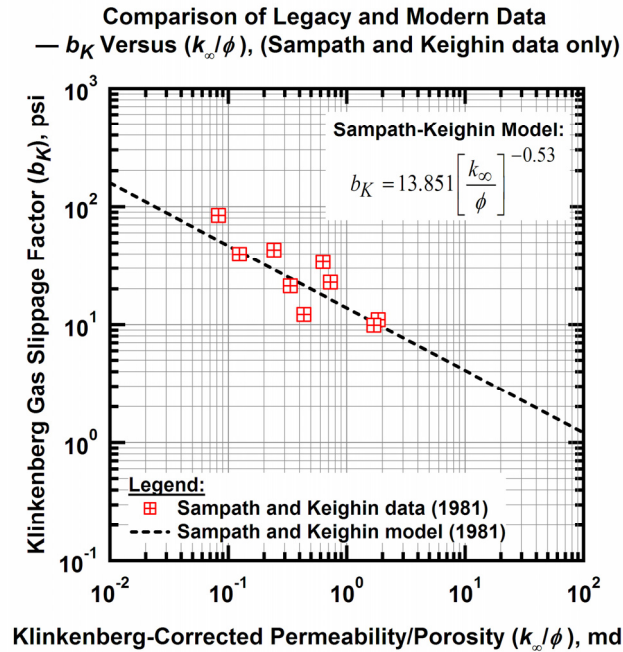


Figure 1.2 — Plot of the gas slippage factor (b_K) versus Klinkenberg-corrected permeability/porosity ratio (k_{∞}/ϕ) for data and correlation from Sampath and Keighin (ref. 4). The correlation is acceptable (*i.e.*, reasonably well-defined).

1.4 Summary

This study begins with the comparison of the existing correlations, on both types of data, steady and unsteady-state, acquired from the literature or from the industry: these correlations are based on the Klinkenberg equation (Eq. 1.1) derived in **Appendix A**.

In the second part of this study, we investigate the gas slippage effect at a fundamental/theoretical level: Klinkenberg derived his result using developments of the *theory of slip* available in 1941; we look at the recent development of this theory and develop a modern equation to model the discrepancies between permeability to gas and true permeability for low permeability sample: the *microflow* model (derived in **Appendix B**).

The last part of this study consists in a comparison between the existing correlations and the microflow model.

CHAPTER II

OVERVIEW OF THE EXISTING CORRELATIONS

2.1 Inventory of the Existing Correlations

The first phase of our work consists mainly of reviewing the available literature — as well as gathering data from the literature and the industry. The literature database consists of the data gathered in the articles from Klinkenberg,¹ Heid *et al*² and Sampath and Keighin.⁴ The industry database is composed of recently acquired datasets obtained from industrial sources — *i.e.*, "Lower Cotton Valley" samples^{7,8}, both datasets are *steady-state measurements*. We also obtained "older" datasets obtained from a Gas Research Institute (GRI) project conducted in the 1980s and early 1990s⁹⁻¹¹. The later datasets are *unsteady-state measurements*.

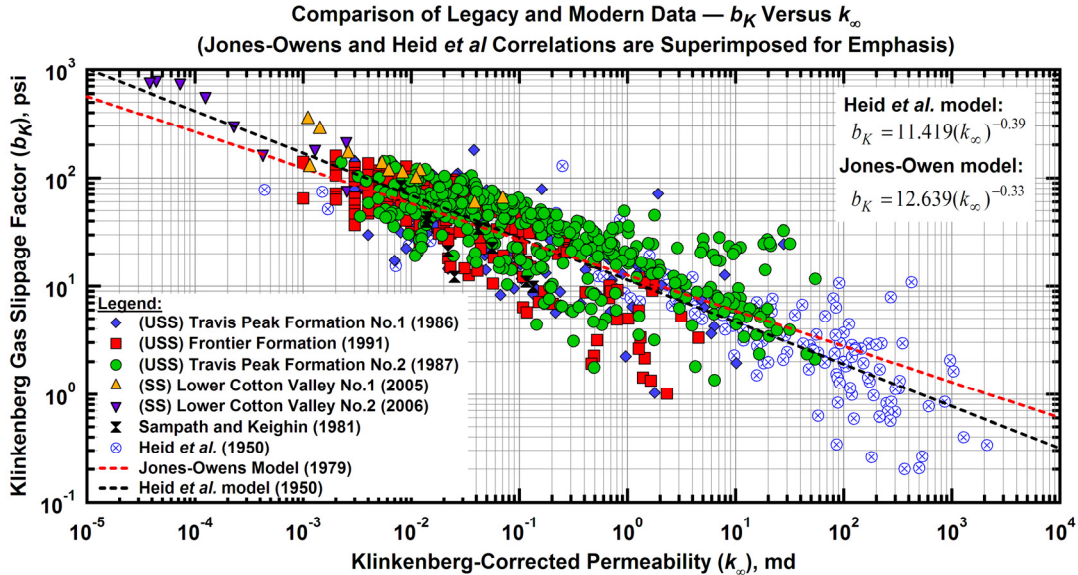


Figure 2.1 — Comparison of the " b_K vs. k_∞ " correlations by Heid *et al* (ref. 2) and Jones-Owens (ref. 3) with various field and literature data, acquired with unsteady-state (USS) or steady-state (SS) techniques — although the correlation appears accurate, the correlation errors are most significant for low permeability data. [k_∞ is determined at 800 psig confining pressure, except for the data of Sampath-Keighin where k_∞ is determined at 1000 psig confining pressure and for the data of Heid *et al* (where no confining pressure was specified).]

The data are correlated in **Fig. 2.1** (the b_K -parameter and the corresponding equivalent liquid permeability (k_∞)), and we note a fair fit of the model proposed by Jones-Owens with the experimental data. The error

spread (vertically) is approximately 1 order of magnitude (factor of 10), which, while far from perfect, at least validates the concept for a correlation of b_K and k_{∞} .

Similarly, a test of the Sampath and Keighin model (ref. 4) using the same data shows an important discrepancy between the model and the data (see **Fig. 2.2**). The model proposed by Sampath and Keighin fits only their data. The data of Heid *et al* lie above the model trend due to the petrophysical properties of the core samples — porosity data ranges from 0.09 to 0.33 (with a median value of 0.14) while the permeability data range from 0.0015 to 2100 md (with a median value of 27.05 md).

Although based on a reduced number of samples, the Sampath-Keighin correlation (Eq. 1.6) is interesting at a theoretical level since it is noted in the literature¹² that the square root of the Klinkenberg-corrected permeability/porosity ratio is considered to be a "characteristic length" (recall that the permeability has the dimension of a length-squared). Eq. 1.2 (repeated below for clarity) shows that the Klinkenberg gas slip-page factor (b_K) is inversely proportional to the capillary radius (r):

$$\frac{b_K}{p} = \frac{4c\bar{\lambda}}{r}, \text{ where } c \approx 1 \text{ (see ref. 5)} \dots\dots\dots (1.2)$$

A theoretical formulation of the capillary radius as a function of the Klinkenberg-corrected permeability/porosity ratio (or, more generally as a function of the permeability/porosity ratio) is given as:

$$r = 8.886 \times 10^{-6} \sqrt{\frac{k_{\infty}}{\phi}} \dots\dots\dots (2.1)$$

Eq. 2.1 is analytically derived in **Appendix B**. In Eq. 2.1, the capillary radius (r) is expressed in cm, the Klinkenberg-corrected porosity (k_{∞}) is expressed in md and the porosity is a fraction. With the appropriate assumptions, it is possible to rigorously derive a general "square-root" k_{∞}/ϕ correlation of the form:

$$b_K = \beta \left[\frac{k_{\infty}}{\phi} \right]^{-0.5} \dots\dots\dots (2.2)$$

The β -term in Eq. 2.2 is a function of the gas used in the core flow experiment — we present Eq. 2.2 computed for different gases on various data correlation and the Sampath-Keighin correlation on **Fig. 2.2**.

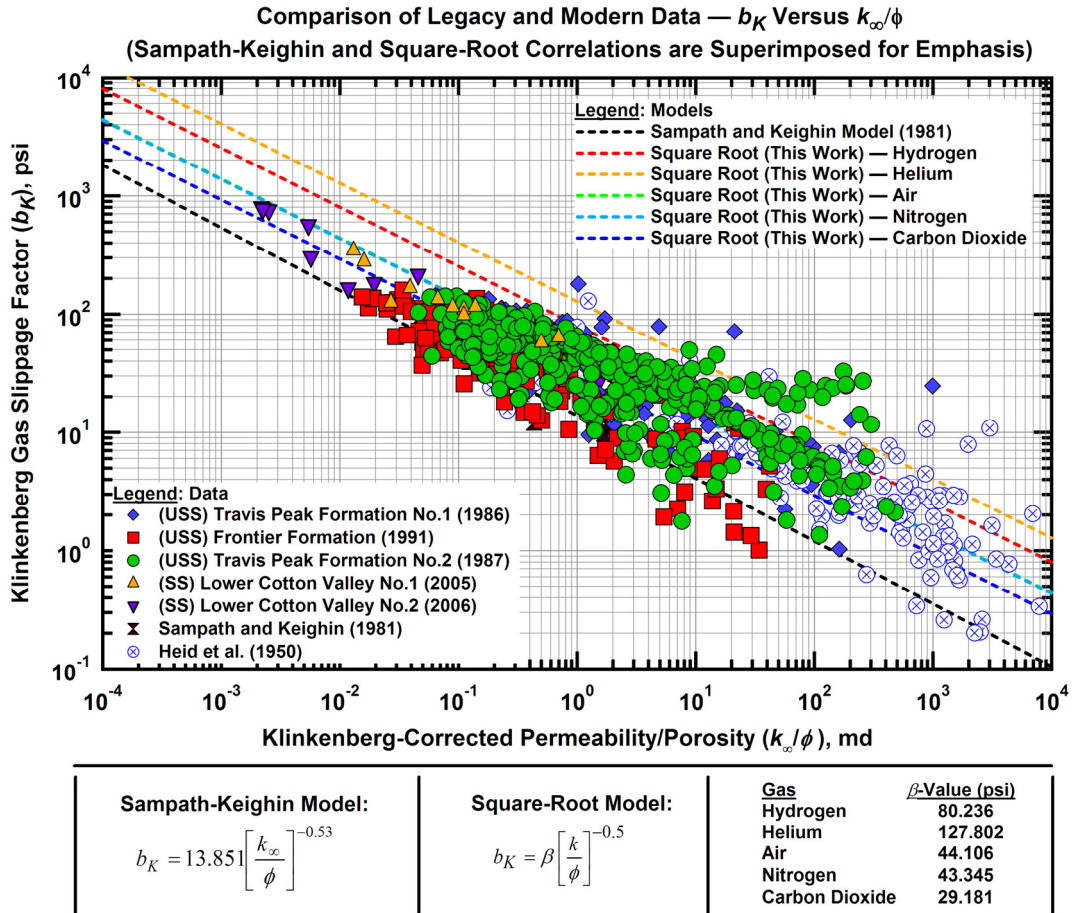


Figure 2.2 — Comparison of the " b_K vs. k_{∞}/ϕ " correlations by Sampath and Keighin (ref. 5) and this work with various field and literature data, acquired with unsteady-state (USS) or steady-state (SS) techniques. Note that Sampath-Keighin model only correlates with the Sampath-Keighin dataset. The square-root model seems to give better results. [k_{∞} is determined at 800 psig confining pressure, except for the data of Sampath-Keighin where k_{∞} is determined at 1000 psig confining pressure, as well as the data of Heid *et al* (where no confining pressure was specified).]

Figs. 2.1 and 2.2 serve to highlight trends in the prescribed data function — as well as to establish that a significant vertical spread exists in these data sets — which can lead to errors in permeability estimates for low permeability reservoirs.

2.2 Comparison for Unsteady-State Data

The correlation previously presented are not meant to be used with unsteady-state measurement — the Klinkenberg-corrected permeability (k_∞) being obtained directly and the flowing pressure data are usually not given in the lab reports, however we will expose them here for the sake of the demonstration. The comparison of the Jones-Owens correlation and the unsteady-state data is shown on **Fig 2.3**.

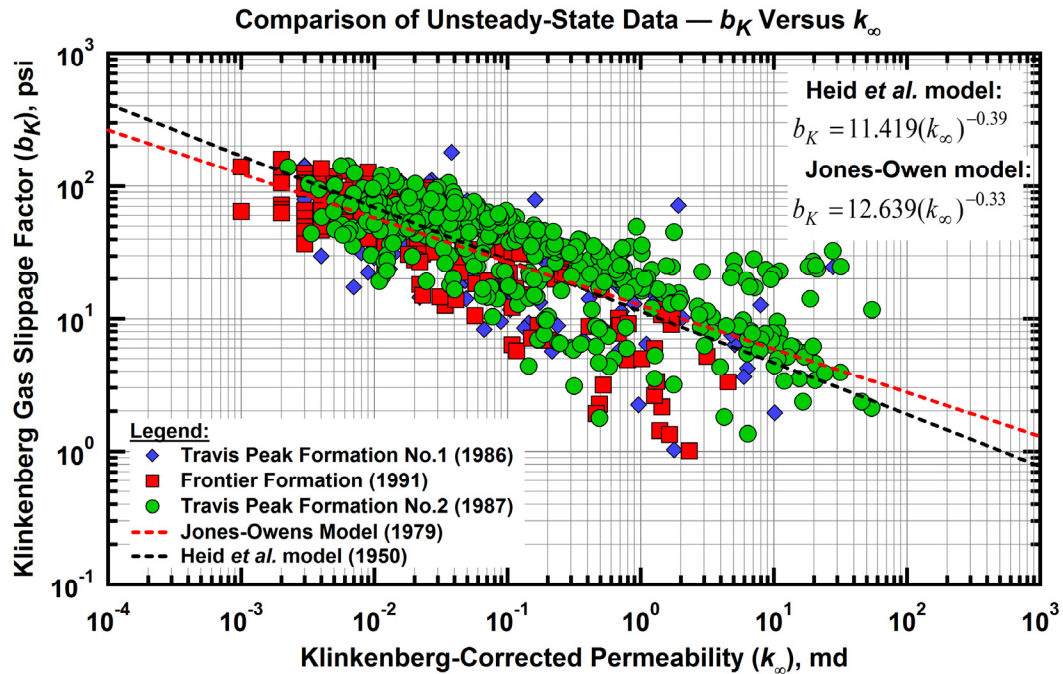


Figure 2.3 — Comparison of the " b_K vs. k_∞ " correlations by Heid et al (ref. 2) and Jones-Owens (ref. 3) with unsteady-state data. The scattering of the data is important in the whole range of permeability, especially in the low permeabilities (data measured permeabilities below 0.001 md were discarded, as these permeabilities are beyond accuracy of the unsteady-state permeameter).

The Jones-Owens correlation follows the trend given by the cloud, but the accuracy is questionable.

The Sampath-Keighin correlation and the proposed square-root correlations also follow the trend: **Fig. 2.4**, present the measured Klinkenberg gas slippage factor (b_K) plotted against the Klinkenberg corrected permeability/porosity ratio (k_∞/ϕ). The vertical scattering is important, and the Sampath-Keighin correlation seems to systematically underestimate the Klinkenberg gas slippage factor, whereas the Square-Root model curve is well centered in the cloud of data points.

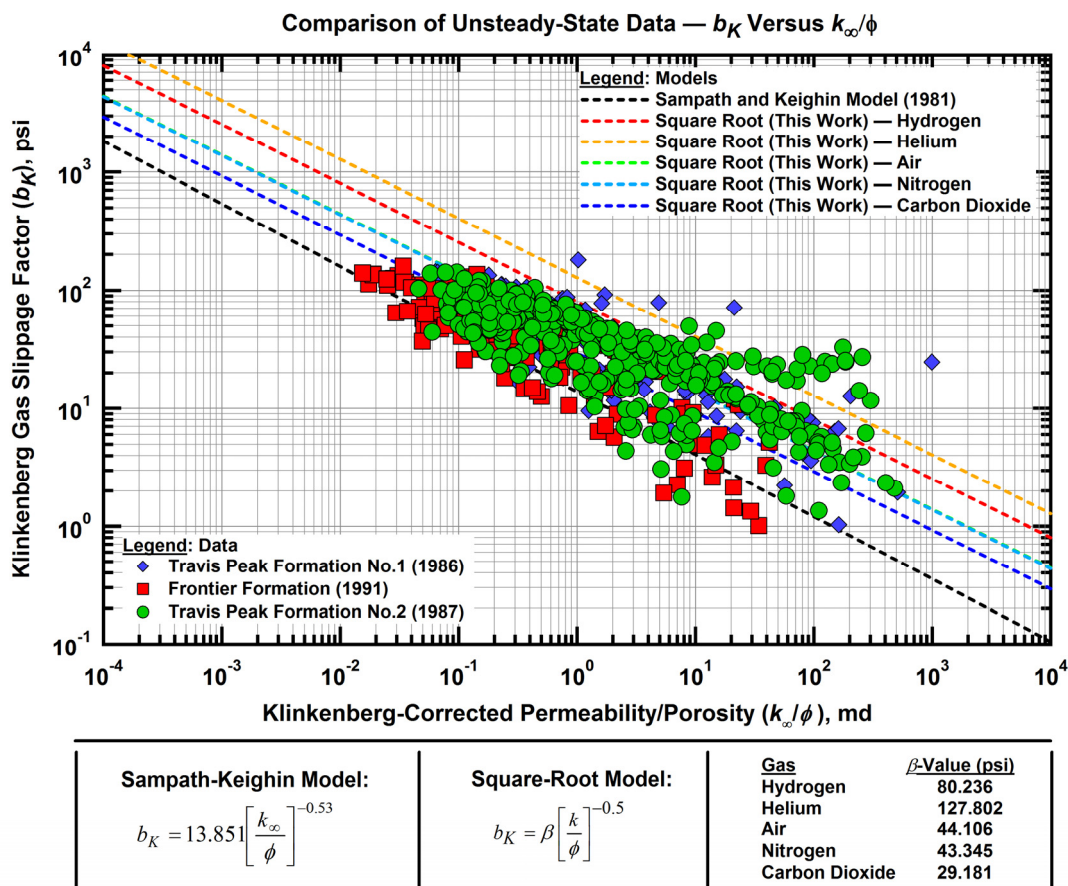


Figure 2.4 — Comparison of the " b_K vs. k_{∞}/ϕ " correlations by Sampath and Keighin (ref. 5) and this work with unsteady-state data. The scattering of the data is important in the whole range of permeability, especially in the low permeabilities (data measured permeabilities below 0.001 md were discarded, as these permeabilities are beyond accuracy of the unsteady-state permeameter). The Square-Root model achieves a better fit than Sampath-Keighin correlation.

The exposed correlations show a reasonable fit with the trend of the data. The principles used in the unsteady-state permeability measurement methods raise fundamental issues (Rushing *et al*¹³). Unsteady-state data should be viewed with concern — especially for permeabilities below 1 microdarcy (0.001 md), as the unsteady-state permeameter tends to overestimate the Klinkenberg-corrected permeabilities.

2.3 Comparison for Steady-State Data

In this section, we compare the Heid *et al* (ref. 2), Jones-Owens (ref. 3), Sampath-Keighin (ref. 4) and our proposed square-root correlation (Eq. 2.2) with the data from the Lower Cotton Valley formation (or modern "standard" database). The first "Cotton Valley" dataset includes 12 core samples; the second has 18 core samples. For each sample, we have the porosity (ϕ) and several measured gas permeabilities (k_a) at various mean core pressure (\bar{p}). From these data points, a Klinkenberg plot is constructed and the Klinkenberg-corrected permeability (k_{∞}) and Klinkenberg gas slippage factor (b_K) are estimated.

The comparison of the Heid *et al* and Jones-Owens correlations with the (Cotton Valley) steady-state data is shown on **Fig 2.5** (b_K vs. k_{∞}). The Sampath-Keighin correlation and our proposed "square-root" correlation are compared to the steady state data in **Fig 2.6** (b_K vs. k_{∞}/ϕ).

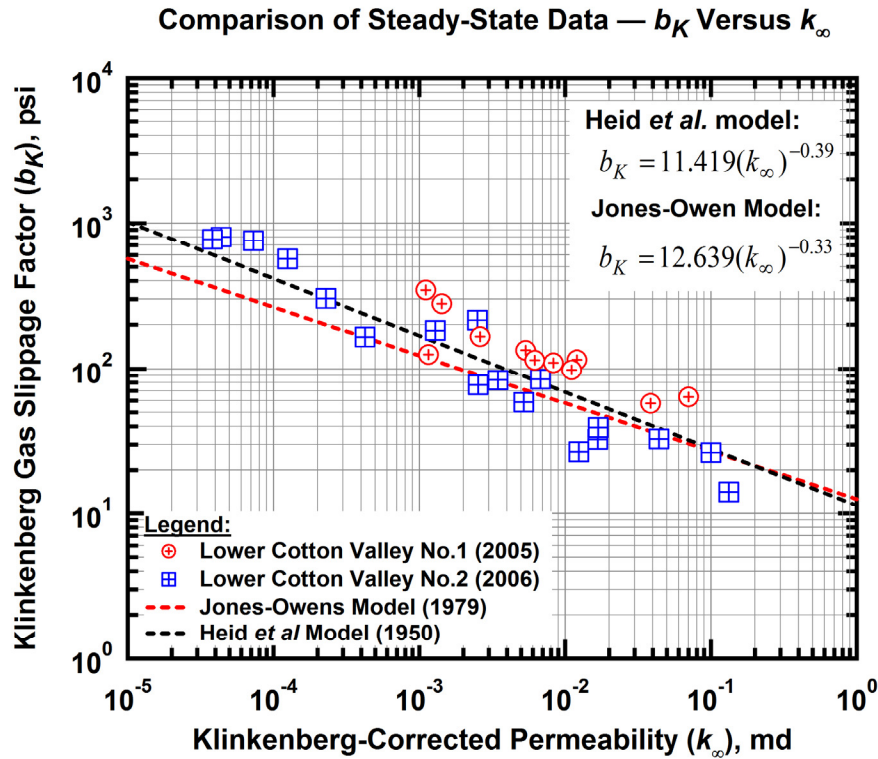


Figure 2.5 — Comparison of the Cotton Valley steady-state data with the Jones-Owens and Heid *et al* correlations. The Heid *et al* correlation seems well adapted for these datasets, whereas the Jones-Owens correlation generally underestimates the gas slippage factor, especially for the first Cotton Valley sample set.

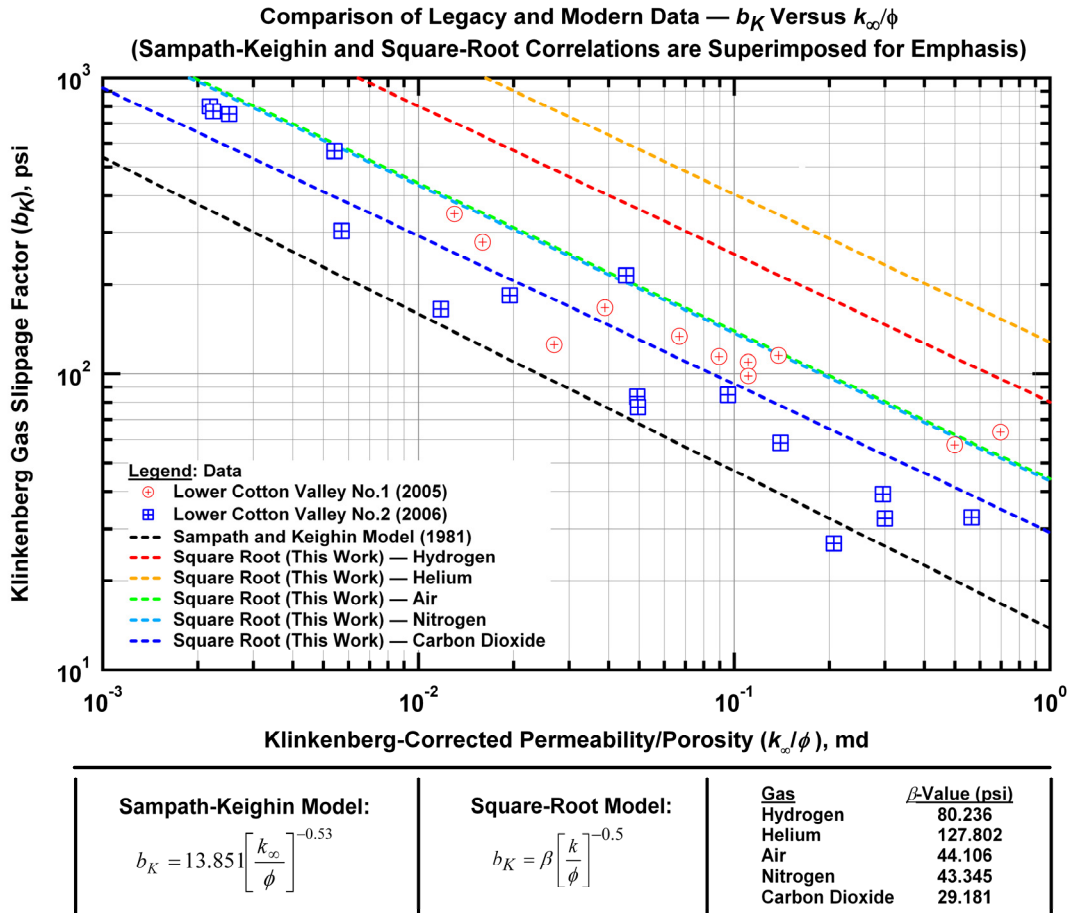


Figure 2.6 — Comparison of the Cotton Valley steady-state data with the Sampath-Keighin and proposed square-root correlations. Although the measurements were performed with nitrogen as the flowing gas, we note that the square-root correlation for carbon dioxide gives the best match (the best fit is actually obtained for a β -value of 34).

For both of the Cotton Valley datasets, the steady-state permeability measurements were performed using nitrogen as the flowing fluid — and we note that the nitrogen curve on Fig. 2.6 overestimates the gas slippage factor (b_K), whereas the carbon dioxide curve provides a good fit. Regardless of the "intercept" issue, our model matches the data trends well.

The objective of this particular effort is to accurately estimate the b_K -term, and then utilize this estimate in Eq. 1.1 to yield the Klinkenberg-corrected permeability. A general procedure for "single-point data" is to use any given pair of k_a and ϕ values to estimate b_K , and then to use the b_K and \bar{p} values to estimate k_{∞} . In our case, we use a model (i.e., correlation) for b_K and substitute this result into Eq. 1.1 to estimate k_{∞} .

As an alternative, one could simply establish a correlation of $k_{\infty} = f(k_a)$ — this process was proposed by Jones and Owens based (ref. 3) on the *gas permeability* (k_a) *estimated at 100 psig*. This correlation is given by Eq. 1.5, repeated below for clarity: (recall that $1\mu\text{d} = 10^{-3} \text{ md}$)

$$k_{\infty} = 10^{(-0.398 \log^2 k_a + 1.067 \log k_a - 0.0825)}, \text{ for } 0.1 \mu\text{d} < k_a < 1 \text{ md} \dots\dots\dots (1.5)$$

The purpose of our work is to establish a relevant correlation of $k_{\infty} = f(\bar{p}, \phi, \dots, k_a)$ — we will pursue a robust correlation as discussed above (*i.e.*, $b_K = f(k_{\infty}, \phi)$, substituted into Eq. 1.1). Recalling the Klinkenberg equation (Eq. 1.1), the Heid *et al* correlation (Eq. 1.3), the Jones-Owens correlation (Eq. 1.4), the Sampath-Keighin correlation (Eq. 1.6), and our proposed square-root correlation (Eq. 2.2) — we have:

$$k_a = k_{\infty} \left[1 + \frac{b_K}{\bar{p}} \right] \quad (\text{Klinkenberg}) \dots\dots\dots (1.1)$$

$$b_K = 11.419(k_{\infty})^{-0.39} \quad (\text{Heid } et \text{ al}) \dots\dots\dots (1.3)$$

$$b_K = 12.639(k_{\infty})^{-0.33} \quad (\text{Jones-Owens}) \dots\dots\dots (1.4)$$

$$b_K = 13.851 \left[\frac{k_{\infty}}{\phi} \right]^{-0.53} \quad (\text{Sampath-Keighin}) \dots\dots\dots (1.6)$$

$$b_K = \beta \left[\frac{k_{\infty}}{\phi} \right]^{-0.5} \quad (\text{this work}) \dots\dots\dots (2.2)$$

Substituting the Heid *et al* correlation (Eq. 1.3) for b_K in Klinkenberg equation (Eq. 1.1) yields:

$$k_a = k_{\infty} \left[1 + \frac{11.419(k_{\infty})^{-0.39}}{\bar{p}} \right] \dots\dots\dots (2.3)$$

Rearranging Eq. 2.3 yields:

$$k_a - k_{\infty} \left[1 + \frac{12.639(k_{\infty})^{-0.33}}{\bar{p}} \right] = 0 \dots\dots\dots (2.4)$$

Substituting Jones-Owens correlation (Eq. 1.4) for b_K in Eq. 1.1 and rearranging yields:

$$k_a - k_{\infty} \left[1 + \frac{12.639(k_{\infty})^{-0.33}}{\bar{p}} \right] = 0 \dots\dots\dots (2.5)$$

Substituting Eq. 1.6 for b_K in Eq. 1.1 and rearranging yields:

$$k_a - k_{\infty} \left[1 + 13.851 \left[\frac{k_{\infty}}{\phi} \right]^{-0.53} \frac{1}{\bar{p}} \right] = 0 \dots\dots\dots (2.6)$$

Substituting Eq. 2.2 for b_K in Eq. 1.1 and rearranging yields:

$$k_a - k_\infty \left[1 + \beta \left[\frac{k_\infty}{\phi} \right]^{-0.5} \frac{1}{\bar{p}} \right] = 0 \dots\dots\dots (2.7)$$

For every steady state measurements (*i.e.*, using a single pair of k_a and \bar{p} values), Eqs. 2.4, 2.5, 2.6 and 2.7 (with the appropriate value for the β -term in Eq. 2.7, *i.e.*, $\beta = 43.345$ for nitrogen), can be solved for the unknown (k_∞) — this method is known as *single point steady-state measurement* and yields the "computed equivalent liquid permeability". **Fig 2.7** and **Fig 2.8** present the computed equivalent liquid permeability plotted against the measured Klinkenberg-corrected permeability on log-log scales for both "Cotton Valley" datasets. In this work we note that the "*Klinkenberg-corrected permeability*" refers only to the value of permeability *actually extrapolated from a Klinkenberg plot* — the permeability values computed from correlations (or computations) are referred as "equivalent liquid permeabilities." However, we will use the same symbol (k_∞) for either case.

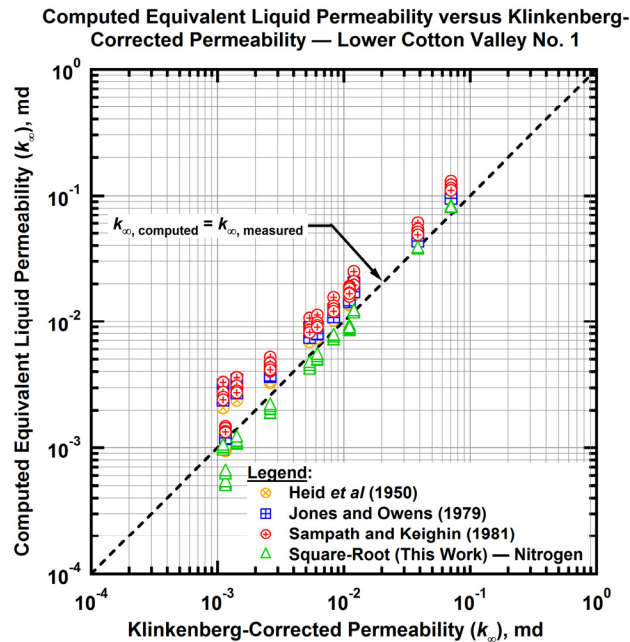


Figure 2.7 — Computed equivalent liquid permeability versus Klinkenberg-corrected permeability, for the Lower Cotton Valley Sample No.1. The Jones-Owens and Sampath-Keighin correlations overestimate k_∞ and the theoretical square-root model for nitrogen underestimates k_∞ . The Heid *et al* correlation gives good results.

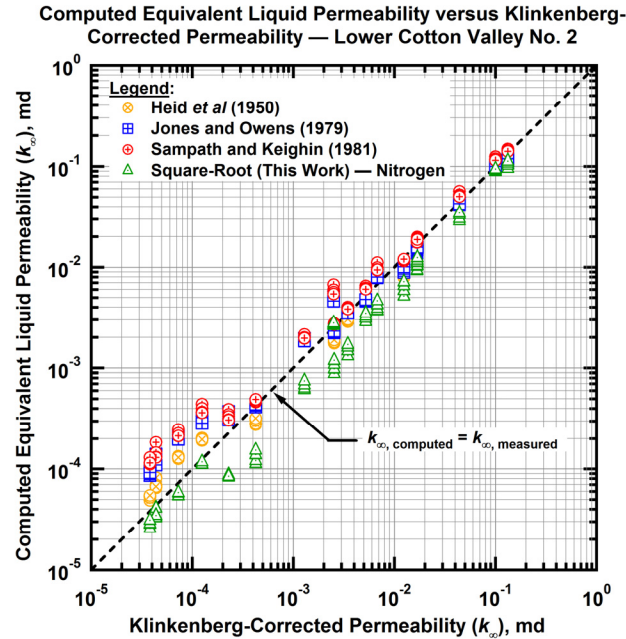


Figure 2.8 — Computed equivalent liquid permeability versus Klinkenberg-corrected permeability, for the Lower Cotton Valley Sample No.2. The Heid *et al*, Jones-Owens and Sampath-Keighin correlations provide fair results for $k_\infty > 0.001$ md. The theoretical square-root model for nitrogen underestimates k_∞ , but performs well for low permeability samples.

In both cases (Cotton Valley samples 1 and 2), the theoretical square-root model (nitrogen curve) underestimates the Klinkenberg-corrected permeability — but the overall performance of the square-root relation is comparable to the other methods.

In **Figs. 2.9 and 2.10** we present the average absolute relative errors for the *computed equivalent liquid permeability* plotted against the measured Klinkenberg-corrected permeability. This format helps us to assess the accuracy of the correlation on a "point-by-point" basis for a particular dataset.

For Cotton Valley Sample No. 1, the Heid *et al*, Jones-Owens and Sampath-Keighin models generally overestimate the permeability. As shown in **Figs. 2.9 and 2.10**, all models exhibit a fairly high absolute relative error (>50 percent for some cases) — however; the "clustering" for both datasets suggests that most samples exhibit less than 25 percent error. Given the data and the relatively approximate nature of the correlations, we consider the performance to be good, perhaps very good.

While it is difficult to discriminate the "best" of the four correlations, based on our results, we believe that the Sampath-Keighin correlation and the generalized square-root correlations are more "consistent" with the theory — and as such, should be favored for this application.

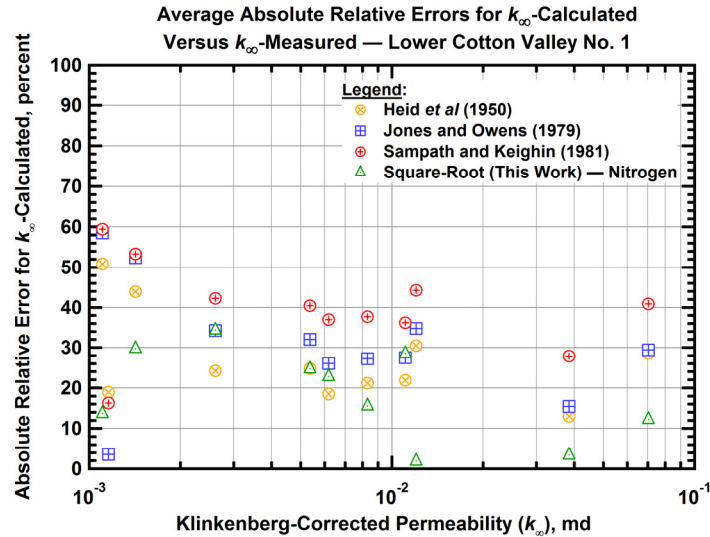


Figure 2.9 — Average absolute relative errors for equivalent liquid permeability versus Klinkenberg-corrected permeability, for Lower Cotton Valley Sample No.1. Errors are generally less than 30 percent.

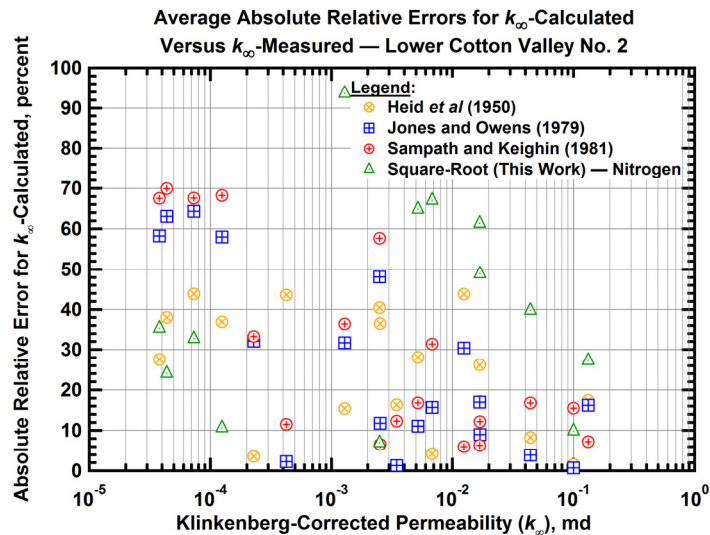


Figure 2.10 — Average absolute relative errors for equivalent liquid permeability versus Klinkenberg-corrected permeability, for Lower Cotton Valley Sample No.2. Errors are generally less than 25 percent, although there are numerous outliers which exhibit greater than 50 percent error.

CHAPTER III

KLINKENBERG MODEL REVISITED

3.1. Preliminary Discussion

Our discussion of the Klinkenberg concept begins with a retreat to the fundamentals — we will utilize the same measurements as with the correlations presented in the previous chapter (*i.e.*, k_a , \bar{p} , ϕ , and back-pressure (if used)), but we now consider the rigorous mechanisms of flow at the microscopic (and smaller) scales. First, we accept the Klinkenberg approximation as a "first order" type of estimate — Eq. 1.1, repeated below for clarity:

$$k_a = k_\infty \left[1 + \frac{b_K}{\bar{p}} \right] \dots\dots\dots (1.1)$$

We "define" k_∞ as *the true, equivalent liquid permeability* of the system, but we will also use estimates of k_∞ *estimated using the Klinkenberg correction as a standard to correlate against*. That is, we will use the Klinkenberg-corrected permeability (k_∞) as reported (or calculated) from our data sources as the reference permeability.

Obviously, we would prefer to use a more rigorous estimate, but for the present study, we must prove concept model (*i.e.*, the microflow model presented in this section) against some standard — and we believe that the Klinkenberg-corrected estimates are appropriate for that purpose.

In **Fig. 3.1**, we present the Klinkenberg-corrected (equivalent liquid) permeability (k_∞) plotted against the measured gas permeability (k_a) on log-log coordinates as a "correlation" to ensure that, at least directionally, Eq. 1 is valid.

As a primer for the development of our microflow model, we consider the phenomenon of gas slippage at a fundamental level — as a phenomenon which occurs as a subset of a much larger area of study known as the theory of rarefied gases.

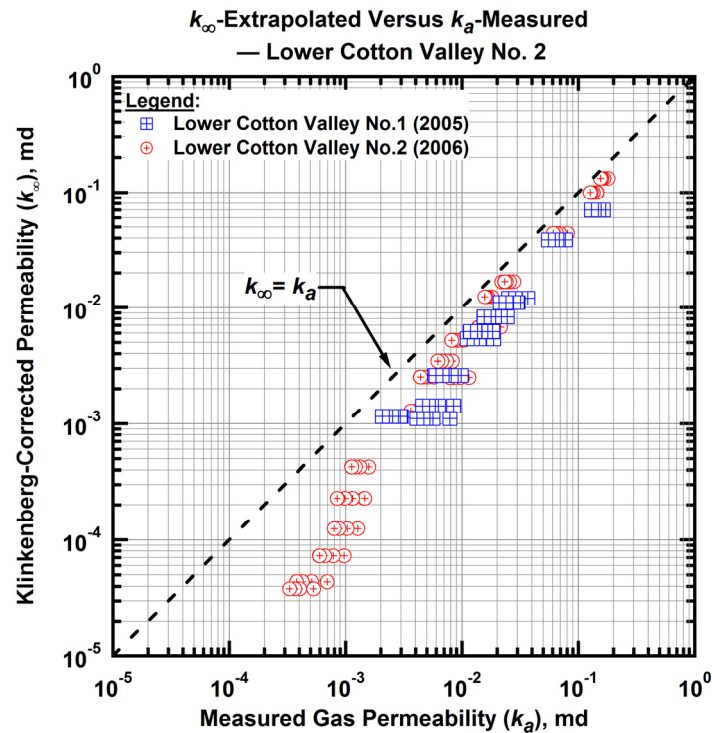


Figure 3.1 — Initial correlation plot of Klinkenberg-corrected (equivalent liquid) permeability (k_{∞}) plotted against the measured gas permeability (k_a) [log-log coordinates]. (data from ref. 7 and 8)

3.2. The Theory of Rarefied Gases (and Surface Phenomena)

Historically, the theory of rarefied gases started being developed as scientists came to the conclusions that some phenomena and equations used for a wide range of pressure, such as the Poiseuille equation for gas flow in capillary tubes or the independence of the gaseous viscosity to pressure, were breaking down at low pressure¹⁴. These failures were ascribed to the fact that the decrease in the gas pressure yields an increase in the mean free path of the gas molecules: the mean free path becomes comparable with the dimensions of the apparatus used. Kundt and Warburg⁵ first observed a deviation between a measured gas flow at low pressure and the flow model predicted by the classical fluid mechanics models (*e.g.*, Navier-Stokes equations): the no-slip condition on the inside surface of the capillary tube no longer holds and is substituted by a slippage condition (the gas molecules have a non-zero velocity at the surface of the wall/capillary tube). Klinkenberg¹ applied this condition to the flow of a gas in a porous medium and derived a first order correction for the gas slippage equation — using the results of the theory available in the late 1930s and early 1940s.

With the development of the common interest for aeronautics and aerospace, as well as, more recently, the development of the MEMS (Micro Electro-Mechanical Systems), the flow of gas at very low pressure — or, more aptly, the flow of gas molecules with a high mean free path (the mean free path (λ) being inversely proportional to the absolute pressure (p)) has been thoroughly studied in the last half century.

In the pursuit of a new microflow model it seems then natural to revisit Klinkenberg model, if for no other reason than to confirm that our new microflow model reverts to the Klinkenberg model under certain conditions (which it does)

The flow regime for a gas flowing in a micro-channel is typically determined by the value of the Knudsen number (Kn) — which is defined as:¹⁵

$$Kn = \frac{\lambda}{l_{char}} \dots\dots\dots (3.1)$$

In Eq. 3.1, λ is the mean free path of the gas molecules (*i.e.*, the average distance (length) between 2 consecutive molecular interactions) and l_{char} is the characteristic length of the flow geometry (*e.g.*, channel height, pipe radius).

For our purposes, the Knudsen number is difficult to define rigorously for a porous medium — but for the sake of argument, we will presume that such a "characteristic length" can be estimated for a porous medium. More generally, we assume that we can define the Knudsen number based on the properties of the porous medium.

The classical definition of the mean free path from thermodynamics is:

$$\lambda(p, T) = \sqrt{\pi/2} \frac{1}{p} \mu \sqrt{\frac{RT}{M}} \quad [\mu \equiv \mu(p, T)] \dots\dots\dots (3.2)$$

This particular definition (*i.e.*, **Eq. 3.2**) is based on the kinetic theory for a perfect gas^{14, 15}. In this definition, R is the universal gas constant, M is the molecular weight of the considered gas and μ is the viscosity of the gas at the corresponding thermodynamic state (*i.e.*, μ is a function of the absolute pressure p , absolute temperature T , and composition of the gas). In the following work, we mostly consider the quantity $\bar{\lambda}$ defined as the mean free path of the gas molecules at the mean absolute pressure, \bar{p} .

In addition to the definitions above, we also must consider different flow regimes for this work are as follows (See **Fig. 3.2**):

- *Continuum Flow Regime*: For $Kn < 0.01$, the mean free path of the gas molecules is *negligible* compared to the characteristic dimension of the flow geometry (*i.e.*, the l_{char} -parameter). In this case the continuum hypothesis of fluid mechanics is applicable (*i.e.*, the system is described by the Navier-Stokes equations).

- "Slip-Flow" Regime: For $0.01 < Kn < 0.1$, the mean free path is *no longer negligible*, and the slippage phenomenon appears in the "Knudsen" layer (layer of gas molecules immediately adjacent to the wall, see ref. 14)
- "Transition" Regime: For $0.1 < Kn < 10$.
- Free Molecular Flow Regime: For $Kn > 10$, the flow is dominated by diffusive effects.

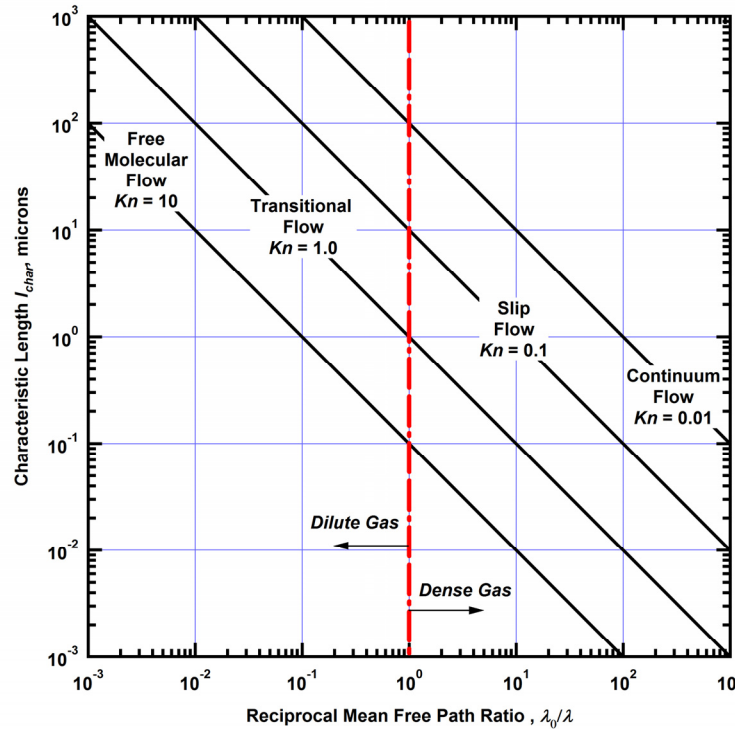


Figure 3.2 — Limits of the different flow regimes, as a function of the characteristic length of the geometry (l_{char}), and the reciprocal mean free path normalized (1 atm, 300 K). The lines defining the various flow regimes are based on the flow of air at isothermal conditions (Modified from ref. 15).

3.3. Unified Flow Model for Gas in Pipes

Karniadakis and Beskok¹⁵ developed a unified model for gas micro-flows in pipe (see **Appendix B**) where this model is valid over the entire range of flow regimes. The volumetric gas flowrate (q) flowing through a capillary of radius r and length L under the pressure drop Δp is given by:

$$q = \frac{\pi r^4}{8 \mu} (1 + \alpha(Kn) Kn) \left[1 + \frac{4Kn}{1 - bKn} \right] \frac{\Delta p}{L}, \text{ with } Kn = \frac{\lambda}{r} \dots\dots\dots(3.3)$$

In Eq. 3.2, b is a generalized slip coefficient (as recommended in ref 15, we apply the condition $b = 1$ in the remainder of this work) and the $\alpha(Kn)$ -term is defined by Karniadakis and Beskok as: (see **Appendix B**)

$$\alpha(Kn) = \frac{128}{15\pi^2} \tan^{-1} [4 Kn^{0.4}] \dots\dots\dots (3.4)$$

Using the same capillary model as Klinkenberg¹, we derived the following "microflow" model which relates the measured permeability to gas (k_a), the equivalent liquid permeability (k_∞), and the Knudsen number (Kn):

$$k_a = k_\infty [1 + \alpha(Kn)Kn] \left[1 + \frac{4Kn}{1 + Kn} \right] \dots\dots\dots (3.5)$$

Eq. 3.5 is rigorously derived (See **Appendix B**) and should be valid for all low pressure/low velocity flow regimes which exist for gas flow in porous media. We have not investigated the application of Eq. 3.5 for high pressure and/or high velocity flow.

3.4. Correlation of the Knudsen Number with Porosity, Permeability and Pressure

The Knudsen number (Kn), unlike the mean pressure (\bar{p}), *cannot be measured by direct laboratory measurements*. It is however possible to derive an analytical expression of the Knudsen number (see **Appendix C**), using the restrictive assumptions already used for deriving the analytical square-root correlation (see **Appendix B**). This analytical formulation is derived using Eqs. 3.1 and 3.2. In Eq. 3.1, the characteristic length of the flow geometry l_{char} (in our case, l_{char} is the theoretical capillary radius r) can be expressed (in m) as a function of the equivalent liquid permeability/porosity ratio (k_∞/ϕ) with Eq. 2.1 (repeated below for clarity):

$$l_{char} = 8.886 \times 10^{-6} \sqrt{k_\infty / \phi} \dots\dots\dots (2.1)$$

The "analytical" Knudsen number is given as:

$$Kn = \eta \frac{1}{p} k_\infty^{-0.5} \phi^{0.5} \dots\dots\dots (3.6)$$

The η -term in Eq. 3.6 is a function of the gas used in the core flow experiment. When the pressure (p) is expressed in psia, and equivalent liquid permeability (k_∞) is given in md and the gas used is nitrogen, Eq. 3.6 becomes:

$$Kn = 10.836 \frac{1}{p} k_\infty^{-0.5} \phi^{0.5} \dots\dots\dots (3.7)$$

Eq. 3.7 is an analytical expression and may not accurately represent the reality of the actual Knudsen number for the specific problem of gas flow in porous media. Our objective is to design a realistic model for estimating the equivalent liquid permeability (k_∞) using single-point, steady state measurements (*i.e.*, using a single pair of k_a and \bar{p} values). To remedy this issue, we propose to define a "pseudo" Knudsen number (Kn_p) — which is defined as a function of the "typically" measured parameters (*i.e.*, \bar{p} , ϕ , k_a).

Assuming that the core flow experiments are conducted in isothermal conditions (*i.e.*, the temperature gradient inside the core is equal to zero) and that the variations of the viscosity are negligible over the range of pressures considered (see Eq. 3.2), the Knudsen number (defined by Eq. 3.1) is *inversely proportional to the mean pressure (\bar{p}) and to the length characteristic of the flow geometry l_{char}* . Typically the pore throat radius, or more conveniently, a function (similar to Eq. 2.1) of the equivalent liquid permeability (k_{∞}) and the porosity (ϕ) is used to estimate l_{char} .

Substituting Eq. 3.4 into Eq. 3-5 yields:

$$k_a = k_{\infty} \left[1 + \frac{128}{15\pi^2} \tan^{-1} \left[4Kn_p^{0.4} \right] Kn_p \right] \left[1 + \frac{4Kn_p}{1 + Kn_p} \right] \dots\dots\dots (3.8)$$

In order to utilize Eq. 3.8, we must assume that the mean pressures, porosities, and the gas and equivalent liquid permeabilities are available. To solve for the "pseudo" Knudsen number (Kn_p) for a particular case, we then rearrange Eq. 3.8 into the following "root solution" form:

$$k_a - k_{\infty} \left[1 + \frac{128}{15\pi^2} \tan^{-1} \left[4Kn_p^{0.4} \right] Kn_p \right] \left[1 + \frac{4Kn_p}{1 + Kn_p} \right] = 0 \dots\dots\dots (3.9)$$

3.5 Application of the Pseudo-Knudsen Number Using Field Data

To demonstrate the application of the "pseudo"-Knudsen number (Kn_p), we only use the Lower Cotton Valley data (No. 2) (ref. 8), from which we derive two correlations for Kn_p (see **Appendix D**). Our first correlation relates the pseudo-Knudsen number (Kn_p) to the reciprocal mean pressure, the porosity, and the gas permeability as follows:

$$Kn_p = 0.59 \frac{1}{\bar{p}} k_a^{-0.5654} \phi^{-0.25} \dots\dots\dots (3.10)$$

As implied, Eq. 3.10 was derived for the specific case of the Cotton Valley No. 2 data, in a process where Kn_p (Eq. 3.9) was estimated using *known data for k_a , \bar{p} , and k_{∞}* . After Kn_p was obtained as the root of Eq. 3.9, we then correlated these Kn_p values with the k_a , \bar{p} , and ϕ data to yield Eq. 3.10.

At this point, Eq. 3.10 can be substituted into Eq. 3.9 — and this result can be solved directly for the equivalent liquid permeability (k_{∞}). Obviously, k_{∞} data must be available to "calibrate" Eq. 3.9 (*i.e.*, to estimate Kn_p). However, we believe that the calibration of Eq. 3.10 may (in future work) be reduced to specific coefficients for the intercept term, as well as the k_a and ϕ exponents.

As an alternative, we can follow the exact same calibration procedure, but this time substitute k_{∞} for k_a in Eq. 3.9 (i.e., the $Kn_p = f(k_a, \bar{p}, \phi)$ correlation). For this case, we obtain:

$$Kn_p = 2.18 \frac{1}{\bar{p}} k_{\infty}^{-0.50225} \phi^{0.253} \dots\dots\dots(3.11)$$

The equivalent liquid permeability values computed using Eq. 3.9 (based on the values of Kn_p from Eqs. 3.10 or 3.11) are correlated with the "given" Klinkenberg-corrected permeability data for this case in **Fig. 3.3**. The equivalent liquid permeability values computed using Eq. 3.9 with the analytical expression of the Knudsen number (Eq. 3.7) are also represented on Fig. 3.3.

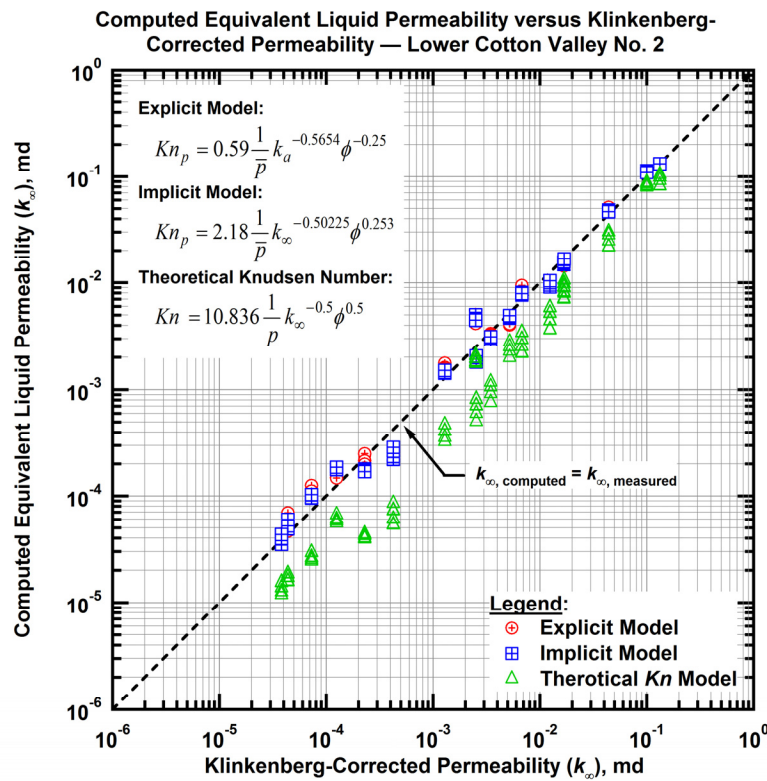


Figure 3.3 — Computed (Klinkenberg) equivalent liquid permeability (k_{∞}) versus Klinkenberg-corrected (extrapolated) permeability (k_a). (theoretical Knudsen number and pseudo-Knudsen number approaches, implicit and explicit relations for Kn_p)

We recognize that Klinkenberg-corrected permeability data may not always be available in practice — and the process of solving simultaneously for the pseudo-Knudsen number (Kn_p) and the equivalent liquid permeability (k_{∞}) will require an implicit formulation (an analog in the field of phase behavior would be an equation-of-state (EOS) which is implicit in fluid density).

In such a case, (*i.e.*, an implicit relation) we would have to determine the coefficients for the $Kn_p = f(k_\infty, \bar{p}, \phi)$ *simultaneously* with the estimation of k_∞ using Eq. 3.7. Writing the correlation for the pseudo-Knudsen number in general form, we have:

$$Kn_p = a_0 \frac{1}{\bar{p}} k_\infty^{a_1} \phi^{a_2} \dots\dots\dots(3.12)$$

Where Eq. 3.12 provides a "correlation" for the variables in this problem — and this relation allows us, in theory, to solve Eq. 3.8 for the equivalent liquid permeability (k_∞) in an implicit fashion. Substituting Eq. 3.12 into Eq. 3.8 and rearranging yields:

$$\frac{k_a}{k_\infty} = \left[1 + \frac{128}{15\pi^2} \tan^{-1} \left[4 \left[a_0 \frac{1}{\bar{p}} k_\infty^{a_1} \phi^{a_2} \right]^{0.4} \right] \left[a_0 \frac{1}{\bar{p}} k_\infty^{a_1} \phi^{a_2} \right] \right] \left[1 + \frac{4}{1 + 1 / \left[a_0 \frac{1}{\bar{p}} k_\infty^{a_1} \phi^{a_2} \right]} \right] \dots\dots\dots(3.13)$$

The "trick" is to obtain the "calibration" coefficients (a_0 , a_1 , and a_2) in Eq. 3.13. As noted above, Eq. 3.13 can be formulated as an "equation-of-state" and the coefficients (a_0 , a_1 , and a_2) can be tuned using non-linear regression — provided that there are sufficient data measurements, and that such measurements are taken for samples from the same depositional sequence.

We must note that we do not in any manner propose that Eq. 3.12 is "universal" (*i.e.*, *one set of coefficients* (a_0 , a_1 , and a_2) *does not apply to all possible data cases*). Eq. 3.12 must be calibrated for each dataset.

For this case, we did formulate Eq. 3.13 as a "fully implicit" solution using non-linear regression and we achieved following results:

- $a_0 = 0.93$
- $a_1 = -0.49$
- $a_2 = 0.13$

The results of our "fully implicit" correlation are shown in **Fig. 3.4**.

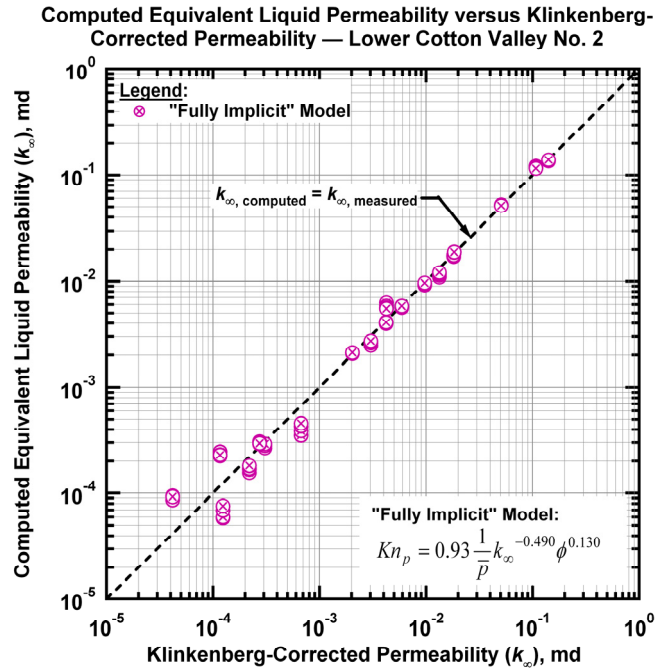


Figure 3.4 — Computed (Klinkenberg) equivalent liquid permeability (k_{∞}) versus Klinkenberg-corrected (extrapolated) permeability (k_{∞}). (fully implicit formulation for the pseudo-Knudsen number)

An overall comparison of all the models and correlations presented in this work is proposed in **Appendix E**.

CHAPTER IV

SUMMARY, CONCLUSIONS AND RECOMMENDATIONS FOR FUTURE WORK

4.1 Summary

The development of the microflow model for permeability prediction in low permeability gas sands offers an alternative to the classical Klinkenberg model, which is the long time reference for measuring permeability. The Klinkenberg model is the universally accepted standard, but we believe that the Klinkenberg model may yield poor results for very low permeability samples.

Our new model has been validated using field data from a low permeability reservoir case, but this "proof" is by no means exhaustive — additional validation is warranted.

4.2 Conclusions

1. The Jones-Owens, Sampath-Keighin, and our square-root correlations may be used satisfactorily for single point, steady-state measurements as mechanisms to estimate the equivalent liquid permeability. The Sampath-Keighin and Square-Root correlations should be preferred based on the theoretical formulations for these models.
2. The microflow model presented in this work is promising as it provides a second-order correction for gas slippage (beyond the "first-order" Klinkenberg formulation). The use of such a correction should be especially relevant for low/ultra low permeability core samples.

4.3 Recommendations, Comments and Future Work

We note that the theoretical square-root correlation (**Appendix B**) has a limited accuracy in this work. However, the square-root model validates the use of the permeability/porosity ratio in the modeling of the gas slippage factor and serves to connect the classical Klinkenberg model with our new "microflow model." Upon further validation, we believe that our microflow model will provide significant improvements for the estimation of equivalent liquid permeability from typical steady-state (gas) permeability measurements.

- Continue validation of the analytical model (Eq. 3.8) through the use of more data (*i.e.*, the "explicit" calibration approach of Eqs. 3.10 and 3.11).
- Continue validation of the "implicit" microflow model (Eq. 3.13).
- Pursue a unique calibration of Eq. 3.13 as a "universal" relation (*i.e.*, an analog to an equation-of-state for fluid phase behavior).

NOMENCLATURE

- b = General slip coefficient
 b_K = Klinkenberg gas slippage factor, psi
 c = Proportionality constant
 Kn = Knudsen number, dimensionless.
 Kn_p = Pseudo-Knudsen number, dimensionless
 k_a = Apparent gas permeability, md
 k_∞ = Equivalent liquid permeability, or Klinkenberg-corrected permeability, md
 l_{char} = Length characteristic of the flow geometry, length.
 \bar{p} = Mean core pressure, psi
 Δp = Differential pressure, psi
 q = Gas flow rate, volume per unit time
 r = Effective pore radius of the considered porous medium, length
 α = Parameter of the rarefaction coefficient, dimensionless
 μ = Gas viscosity, cp
 λ = Mean free path of the gas molecules, length
 ϕ = Porosity, fraction

REFERENCES

1. Klinkenberg, L.J.: "The Permeability of Porous Media to Liquid and Gases," paper presented at the API 11th Mid Year Meeting, Tulsa, Oklahoma (May 1941); in *API Drilling and Production Practice* (1941), 200-213
2. Heid, J.G., McMahon, J.J., Nielsen, R.F. and Yuster, S.T.: "Study of the Permeability of Rocks to Homogeneous Fluids," paper presented at the Spring Meeting of the Southwestern District, Division of Production, Dallas, TX (March 1950); in *API Drilling and Production Practice* (1950), 230-246
3. Jones, F.O. and Owens, W.W.: "A Laboratory Study of Low Permeability Gas Sands," paper SPE 7551 presented at the 1979 SPE Symposium on Low-Permeability Gas Reservoirs, May 20-22, 1979, Denver, CO.
4. Sampath, K. and Keighin, C.W.: "Factors Affecting Gas Slippage in Tight Sandstones," paper SPE 9872 presented at the 1981 SPE/DOE Low Permeability Symposium, May 27-29, 1981, Denver, CO.
5. Kundt, A. and Warburg, E.: "Über Reibung und Wärmeleitung verdünnter Gase," *Poggendorfs Annalen der Physik und Chemie* (1875), **155**, 337.
6. Maxwell, J. C.: "On the Viscosity or Internal Friction of Air and Other Gases," *Philosophical Transactions of the Royal Society of London* (1866), **156**, 249-268.
7. *Lower Cotton Valley Formation Core Report* — Anadarko Petroleum Corp., (2005), Houston, TX.
8. *Lower Cotton Valley Formation Core Report* — Anadarko Petroleum Corp., (2006), Houston, TX.
9. *Travis Peak Formation Core Report* — Well S.F.E. No 2, S.A. Holditch, (1987), College Station, TX.
10. *Travis Peak Formation Core Report* — Well 5 Howell, S.A. Holditch, (1986), College Station, TX.
11. *Frontier Formation Core Report* — Well S.F.E. 4-24, S.A. Holditch, (1991), College Station, TX.
12. Jones, S.C.: "Using the Inertial Coefficient, β , to Characterize Heterogeneity in Reservoir Rock," paper SPE 16949 presented at the 1987 SPE Annual Technical Conference and Exhibition, September 27-30, 1987, Dallas, TX.
13. Rushing, J.A., Newsham, K.E., Lasswell, P.M., Cox, J.C. and Blasingame, T.A.: "Klinkenberg-Corrected Permeability Measurements in Tight Gas: Steady-State versus Unsteady-State Techniques," paper SPE 89867 presented at the 2004 SPE Annual Technical Conference and Exhibition, September 26-29, 2004, Houston, TX.

14. Loeb, L.B.: *The Kinetic Theory of Gases*, second edition, McGraw-Hill Co. Inc., New York (1934).
15. Karniadakis, G.E. and Beskok, A.: *Micro-flows, Fundamentals and Simulation*, Springer-Verlag, New-York (2002).

APPENDIX A

KLINKENBERG DERIVATION

This appendix presents the derivation of the Klinkenberg equation.¹ However, the derivation of the Klinkenberg relation uses components that Klinkenberg did not employ (*i.e.*, elements of the literature for the kinetic theory of gases).²

A.1 Flow of Gas through a Straight Capillary

We consider a capillary tube of radius (R_0) and length (L) with its axis coincident with the x -axis. Gas is flowing through the capillary as a result of a pressure drop ($\Delta p = (p_1 - p_2)$) across the length (L) of the capillary tube. Assume that the velocity of the flowing gas (v) is a function only of the distance r from the x -axis. Consider now a cylindrical shell of length (L) comprised between the cylinders of radii r and $r + \delta r$. The force (F_1) acting on the cross-section of this shell is the normal pressure due to the flowing gas:

$$dF_1 = 2\pi\Delta p r \delta r \dots\dots\dots(A-1)$$

Assuming that the fluid motion is in steady-state, this force is balanced by the viscous drag exerted by the flowing gas on the outer and the inner surfaces (along the x -axis) of the cylindrical shell. The viscous drag is defined by:

$$F = \mu S \frac{dv}{dr} \dots\dots\dots(A-2)$$

Where:

μ = Coefficient of viscosity of the gas.

S = Surface considered ($2\pi rL$ for the inner surface, $2\pi(r + \delta r)L$ for the outer surface).

The gas velocity reaches its maximum on the axis of the cylinder (*i.e.*, $r=0$) and decreases radially towards the wall to a velocity of zero — therefore the velocity gradient dv/dr is negative. The viscous drag exerted on the inner surfaces is:

$$dF_{\text{inner Surface}} = -2\pi\mu L r \frac{dv}{dr} \dots\dots\dots(A-3)$$

The component of the viscous drag on the outer surface of the cylindrical shell, where the gas velocity is lower, is:

$$dF_{\text{Outer Surface}} = -2\pi\mu L (r + \delta r) \frac{d\left[v + \frac{dv}{dr} \delta r\right]}{dr} \dots\dots\dots(A-4)$$

The resulting viscous drag exerted on the entire shell is given by:

$$dF_2 = dF_{\text{OuterSurface}} - dF_{\text{InnerSurface}}$$

The equilibrium yields $dF_1 = dF_2$, hence:

$$2\pi\Delta p r \delta r = 2\pi\mu L r \frac{dv}{dr} - 2\pi\mu L (r + \delta r) \frac{d\left[v + \frac{dv}{dr} \delta r\right]}{dr} \dots\dots\dots (\text{A-5})$$

Expanding the second term on the right-hand side of Eq. A-5 yields:

$$2\pi\mu L (r + \delta r) \frac{d\left(v + \frac{dv}{dr} \delta r\right)}{dr} = 2\pi\mu L \left[r \frac{dv}{dr} + \delta r \left(r \frac{d^2v}{dr^2} + \frac{dv}{dr} \right) + \delta r^2 \frac{d^2v}{dr^2} \right] \dots\dots\dots (\text{A-6})$$

In Eq. A-6, the term $\delta r^2(d^2v/dr^2)$ is negligible compared to the other terms — neglecting this term and substituting Eq. A-6 into Eq. A-5 yields:

$$2\pi\Delta p r \delta r = 2\pi\mu L r \frac{dv}{dr} - 2\pi\mu L \left[r \frac{dv}{dr} + \delta r \left(r \frac{d^2v}{dr^2} + \frac{dv}{dr} \right) \right] \dots\dots\dots (\text{A-7})$$

Expanding and simplifying Eq. A-7 gives:

$$r\Delta p = -\mu L \left[r \frac{d^2v}{dr^2} + \frac{dv}{dr} \right] \dots\dots\dots (\text{A-8})$$

Dividing Eq. A-8 by $(-r\mu L)$ yields the following differential equation:

$$\frac{d^2v}{dr^2} + \frac{1}{r} \frac{dv}{dr} = -\frac{\Delta p}{\mu L} \dots\dots\dots (\text{A-9})$$

A particular solution of Eq. A-9 (*i.e.*, a non-linear differential equation) is:

$$v = A_0 - \frac{\Delta p}{4\mu L} r^2 \dots\dots\dots (\text{A-10})$$

Where A_0 is a constant fixed by the boundary conditions. Two different boundary conditions can be used — slip-flow at the wall or no slip-flow at the wall.

If no slip-flow is assumed at the wall, the condition is $v = 0$ for $r = R_0$; this imposes $A_0 = \frac{\Delta p}{4\mu L} R_0^2$. The

velocity solution to Eq. A-10 is then:

$$v = \frac{\Delta p}{4\mu L} (R_0^2 - r^2) \dots\dots\dots (\text{A-11})$$

The gas flowrate (q_g) is obtained by integrating the gas flow-rate through the considered cylinder shell section ($v(2\pi r dr)$) over the whole cross-section of the capillary tube, which yields the Poiseuille equation:

$$q_g = \int_0^{R_0} 2\pi r \frac{\Delta p}{4\mu L} (R_0^2 - r^2) dr = \frac{\pi}{8} \frac{\Delta p}{\mu L} R_0^4 \quad \text{.....(A-12)}$$

If the gas slippage is considered at the wall, the condition can be written $v = v_0$ for $r = R_0$ (where v_0 is non-zero). Kundt and Warburg³ proved that the velocity at the wall (v_0) is proportional to the velocity gradient at the wall ($[dv/dr]_{r=R_0}$), as given by:

$$v_0 = -c\bar{\lambda} [dv/dr]_{r=R_0} \quad \text{.....(A-13)}$$

In Eq. A-13, c is a constant with a value slightly less than 1 (as given by Kundt and Warburg) and $\bar{\lambda}$ is the average mean free path of the gas molecules (i.e., the mean free path of the gas molecules at the mean pressure \bar{p} (see ref. 14)), defined by $\bar{p} = [p_1 + p_2]/2$). The velocity gradient at the wall is obtained by differentiating Eq. A-10:

$$\frac{dv}{dr} = -\frac{\Delta p}{2\mu L} r \quad \text{.....(A-14)}$$

Applying the condition given by Eq. A-13 to Eq. A-14 yields:

$$v_0 = c\bar{\lambda} \frac{\Delta p}{2\mu L} R_0 \quad \text{.....(A-15)}$$

Using Eq. A-12 in Eq. A-9, at $r = R_0$, and rearranging yields:

$$A_0 = \frac{\Delta p}{4\mu L} [R_0^2 + 2c\bar{\lambda}R_0] \quad \text{.....(A-16)}$$

Substituting Eq. A-16 for A_0 in Eq. A-10 gives:

$$v = \frac{\Delta p}{4\mu L} [R_0^2 - r^2 + 2c\bar{\lambda}R_0] \quad \text{.....(A-17)}$$

As previously done for Eq. A-12, the gas flowrate (q_g) is obtained by integrating $v(2\pi r dr)$ over the whole radius of the capillary:

$$\begin{aligned} q_g &= \int_0^{R_0} \frac{\Delta p}{4\mu L} [R_0^2 - r^2 + 2c\bar{\lambda}R_0] 2\pi r dr \\ &= \frac{\pi}{8} \frac{\Delta p}{\mu L} R_0^4 \left[1 + \frac{4c\bar{\lambda}}{R_0} \right] \quad \text{.....(A-18)} \\ &= \frac{R_0^2}{8} \pi R_0^2 \frac{1}{\mu} \frac{\Delta p}{L} \left[1 + \frac{4c\bar{\lambda}}{R_0} \right] \end{aligned}$$

Re-writing Eq. A-18 in terms of superficial velocity (v_l):

$$\begin{aligned} v_g &= \frac{q_l}{A_{\text{tube}}} \\ &= \frac{q_l}{\pi R_0^2} = \frac{R_0^2}{8} \frac{1}{\mu} \frac{\Delta p}{L} \left[1 + \frac{4c\bar{\lambda}}{R_0} \right] \quad \text{.....(A-19)} \end{aligned}$$

A.2 Flow of Gas through an Idealized Porous Medium

Klinkenberg's idealized porous medium is composed of solid material through which the capillaries are oriented randomly and have all the same radius r . The direction of flow is parallel to one of the planes of the cube, and let there be N capillaries. The system for Klinkenberg's idealized porous medium is shown in **Fig. A-1**.

The liquid flowrate (q_l) through the capillary is given by Poiseuille's law as: (3 dimensional flow, so Klinkenberg used 1/3 of the total flow for a particular direction).

$$q_l = \frac{1}{3} N \frac{R_0^2}{8} \pi R_0^2 \frac{1}{\mu} \frac{\Delta p}{L} \quad (\pi R_0^2 = A_{\text{tube}}) \dots\dots\dots (\text{A-20})$$

Re-writing Eq. A-20 in terms of superficial velocity (v_l):

$$\begin{aligned} v_l &= \frac{q_l}{A_{\text{tube}}} \quad (\pi R_0^2 = A_{\text{tube}}) \dots\dots\dots (\text{A-21}) \\ &= \frac{1}{3} N \frac{R_0^2}{8} \frac{1}{\mu} \frac{\Delta p}{L} \end{aligned}$$

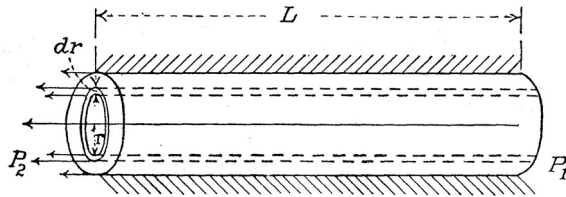


Figure A.1 — System schematic for a tube (Loeb²).

Darcy's law gives:

$$q_l = k_l (L^2) \frac{1}{\mu} \frac{\Delta p}{L} \quad (L^2 = A_{\text{cube}} \text{ (i.e., rock sample)}) \dots\dots\dots (\text{A-22})$$

Re-writing Eq. A-22 in terms of superficial velocity (v_l):

$$\begin{aligned} v_l &= \frac{q_l}{A_{\text{cube}}} \quad (L^2 = A_{\text{cube}} \text{ (i.e., rock sample)}) \dots\dots\dots (\text{A-23}) \\ &= k_l \frac{1}{\mu} \frac{\Delta p}{L} \end{aligned}$$

Where k_l is the permeability to liquid of the porous medium — which is also the absolute permeability of the porous medium (provided that the saturation is 100 percent — *i.e.*, single-phase flow). Equating Eqs. A-19 and A-20 and simplifying yields:

$$k_l = \frac{1}{3} N \frac{R_0^2}{8} \dots\dots\dots (\text{A-24})$$

If we assume that the flowing fluid is a gas, with a gas slippage condition at the wall ($v_0 \neq 0$), the gas flowrate (q_g) is given by Eq. A-18:

$$v_g = \frac{q_g}{\pi R_0^2} = \frac{R_0^2}{8} \frac{1}{\mu} \frac{\Delta p}{L} \left[1 + \frac{4c\bar{\lambda}}{R_0} \right] \dots\dots\dots (A-19)$$

Substituting $k_l = \frac{1}{3} N \frac{R_0^2}{8}$ into Eq. A-19 for yields:

$$v_g = k_l \frac{1}{\mu} \frac{\Delta p}{L} \left[1 + \frac{4c\bar{\lambda}}{R_0} \right] \dots\dots\dots (A-25)$$

For the same gas flowrate, Darcy's law gives:

$$v_g = k_a \frac{1}{\mu} \frac{\Delta p}{L} \dots\dots\dots (A-26)$$

Where k_a is the *apparent permeability to gas*. Setting Eq. A-25 equal to Eq. A-26 and simplifying, yields:

$$k_a = k_l \left[1 + \frac{4c\bar{\lambda}}{R_0} \right] \dots\dots\dots (A-27)$$

As the mean free path ($\bar{\lambda}$) is proportional to the reciprocal mean pressure (\bar{p}), we can define:

$$\frac{4c\bar{\lambda}}{r} \equiv \frac{b_K}{\bar{p}} \dots\dots\dots (A-28)$$

Where b_K is a coefficient of proportionality, *known as the Klinkenberg gas slippage factor*. Substituting Eq. A-28 for $4c\bar{\lambda}/r$ in Eq. A-27 gives the Klinkenberg equation:

$$k_a = k_l \left[1 + \frac{b_K}{\bar{p}} \right] \dots\dots\dots (A-29)$$

References

1. Klinkenberg, L.J.: "The Permeability of Porous Media to Liquid and Gases, " paper presented at the API 11th Mid Year Meeting, Tulsa, Oklahoma (May 1941); in *API Drilling and Production Practice* (1941), 200-213
2. Loeb, L.B.: *The Kinetic Theory of Gases*, second edition, McGraw-Hill Co. Inc., New York City (1934).
3. Kundt, A. and Warburg, E.: "Über Reibung und Wärmeleitung verdünnter Gase, " *Poggendorfs Annalen der Physik und Chemie* (1875), **155**, 337.

APPENDIX B

DERIVATION OF A THEORETICAL SQUARE-ROOT CORRELATION

B.1 Theoretical Capillary Radius

Considering the flow of a liquid through a capillary tube of inner radius r and length L , the fluid flowrate (q) is given by Poiseuille law as:

$$q = \pi r^2 \frac{r^2}{8} \frac{1}{\mu} \frac{\Delta p}{L} = \frac{\pi}{8} \frac{1}{\mu} \frac{\Delta p}{L} r^4 \dots\dots\dots (B-1)$$

In Eq. B-1, μ is the viscosity of the fluid and Δp is the pressure drop across the length of the tube. Considering a cylinder of idealized porous medium with a radius R_0 and a length L , composed of n identical capillary tubes (such as described above), with the same orientation — parallel to the axis of the cylinder. We note that for this discussion (as opposed to our previous work in this section), that R_0 is now defined as the outer radius of the bulk core sample. By definition, the porosity ϕ of a porous medium is given by:

$$\phi = \frac{\text{Void Volume}}{\text{Bulk Volume}} = n \frac{\pi r^2 L}{\pi R_0^2 L} = n \frac{r^2}{R_0^2} \dots\dots\dots (B-2)$$

The total volumetric flowrate (q_{tot}) of a fluid flowing through this cylinder is defined by multiplying Eq. B-1 by the number of tubes, n . This gives:

$$q_{tot} = n \frac{r^2}{8} \frac{1}{\mu} (\pi r^2) \frac{\Delta p}{L} = n \frac{\pi}{8} \frac{1}{\mu} \frac{\Delta p}{L} r^4 \dots\dots\dots (B-3)$$

For flow in a porous medium, Darcy's law is defined as:

$$q_{tot} = \frac{k}{\mu} A \frac{\Delta p}{L} \dots\dots\dots (B-4)$$

In Eq. B-4, k is the permeability of the porous medium and A is the cross-sectional area of the cylinder. Since $A = \pi R_0^2$, Eq. B-4 yields:

$$q_{tot} = \frac{k}{\mu} (\pi R_0^2) \frac{\Delta p}{L} \dots\dots\dots (B-5)$$

Equating Eqs. B-3 and B-5, and rearranging yields:

$$n \frac{r^4}{8} = k R_0^2 \dots\dots\dots (B-6)$$

Rearranging Eq. B-6 gives:

$$\left[n \frac{r^2}{R_0^2} \right] \times r^2 = 8k$$

Substituting Eq. B-2 into the above result, we have:

$$\left[n \frac{r^2}{R_0^2} \right] \times r^2 = 8k \rightarrow \phi r^2 = 8k \dots\dots\dots (B-7)$$

Or, solving Eq. B-7 for the "equivalent capillary" radius, r , we obtain:

$$r = 2 \sqrt{2} \times \sqrt{k/\phi} \dots\dots\dots (B-8)$$

In Eq. B-8, the "units" of permeability depend on the units system. For consistency, we must apply a conversion factor, C_0 , as a multiplier (e.g., when k is in md and r is in cm — $C_0 = 3.1415 \times 10^{-6} \text{ cm}/\sqrt{\text{md}}$, recall that 1 Darcy = $9.86923 \times 10^{-9} \text{ cm}^2$). The general form of Eq. B-8 with the units conversion factor (C_0) is:

$$r = 2 \sqrt{2} \times C_0 \times \sqrt{k/\phi} \dots\dots\dots (B-9)$$

Using $C_0 = 3.1415 \times 10^{-6}$, Eq. B-9 becomes:

$$r = 8.886 \times 10^{-6} \sqrt{k/\phi} \dots\dots\dots (B-10)$$

B.2 Theoretical Square-Root Correlation

To correct for the effects of gas slippage in permeability measurements, Klinkenberg¹ derived an approximate linear relationship between the measured gas permeability (k_a) and the reciprocal mean pressure (\bar{p}). This result is given as:

$$k_a = k_\infty \left[1 + \frac{b_K}{\bar{p}} \right] \dots\dots\dots (B-11)$$

In Eq. B-11, k_∞ is the *Klinkenberg-corrected permeability* and b_K is the *Klinkenberg gas slippage factor*. The gas slippage factor (b_K) is a "constant" which relates the mean free path of the gas molecules ($\bar{\lambda}$) at the mean (absolute) pressure (\bar{p}) and the effective pore-throat radius (r), as given by:

$$\frac{4c\bar{\lambda}}{r} = \frac{b_K}{\bar{p}} \dots\dots\dots (B-12)$$

In Eq. B-12, c is a constant very close to unity.² We will consider $c = 1$ for the remainder of this derivation. Re-arranging Eq. B-12 yields:

$$b_K = \frac{4}{r} \bar{\lambda} \bar{p} \dots\dots\dots (B-13)$$

Substituting r in Eq. B-13 with Eq. B-10 gives:

$$b_K = \frac{4}{8.886 \times 10^{-6}} \bar{\lambda} \bar{p} \left[\frac{k}{\phi} \right]^{-0.5} \dots\dots\dots (B-14)$$

In Eq. B-14, the mean free path of the gas molecules is defined by:³

$$\bar{\lambda}(p,T) = \sqrt{\pi/2} \frac{1}{\bar{p}} \mu \sqrt{\frac{RT}{M}} \quad [\mu \equiv \mu(\bar{p},T)] \dots\dots\dots(B-15)$$

In this definition, R is the universal gas constant, M is the molecular weight of the gas and μ is the viscosity of the gas at the corresponding thermodynamic state (*i.e.*, μ is a function of the absolute (mean) pressure, \bar{p} , absolute temperature, T , and composition of the gas). For clarity, the subsequent formulae are expressed in S.I. units, unless specified otherwise.

The square-root correlation developed in this work conforms to the following assumptions:

- The temperature in the core sample is uniform during steady-state flow (assumed: $T = 298$ K).
- The gas used for the experiments is nitrogen ($M = 28.01348$ kg/kg-mole).
- Assuming that, in the range of pressure applied in the laboratory, nitrogen behaves as ideal gas, the variation of the nitrogen viscosity with pressure is negligible, hence $\mu_{N_2}(T, \bar{p}) \approx \mu_{N_2,1\text{atm}}(T)$.

Nitrogen viscosity as a function of temperature ($\mu_{N_2,1\text{atm}}(T)$, expressed in Pa.s) is computed using Sutherland's equation:⁴

$$\mu_{N_2,1\text{atm}}(T) = \frac{13.85T^{1.5}}{T + 102} \times 10^{-7} \dots\dots\dots(B-16)$$

The value of the universal gas constant R is: $R = 8,314$ J/K/kg-mole. The product $\bar{\lambda}\bar{p}$ in Eq. B-15 can be calculated using Eq. B-15 and B-16:

$$\bar{\lambda}\bar{p} = \sqrt{\pi/2} \frac{1}{\bar{p}} \sqrt{\frac{8314 \times 298}{28.01348}} \times \frac{13.85 \times 298^{1.5}}{298 + 102} \times 10^{-7} \times \bar{p} = 0.00664 \dots\dots\dots(B-17)$$

To obtain the radius, r , in meters (recall that the base unit of the mean free path λ is the meter), Eq. B-10 (expressed in traditional units) becomes;

$$r = 8.886 \times 10^{-8} \sqrt{k/\phi} \dots\dots\dots(B-18)$$

Using the result from Eq. B-17 and Eq. B-18 in Eq. B-14 yields:

$$b_K = \frac{4 \times 0.00664}{8.886 \times 10^{-8}} \left[\frac{k}{\phi} \right]^{-0.5} = 2.9885 \times 10^5 \left[\frac{k}{\phi} \right]^{-0.5} \dots\dots\dots(B-19)$$

Where b_K is expressed in Pa. Converting b_K to psi yields:

$$b_K = 43.345 \left[\frac{k}{\phi} \right]^{-0.5} \dots\dots\dots(B-20)$$

The significance of Eq. B-20 is that this result establishes the basis for the b_K versus $\sqrt{k/\phi}$ correlation given by Sampath and Keighin⁵. The exponent (-0.5) is established rigorously from theory as shown above.

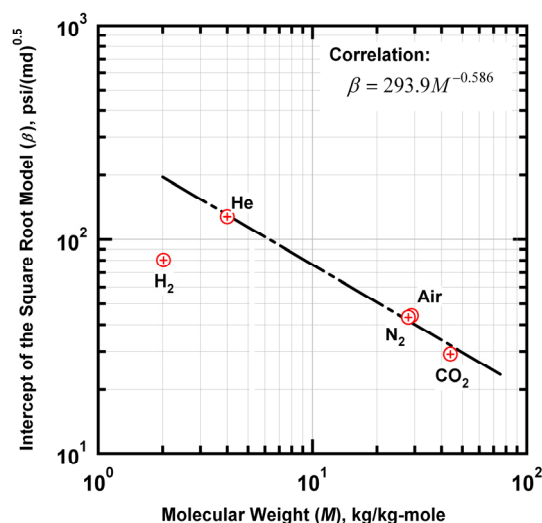


Figure B.1 — Intercept of the square root model versus molecular weight of the gas used in the measurements — the viscosity of the different gases except H_2 is similar (see Table B.1), hence the $\bar{\lambda}\bar{p}$ -term (Eq. B-17) varies approximately with the reciprocal square-root of the molecular weight.

The intercept (43.345) is based on the assumptions of ambient temperature ($T = 298 \text{ K}$) and pressure (1 atm), but these assumptions are probably not significant compared to the assumption of nitrogen as the reference gas. The table below summarizes our estimates of the intercept coefficient for hydrogen, helium, air, nitrogen, and carbon dioxide.

Table B.1 — Intercept for Eq. B-20, various gases.

Flowing Gas	Molecular Weight (kg/kg-mole)	Gas Viscosity at 1atm and 298 K (Pa.s)	Eq. B-20 Intercept (psi)
hydrogen	2.0159	8.845×10^{-6}	80.236
helium	4.0026	1.985×10^{-5}	127.802
air	28.9586	1.842×10^{-5}	44.106
nitrogen	28.01348	1.781×10^{-5}	43.345
carbon dioxide	44.0095	1.503×10^{-5}	29.181

These estimates are based on the fluid properties of ref. 3 and the NIST correlations⁶ as appropriate.

References

1. Klinkenberg, L.J.: "The Permeability of Porous Media to Liquid and Gases," paper presented at the API 11th Mid Year Meeting, Tulsa, Oklahoma (May 1941); in *API Drilling and Production Practice* (1941), 200-213
2. Kundt, A. and Warburg, E.: "Über Reibung und Wärmeleitung verdünnter Gase, " *Poggendorfs Annalen der Physik und Chemie* (1875), **155**, 337.
3. Loeb, L.B.: *The Kinetic Theory of Gases*, second edition, McGraw-Hill Co. Inc., New York (1934).

4. *RP-40, Recommended Practices for Core Analysis*, 2nd edition, API, Washington, DC (1998).
5. Sampath, K. and Keighin, C.W.: "Factors Affecting Gas Slippage in Tight Sandstones," paper SPE 9872 presented at the 1981 SPE/DOE Low Permeability Symposium, May 27-29, 1981, Denver, Colorado.
6. NIST Chemistry Webbook, NIST, <http://webbook.nist.gov>

APPENDIX C

A RIGOROUS MICRO-FLOW MODEL APPLIED TO THE PROBLEM OF GAS FLOW THROUGH POROUS MEDIA

C.1 Unified Flow Model for Pipe Flow

Karniadakis and Beskok¹ developed a unified model that predicts volumetric and mass flowrates for gas flow in channels and pipes, over the entire Knudsen regime (*i.e.*, all flow regimes). The Karniadakis-Beskok "micro-flow" model is given (without derivation) as:

$$q = \frac{\pi}{8} l_{char}^4 \frac{1}{\mu} \frac{\Delta p}{L} [1 + \alpha(Kn) Kn] \left[1 + \frac{4Kn}{1 - bKn} \right] \dots\dots\dots (C-1)$$

Where:

- q = Volumetric flowrate in the conduit, cc/sec
- l_{char} = Characteristic length of the flow geometry (*e.g.*, channel height, pipe radius), cm
- L = Length of conduit, cm
- Δp = Pressure drop across the length of the conduit, atm
- μ = Gas viscosity at temperature and pressure, cp
- b = Dimensionless slip coefficient, (b is defined as -1)
- $\alpha(Kn)$ = Dimensionless term in the rarefaction coefficient

In Eq. C-1, the Knudsen number (Kn) is defined by:

$$Kn = \frac{\bar{\lambda}}{l_{char}} \dots\dots\dots (C-2)$$

Where $\bar{\lambda}$ is the mean free path of the gas molecules (*i.e.*, the average distance (length) between 2 consecutive molecular interactions at the mean pressure (\bar{p})).

We use a value of -1 for the general slip coefficient (b) as recommended by Karniadakis and Beskok. The role of the rarefaction coefficient $[1 + \alpha(Kn) Kn]$ is to account for the transition between the "*slip-flow*" regime (for which Klinkenberg model was developed²) and the "*free molecular flow*" regime. In the "*slip-flow*" regime (*i.e.*, $0.01 < Kn < 0.1$), the rarefaction coefficient is equal to 1 (*i.e.*, $\alpha = 0$); in the "*free molecular flow*" regime (*i.e.*, $Kn > 10$), the volumetric flow-rate is independent of the Knudsen number and the parameter α tends toward a constant value (for $Kn \rightarrow \infty$).

For reference, the "Knudsen" flow regimes are defined as follows below and are illustrated graphically in Fig. C.1.

- *Continuum Flow Regime*: For $Kn < 0.01$, the mean free path of the gas molecules is *negligible* compared to the characteristic dimension of the flow geometry (*i.e.*, the l_{char} -parameter). In this case the continuum hypothesis of fluid mechanics is applicable (*i.e.*, the system is described by the Navier-Stokes equations).
- *"Slip-Flow" Regime*: For $0.01 < Kn < 0.1$, the mean free path is *no longer negligible*, and the slippage phenomenon appears in the "Knudsen" layer (layer of gas molecules immediately adjacent to the wall)
- *"Transition" Regime*: For $0.1 < Kn < 10$.
- *Free Molecular Flow Regime*: For $Kn > 10$, the flow is dominated by diffusive effects.

The variation of the α -parameter as a function of Kn is represented using:¹

$$\alpha(Kn) = \alpha_0 \frac{2}{\pi} \tan^{-1} [c_1 Kn^{c_2}] \dots\dots\dots (C-3)$$

Where α_0 , c_1 and c_2 are constants. The values for the constants c_1 and c_2 are respectively 4.0 and 0.4 and the parameter α_0 is given by:

$$\alpha_0 = \frac{64}{3\pi} \frac{1}{\left[1 - \frac{4}{b}\right]} = \frac{64}{15\pi} \dots\dots\dots (C-4)$$

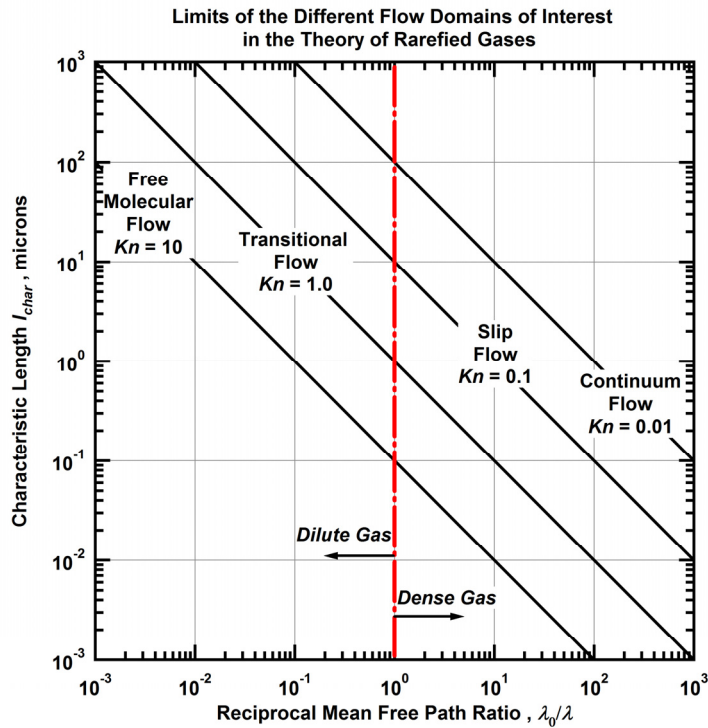


Figure C.1 — Limits of the different flow regimes as a function of the length characteristic of the geometry, l_{char} , and the reciprocal mean free path normalized at atmospheric conditions and 300 K. The lines defining the various Knudsen number regimes are based on air at isothermal conditions (Modified from ref. 1).

C.2 Validation of the Micro-Flow Model Concept

In order to validate the applicability of the concept of the unified flow model (Eq. C-1) for the problem of steady-state gas flow through a porous medium, we computed the Knudsen number for a given data set composed of 11 core samples tested at various mean pressures.

The mean free path of gas molecules is defined by:¹

$$\bar{\lambda}(p, T) = \sqrt{\pi/2} \frac{1}{\bar{p}} \mu \sqrt{\frac{RT}{M}} \quad [\mu \equiv \mu(\bar{p}, T)] \dots\dots\dots (C-5)$$

The mean free path ($\bar{\lambda}$) is computed using the following (all terms in S.I. units):

- The core flow experiments were performed at a constant room temperature ($T = 298$ K).
- The gas used for the experiments was nitrogen ($M = 28.01348$ lb/lbmole).
- The nitrogen viscosity was computed using Sutherland's equation³:

$$\begin{aligned} \mu_{N_2, 1 \text{ atm}}(T) &= \frac{13.85T^{1.5}}{T + 102} \\ \mu_{N_2}(T, p) &= \mu_{N_2, 1 \text{ atm}}(T) - 0.12474 + 0.123688p \dots\dots\dots (C-6) \\ &\quad + 1.05452 \times 10^{-3} p^2 - 1.5052 \times 10^{-6} p^3 \end{aligned}$$

The characteristic length of the conduit (l_{char}) is required in order to estimate the required Knudsen numbers. The "typical" characteristic length is estimated from capillary pressure data or an equivalent single capillary concept — and these "lengths" are typically the capillary radii. We use this exercise simply to evaluate one definition over another — conceptually, there is no perfect definition because we are investigating flow in porous media, not uniform capillaries.

The definitions we consider for l_{char} are:

- The *computed* average pore throat radius estimated from capillary pressure data (these data are given in the various reports from which the sample data were extracted).
- The theoretical "capillary radius" given by:

$$l_{char} = 8.886 \times 10^{-6} \sqrt{k_{\infty} / \phi} \dots\dots\dots (C-7)$$

The minimum and maximum computed Knudsen numbers (based on mean pressures) for each sample are presented in **Table C.1**. Since most of the Knudsen numbers are greater than 0.1, the "*Transition*" *Regime* ($0.1 < Kn < 10$) is the dominant type of flow regime — therefore, the rarefaction coefficient defined in the previous section plays a major role for modeling the volumetric flowrate. In concept, this observation validates the application of the micro-flow model for (steady-state) gas flow in porous media.

Table C.1 — Minimum and maximum Knudsen numbers corresponding to the models used to represent the characteristic length l_{char} .

Sample ID	Kn Estimated from the Average Pore Throat Radius		Kn Estimated from Eq. C-7	
	min Kn	max Kn	min Kn	max Kn
1	0.15	0.34	0.64	1.51
2	0.15	0.36	0.32	0.77
3	0.43	0.97	0.40	0.91
4	0.06	0.15	0.72	1.67
5	0.15	0.34	0.12	0.27
6	0.37	0.72	0.41	0.80
7	0.15	0.34	0.22	0.50
8	0.05	0.09	0.16	0.26
9	0.15	0.33	0.28	0.63
10	0.18	0.34	0.28	0.52
12	0.18	0.34	0.31	0.57

C.3 Derivation of a Theoretical Knudsen Number as a Function of Pressure, Permeability and Porosity.

It is possible to derive analytically an expression of the Knudsen number (Kn) as a function of the pressure (p), equivalent liquid permeability (k_{∞}) and porosity (ϕ) only, using Eqs. C-2, C-5 and C-7. It is assumed in the following section that nitrogen behaves as an ideal gas over the range of pressure considered: nitrogen viscosity is then a constant. Substituting Eqs. C-5 and C-7 in Eq. C-2 yields:

$$Kn = \sqrt{\pi/2} \frac{1}{p} \mu \sqrt{\frac{RT}{M}} \frac{1}{8.886 \times 10^{-8}} \left[\frac{k_{\infty}}{\phi} \right]^{-0.5} \dots\dots\dots (C-8)$$

The units in Eq. C-8 are as follows: the pressure is expressed in Pa, the viscosity (μ) in Pa.s, R in J/K/kg-mole, T in K, M in kg/kg-mole and k_{∞} in md. The Knudsen number formulation developed in this work conforms to the following assumptions:

- The temperature in the core sample is uniform during steady-state flow (assumed: $T = 298$ K).
- The gas used for the experiments is nitrogen ($M = 28.01348$ kg/kg-mole).
- Assuming that, in the range of pressure applied in the laboratory, nitrogen behaves as ideal gas, the variation of the nitrogen viscosity with pressure is negligible, hence $\mu_{N_2}(T, \bar{p}) \approx \mu_{N_2,1atm}(T)$.

Nitrogen viscosity as a function of temperature ($\mu_{N_2,1atm}(T)$), expressed in Pa.s) is computed using Sutherland's equation:³

$$\mu_{N_2,1atm}(T) = \frac{13.85T^{1.5}}{T + 102} \times 10^{-7} \dots\dots\dots (C-9)$$

The value of the universal gas constant R is: $R = 8,314$ J/K/kg-mole.

With the afore mentioned assumptions, Kn is written as:

$$Kn = \sqrt{\pi/2} \left[\frac{13.85 (298)^{1.5}}{298 + 102} \times 10^{-7} \right] \sqrt{\frac{8,314 \times 298}{28.01348}} \frac{1}{8.886 \times 10^{-8}} \frac{1}{p} \left[\frac{k_{\infty}}{\phi} \right]^{-0.5}$$

$$= 74,713 \frac{1}{p} \left[\frac{k_{\infty}}{\phi} \right]^{-0.5}$$

.....(C-10)

In Eq. C-10, the absolute pressure (p) is given in Pa. For p given in psia, Eq. C-10 becomes:

$$Kn = 74,713 \frac{1}{p} \left[\frac{k_{\infty}}{\phi} \right]^{-0.5} \times 0.000145038 = 10.836 \frac{1}{p} \left[\frac{k_{\infty}}{\phi} \right]^{-0.5}$$

.....(C-11)

This expression (Eq. C-11), although derived theoretically using restrictive assumptions, establishes the basis for expressing Kn as a function of p , k_{∞} and ϕ .

C.4 A Rigorous Micro-Flow Model for Gas Flow in an Idealized Porous Medium.

The "micro-flow" model is defined in the previous section as:

$$q = \frac{\pi}{8} l_{char}^4 \frac{1}{\mu} \frac{\Delta p}{L} [1 + \alpha(Kn) Kn] \left[1 + \frac{4Kn}{1 - bKn} \right] \dots\dots\dots(C-1)$$

Poiseuille's law for fluid flow in a pipe (or tube) is given by:

$$q = \frac{\pi}{8} l_{char}^4 \frac{1}{\mu} \frac{\Delta p}{L} \dots\dots\dots(C-12)$$

Darcy's law for fluid flow in a porous media:

$$q = k A_{core} \frac{1}{\mu} \frac{\Delta p}{L} \dots\dots\dots(C-13)$$

In Eq. C-13, A is the cross-sectional area of the porous medium (perpendicular to the direction of the flow). Following the procedure given by Klinkenberg,² we can equate Poiseuille's and Darcy's laws to yield an expression for the permeability (k). This procedure requires us to equate Eqs. C-12 and C-13, which yields:

$$k = \frac{\pi}{8} \frac{l_{char}^4}{A_{core}} \dots\dots\dots(C-14)$$

Substituting Eq. C-14 into Eq. C-1, we have:

$$q = \frac{k}{\mu} A_{core} \frac{\Delta p}{L} [1 + \alpha(Kn) Kn] \left[1 + \frac{4Kn}{1 - bKn} \right] \dots\dots\dots(C-15)$$

Where:

- k = Permeability, D
- q = Volumetric flowrate in the conduit, cc/sec
- l_{char} = The characteristic length of the flow geometry (e.g., channel height, pipe radius), cm
- L = Length of conduit, cm

- Δp = Pressure drop across the length of the conduit, atm
- μ = Gas viscosity at temperature and pressure, cp
- b = Dimensionless slip coefficient (b is defined as -1)
- $\alpha(Kn)$ = Dimensionless rarefaction coefficient
- Kn = Knudsen number, dimensionless

Multiplying through Eq. C-15 by $\frac{\mu}{A} \frac{L}{\Delta p}$ and using $b=-1$, we obtain:

$$q \frac{\mu}{A} \frac{L}{\Delta p} = k_{\infty} [1 + \alpha(Kn) Kn] \left[1 + \frac{4Kn}{1 - bKn} \right] \dots\dots\dots (C-16)$$

Where we note that the left-hand-side of Eq. C-16 is simply the "gas" permeability (k_a) as defined by Darcy's law (*i.e.*, the "uncorrected" permeability). Making this reduction, we have our base form:

$$k_a = k_{\infty} [1 + \alpha(Kn) Kn] \left[1 + \frac{4Kn}{1 + Kn} \right] \dots\dots\dots (C-17)$$

Eq. C-17 provides an independent relation between the apparent gas permeability (k_a) the slip-corrected permeability (or Klinkenberg-corrected permeability) (k_{∞}) and the Knudsen number (Kn). We now need to finalize Eq. C-17 by substitution of the relations for $\alpha(Kn)$. We substitute Eq. C-3 into Eq. C-1 (and assume that $c_1 = 4.0$ and $c_2 = 0.4$ in Eq. C-3), which yields a direct relation for $\alpha(Kn)$ of the form of:

$$\alpha(Kn) = \frac{128}{15\pi^2} \tan^{-1} [4 Kn^{0.4}] \dots\dots\dots (C-18)$$

We now substitute Eq. C-18 into Eq. C-17 to yield our formal (or complete) result for this work:

$$k_a = k_{\infty} \left[1 + \left[\frac{128}{15\pi^2} \tan^{-1} [4 Kn^{0.4}] \right] Kn \right] \left[1 + \frac{4Kn}{1 + Kn} \right] \dots\dots\dots (C-19)$$

C.5 Klinkenberg Model as a Simplified Microflow Model for Slip-Flow Regime

We can prove "mathematically" (using rigorous assumptions) that the model developed by Klinkenberg is actually a simplification of the microflow model for the case of the slip-flow regime ($0.01 < Kn < 0.1$).

Recalling the Klinkenberg equation:

$$k_a = k_{\infty} \left[1 + \frac{b_K}{\bar{p}} \right] \dots\dots\dots (C-20)$$

Where:

- k_{∞} = Klinkenberg-corrected permeability, D
- k_a = Apparent gas permeability, D
- b_K = Klinkenberg gas slippage factor, atm
- \bar{p} = Mean core pressure, atm

The Klinkenberg gas slippage factor (b_K) is defined by Klinkenberg as a coefficient of proportionality:

$$\frac{4c\bar{\lambda}}{r} = \frac{b_K}{\bar{p}} \dots\dots\dots (C-21)$$

Where c is a constant close to 1 (see ref. 4) and r is the effective pore throat radius (in our case r is the characteristic length l_{char}).

Applying Eq. C-21 to Eq. C-20 yields:

$$k_a = k_\infty \left[1 + 4c \frac{\bar{\lambda}}{r} \right] \dots\dots\dots (C-22)$$

Recall the base form of our microflow model (Eq. C-17):

$$k_a = k_\infty [1 + \alpha(Kn) Kn] \left[1 + \frac{4Kn}{1 + Kn} \right] \dots\dots\dots (C-17)$$

We assume that we are in a slip-flow regime, then by definition, $\alpha(Kn) = 0$. Hence Eq. C-17 becomes:

$$k_a = k_\infty \left[1 + \frac{4Kn}{1 + Kn} \right] \dots\dots\dots (C-23)$$

Also, for $0.01 < Kn < 0.1$, we have:

$$\frac{1}{1 + Kn} \approx 1 - Kn + o(Kn) \dots\dots\dots (C-24)$$

Hence:

$$\begin{aligned} \frac{4Kn}{1 + Kn} &\approx 4Kn - 4Kn^2 + o(Kn^2) \dots\dots\dots (C-25) \\ &\approx 4Kn \end{aligned}$$

By definition of the Knudsen number (Eq. C-2):

$$Kn = \frac{\bar{\lambda}}{l_{char}} \dots\dots\dots (C-2)$$

Eq. C-23 now yields:

$$\begin{aligned} k_a &\approx k_\infty [1 + 4Kn] \\ &\approx k_\infty \left[1 + 4 \frac{\bar{\lambda}}{l_{char}} \right] \dots\dots\dots (C-26) \end{aligned}$$

Eq. C-26 is very similar (and almost identical) to Eq. C-22, provided that the constant c in Eq. C-22 is equal to one and the mean free path of the gas molecules used in the microflow model ($\bar{\lambda}$) is defined as the average mean free path of the gas molecules ($\bar{\lambda}$ in the Klinkenberg model, evaluated at the mean core pressure). We can consider that the Klinkenberg model is an approximation of the microflow model.

References

1. Karniadakis, G.E. and Beskok, A.: *Micro-flows, Fundamentals and Simulation*, Springer-Verlag, New-York (2002).
2. Klinkenberg, L.J.: "The Permeability of Porous Media to Liquid and Gases, " paper presented at the API 11th Mid Year Meeting, Tulsa, Oklahoma (May 1941); in *API Drilling and Production Practice* (1941), 200-213
3. *RP40, Recommended Practices for Core Analysis*, 2nd edition, API, Washington, DC (1998).
4. Kundt, A. and Warburg, E.: "Über Reibung und Wärmeleitung verdünnter Gase, " *Poggendorfs Annalen der Physik und Chemie* (1875), **155**, 337.

APPENDIX D

CORRELATIONS FOR THE "PSEUDO-KNUDSEN" NUMBER — APPLICATION TO A TIGHT GAS EXAMPLE (LOUISIANA, USA)

D.1 Definitions

The Knudsen number is a dimensionless variable that is used to characterize the flow regime of a gas flowing through a conduit — and is defined as:¹

$$Kn = \frac{\lambda}{l_{char}} \dots\dots\dots (D-1)$$

Where:

- λ = The mean free path of the gas molecules (*i.e.*, the average distance (length) between 2 consecutive molecular interactions).
- l_{char} = The characteristic length of the conduit (*e.g.*, channel height, pipe radius).

The mean free path of gas molecules is defined by:

$$\lambda(p, T) = \sqrt{2/\pi} \frac{1}{p} \mu \sqrt{\frac{RT}{M}} \quad [\mu \equiv \mu(p, T)] \dots\dots\dots (D-2)$$

This particular definition (*i.e.*, Eq. D-2) is based on the kinetic theory for a perfect gas^{1,2}. In this definition, R is the universal gas constant, M is the molecular weight of the considered gas and μ is the viscosity of the gas at the corresponding thermodynamic state (*i.e.*, μ is a function of the pressure p , absolute temperature T (in degrees Rankine), and composition of the gas). Our objective is to validate our new model for equivalent liquid permeability: (see Appendix C for derivation)

$$k_a = k_\infty \left[1 + \left[\frac{128}{15\pi^2} \tan^{-1} \left[4Kn^{0.4} \right] \right] Kn \right] \left[1 + \frac{4Kn}{1 + Kn} \right] \dots\dots\dots (D-3)$$

Where:

- k_a = Permeability to gas (units must be consistent with k_∞)
- k_∞ = Equivalent liquid permeability (units must be consistent with k_a)
- Kn = Knudsen number, dimensionless

D.2 Determination of the Pseudo-Knudsen Numbers

This data set (ref. 3) includes 18 core samples where the Klinkenberg analysis (ref. 4) was performed in order to estimate the liquid equivalent permeability (k_∞). The measured mean pressure, the permeability to gas, and the porosity are given for each sample — and using the mean pressure and permeability to gas data, a Klinkenberg plot is constructed, and the gas slippage factor (b_K) and the Klinkenberg-corrected permeability (k_∞) are estimated.

As noted, the porosity of the sample is also given, but no reference conditions were given, so we assumed 300 K (80 Deg F) and 1 atm. The data summary is given in **Table D.1**.

Table D.1 — Summary of the core data (given data and computed results).

Sample ID	k_∞ (md)	b_K (psi)	ϕ (fraction)
1-8	0.0001	565.3	0.023
2-10	0.1322	14.2	0.063
2-22	0.0168	32.5	0.056
3-8	0.0439	32.8	0.078
3-48	0.0035	83.6	0.07
1-1	0.00007	753.5	0.029
1-5	0.00004	801.0	0.02
1-7	0.00003	771.0	0.017
2-2	0.0004	165.1	0.036
2-7	0.0124	26.8	0.06
2-8	0.0025	77.1	0.051
2-12	0.0025	215.1	0.055
2-28	0.0052	58.6	0.037
3-4	0.0002	303.1	0.04
3-6	0.0999	26.4	0.066
3-10	0.0067	84.8	0.071
3-36	0.0168	39.2	0.057
3-55	0.0013	183.7	0.066

Since we cannot compute the Knudsen number explicitly, the goal of this step is to evaluate a "pseudo Knudsen" number (Kn_p) using the relation below:

$$k_a - k_\infty \left[1 + \left[\frac{128}{15\pi^2} \tan^{-1} \left[4Kn^{0.4} \right] \right] Kn \right] \left[1 + \frac{4Kn}{1+Kn} \right] = 0 \dots\dots\dots(D-4)$$

It is easily proven that for any pair of values for k_a and k_∞ , Eq. D-4 has a unique positive solution: we refer to this solution as the "pseudo Knudsen" number.

Analytical Considerations

For each Klinkenberg-corrected permeability (k_∞) value, we can define the following function f_{k_∞} :

$$f_{k_\infty}(x) \equiv k_\infty \left[1 + \left[\frac{128}{15\pi^2} \tan^{-1} \left[4x^{0.4} \right] \right] x \right] \left[1 + \frac{4x}{1+x} \right] \dots\dots\dots(D-5)$$

In this particular example case, we have 8 data measurements per sample which are used to construct a plot of k_a versus $1/p$ — and from which a single k_∞ -value is obtained. We also note that the Knudsen number is a real number, strictly positive — therefore f_{k_∞} is then defined on $]0, +\infty[$. The first step of our approach is to find a root of the equation $f_{k_\infty}(x) = k_a$.

It is easily proven that, for each and every value of k_{∞} , $f_{k_{\infty}}$ is a strictly increasing function. The limits of the $f_{k_{\infty}}(x)$ are given as:

$$\begin{aligned} f_{k_{\infty}} &\xrightarrow{x \rightarrow 0} k_{\infty} \\ f_{k_{\infty}} &\xrightarrow{x \rightarrow +\infty} +\infty \end{aligned}$$

Since the Klinkenberg-corrected permeability (k_{∞}) of a sample is always lower than any measured permeability to gas (k_a) value for the same sample, the equation $f_{k_{\infty}}(x) = k_a$ (which is strictly equivalent to Eq.D-1) has a unique solution on $[0, +\infty[$. The solutions of the equations ($f_{k_{\infty}}(x) = k_a$) for the different samples and for each value of k_a have been computed using both MS *Excel* and *MATLAB* (the same results were obtained). This process yields the "pseudo-Knudsen" numbers presented in **Table D.2**.

Table D.2 — Data and Kn_p solutions computed using Eq. D-5.

	k_{as} , md	k_{cs} , md	\bar{p} , psia	ϕ , fraction	Kn_p
Sample_1_8	1.27E-03	1.25E-04	60.0	0.023	1.6309
	1.27E-03	1.25E-04	60.0	0.023	1.6314
	1.03E-03	1.25E-04	75.4	0.023	1.3121
	1.03E-03	1.25E-04	75.4	0.023	1.3135
	8.77E-04	1.25E-04	90.1	0.023	1.1024
	8.78E-04	1.25E-04	90.0	0.023	1.1039
	7.95E-04	1.25E-04	104.9	0.023	0.9897
	7.95E-04	1.25E-04	104.9	0.023	0.9904
Sample_2_10	1.80E-01	1.32E-01	39.6	0.063	0.0760
	1.80E-01	1.32E-01	39.6	0.063	0.0756
	1.66E-01	1.32E-01	54.9	0.063	0.0535
	1.66E-01	1.32E-01	54.9	0.063	0.0537
	1.59E-01	1.32E-01	69.7	0.063	0.0437
	1.58E-01	1.32E-01	69.7	0.063	0.0420
	1.55E-01	1.32E-01	84.7	0.063	0.0371
	1.55E-01	1.32E-01	84.7	0.063	0.0371
Sample_2_22	2.57E-02	1.68E-02	59.7	0.056	0.1095
	2.60E-02	1.68E-02	59.7	0.056	0.1132
	2.41E-02	1.68E-02	74.6	0.056	0.0903
	2.41E-02	1.68E-02	74.5	0.056	0.0910
	2.28E-02	1.68E-02	89.9	0.056	0.0753
	2.29E-02	1.68E-02	89.9	0.056	0.0762
	2.19E-02	1.68E-02	104.8	0.056	0.0638
	2.20E-02	1.68E-02	104.7	0.056	0.0649
Sample_3_8	8.05E-02	4.40E-02	39.5	0.078	0.1685
	8.05E-02	4.40E-02	39.5	0.078	0.1686
	6.89E-02	4.40E-02	54.8	0.078	0.1166
	6.89E-02	4.40E-02	54.8	0.078	0.1167
	6.47E-02	4.40E-02	69.8	0.078	0.0977
	6.48E-02	4.40E-02	69.8	0.078	0.0980
	6.10E-02	4.40E-02	84.8	0.078	0.0807
	6.09E-02	4.40E-02	84.8	0.078	0.0804
Sample_3_48	8.28E-03	3.45E-03	59.6	0.070	0.2778
	8.27E-03	3.45E-03	59.6	0.070	0.2773
	7.35E-03	3.45E-03	74.7	0.070	0.2265
	7.35E-03	3.45E-03	74.7	0.070	0.2264
	6.69E-03	3.45E-03	90.0	0.070	0.1899
	6.69E-03	3.45E-03	90.0	0.070	0.1897
	6.19E-03	3.45E-03	104.7	0.070	0.1616
	6.19E-03	3.45E-03	104.7	0.070	0.1616

Table D.2 — Continued

	k_a , md	k_{cs} , md	\bar{p} , psia	ϕ , fraction	Kn_p
Sample_1_1	9.71E-04	7.29E-05	59.2	0.029	2.1436
	9.71E-04	7.29E-05	59.2	0.029	2.1436
	7.80E-04	7.29E-05	74.6	0.029	1.7142
	7.80E-04	7.29E-05	74.5	0.029	1.7151
	6.61E-04	7.29E-05	89.3	0.029	1.4440
	6.62E-04	7.29E-05	89.3	0.029	1.4460
	5.95E-04	7.29E-05	104.4	0.029	1.2921
	5.97E-04	7.29E-05	104.4	0.029	1.2980
Sample_1_5	6.95E-04	4.37E-05	59.9	0.020	2.5613
	6.94E-04	4.37E-05	59.9	0.020	2.5589
	5.10E-04	4.37E-05	75.1	0.020	1.8738
	5.11E-04	4.37E-05	75.1	0.020	1.8776
	4.22E-04	4.37E-05	89.7	0.020	1.5438
	4.23E-04	4.37E-05	89.7	0.020	1.5471
	3.79E-04	4.37E-05	104.6	0.020	1.3795
	3.78E-04	4.37E-05	104.6	0.020	1.3757
Sample_1_7	5.28E-04	3.80E-05	59.8	0.017	2.2379
	5.28E-04	3.80E-05	59.8	0.017	2.2379
	4.03E-04	3.80E-05	76.0	0.017	1.6975
	4.03E-04	3.80E-05	76.0	0.017	1.6967
	3.63E-04	3.80E-05	89.9	0.017	1.5239
	3.64E-04	3.80E-05	89.9	0.017	1.5293
	3.30E-04	3.80E-05	104.8	0.017	1.3776
	3.30E-04	3.80E-05	104.8	0.017	1.3795
Sample_2_2	1.57E-03	4.24E-04	59.6	0.036	0.5209
	1.58E-03	4.24E-04	59.6	0.036	0.5240
	1.32E-03	4.24E-04	75.0	0.036	0.4137
	1.33E-03	4.24E-04	75.0	0.036	0.4144
	1.21E-03	4.24E-04	90.1	0.036	0.3621
	1.21E-03	4.24E-04	90.1	0.036	0.3645
	1.12E-03	4.24E-04	104.8	0.036	0.3255
	1.12E-03	4.24E-04	104.8	0.036	0.3261
Sample_2_7	1.80E-02	1.24E-02	59.5	0.060	0.0932
	1.80E-02	1.24E-02	59.5	0.060	0.0929
	1.67E-02	1.24E-02	75.0	0.060	0.0723
	1.67E-02	1.24E-02	75.0	0.060	0.0719
	1.61E-02	1.24E-02	89.9	0.060	0.0626
	1.60E-02	1.24E-02	89.9	0.060	0.0617
	1.57E-02	1.24E-02	104.8	0.060	0.0556
	1.57E-02	1.24E-02	104.8	0.060	0.0558

Table D.2 — Continued

	k_a , md	k_s , md	\bar{p} , psia	ϕ , fraction	Kn_p
Sample_2_8	5.76E-03	2.53E-03	59.5	0.051	0.2555
	5.76E-03	2.53E-03	59.5	0.051	0.2554
	5.06E-03	2.53E-03	74.7	0.051	0.2024
	5.06E-03	2.53E-03	74.7	0.051	0.2024
	4.67E-03	2.53E-03	89.7	0.051	0.1723
	4.67E-03	2.53E-03	89.7	0.051	0.1718
	4.38E-03	2.53E-03	104.8	0.051	0.1499
	4.39E-03	2.53E-03	104.8	0.051	0.1502
Sample_2_12	1.15E-02	2.50E-03	59.7	0.055	0.6790
	1.15E-02	2.50E-03	59.7	0.055	0.6790
	9.58E-03	2.50E-03	74.7	0.055	0.5429
	9.57E-03	2.50E-03	74.6	0.055	0.5422
	8.55E-03	2.50E-03	89.8	0.055	0.4679
	8.55E-03	2.50E-03	89.8	0.055	0.4679
	7.87E-03	2.50E-03	104.9	0.055	0.4180
	7.88E-03	2.50E-03	104.9	0.055	0.4184
Sample_2_28	1.03E-02	5.19E-03	59.7	0.037	0.2006
	1.03E-02	5.19E-03	59.7	0.037	0.2001
	9.24E-03	5.19E-03	75.3	0.037	0.1591
	9.23E-03	5.19E-03	75.3	0.037	0.1586
	8.52E-03	5.19E-03	89.8	0.037	0.1319
	8.53E-03	5.19E-03	89.8	0.037	0.1320
	8.15E-03	5.19E-03	105.0	0.037	0.1177
	8.14E-03	5.19E-03	104.9	0.037	0.1174
Sample_3_4	1.44E-03	2.28E-04	59.1	0.040	0.9795
	1.46E-03	2.28E-04	59.1	0.040	0.9918
	1.14E-03	2.28E-04	74.7	0.040	0.7513
	1.15E-03	2.28E-04	74.7	0.040	0.7567
	9.80E-04	2.28E-04	89.4	0.040	0.6254
	9.86E-04	2.28E-04	89.4	0.040	0.6303
	8.52E-04	2.28E-04	104.5	0.040	0.5251
	8.45E-04	2.28E-04	104.5	0.040	0.5191
Sample_3_6	1.45E-01	9.99E-02	59.8	0.066	0.0930
	1.44E-01	9.99E-02	59.8	0.066	0.0918
	1.35E-01	9.99E-02	74.8	0.066	0.0726
	1.34E-01	9.99E-02	74.8	0.066	0.0725
	1.29E-01	9.99E-02	89.8	0.066	0.0619
	1.29E-01	9.99E-02	89.8	0.066	0.0620
	1.26E-01	9.99E-02	104.5	0.066	0.0560
	1.26E-01	9.99E-02	104.5	0.066	0.0556

Table D.2 — Continued

	k_a , md	k_{cs} , md	\bar{p} , psia	ϕ , fraction	Kn_p
Sample_3_10	2.13E-02	6.78E-03	39.6	0.071	0.4162
	2.14E-02	6.78E-03	39.6	0.071	0.4200
	1.69E-02	6.78E-03	55.0	0.071	0.2964
	1.69E-02	6.78E-03	55.0	0.071	0.2964
	1.49E-02	6.78E-03	69.9	0.071	0.2398
	1.50E-02	6.78E-03	69.9	0.071	0.2413
	1.39E-02	6.78E-03	84.8	0.071	0.2100
	1.39E-02	6.78E-03	84.8	0.071	0.2107
Sample_3_36	2.80E-02	1.68E-02	60.3	0.057	0.1353
	2.78E-02	1.68E-02	60.3	0.057	0.1335
	2.55E-02	1.68E-02	75.4	0.057	0.1067
	2.56E-02	1.68E-02	75.4	0.057	0.1079
	2.40E-02	1.68E-02	90.3	0.057	0.0884
	2.40E-02	1.68E-02	90.3	0.057	0.0887
	2.32E-02	1.68E-02	105.1	0.057	0.0790
	2.33E-02	1.68E-02	105.1	0.057	0.0796
Sample_3_55	5.18E-03	1.28E-03	60.1	0.066	0.5795
	5.18E-03	1.28E-03	60.1	0.066	0.5796
	4.37E-03	1.28E-03	74.8	0.066	0.4656
	4.38E-03	1.28E-03	74.8	0.066	0.4657
	3.91E-03	1.28E-03	90.1	0.066	0.3990
	3.91E-03	1.28E-03	90.1	0.066	0.3984
	3.63E-03	1.28E-03	105.2	0.066	0.3587
	3.63E-03	1.28E-03	105.2	0.066	0.3589

D.3 Correlation of the Pseudo-Knudsen Number with Pressure, Permeability and Porosity.

Using the data in **Table D.2**, we developed two correlations to relate the "pseudo-Knudsen" numbers (Kn_p) and the available data (k_a , k_∞ , ϕ , p). The first correlation given below relates the "pseudo-Knudsen" number (Kn_p) to the reciprocal mean pressure, the porosity (ϕ), and the gas permeability (k_a):

$$Kn_p = 0.59 \frac{1}{\bar{p}} k_a^{-0.5654} \phi^{-0.25} \dots\dots\dots (D-6)$$

Applying Eq. D-6 to Eq. D-4 yields:

$$k_a = k_\infty \left[1 + \frac{128}{15\pi^2} \tan^{-1} \left[4 \left[0.59 \frac{1}{\bar{p}} k_a^{-0.5654} \phi^{-0.25} \right]^{0.4} \right] 0.59 \frac{1}{\bar{p}} k_a^{-0.5654} \phi^{-0.25} \right] \left[1 + \frac{4 \left[0.59 \frac{1}{\bar{p}} k_a^{-0.5654} \phi^{-0.25} \right]}{1 + 0.59 \frac{1}{\bar{p}} k_a^{-0.5654} \phi^{-0.25}} \right] \dots\dots\dots (D-7)$$

The equivalent liquid permeability can then be easily computed by:

$$k_\infty = k_a / \left[1 + \frac{128}{15\pi^2} \tan^{-1} \left[4 \left[0.59 \frac{1}{\bar{p}} k_a^{-0.5654} \phi^{-0.25} \right]^{0.4} \right] 0.59 \frac{1}{\bar{p}} k_a^{-0.5654} \phi^{-0.25} \right] \left[1 + \frac{4 \left[0.59 \frac{1}{\bar{p}} k_a^{-0.5654} \phi^{-0.25} \right]}{1 + 0.59 \frac{1}{\bar{p}} k_a^{-0.5654} \phi^{-0.25}} \right] \dots\dots\dots (D-8)$$

For the second correlation we replaced the gas permeability with the equivalent liquid permeability:

$$Kn_p = 2.18 \frac{1}{\bar{p}} k_\infty^{-0.50225} \phi^{0.253} \dots\dots\dots (D-9)$$

Substitution of Eq. D-9 into Eq. D-4 yields:

$$k_a = k_\infty \left[1 + \frac{128}{15\pi^2} \tan^{-1} \left[4 \left[2.18 \frac{1}{\bar{p}} k_\infty^{-0.50225} \phi^{0.253} \right]^{0.4} \right] 2.18 \frac{1}{\bar{p}} k_\infty^{-0.50225} \phi^{0.253} \right] \left[1 + \frac{4 \left[2.18 \frac{1}{\bar{p}} k_\infty^{-0.50225} \phi^{0.253} \right]}{1 + 2.18 \frac{1}{\bar{p}} k_\infty^{-0.50225} \phi^{0.253}} \right] \dots\dots\dots (D-10)$$

Rearranging Eq. D-10 yields:

$$k_a - k_\infty \left[1 + \frac{128}{15\pi^2} \tan^{-1} \left[4 \left[2.18 \frac{1}{\bar{p}} k_\infty^{-0.50225} \phi^{0.253} \right]^{0.4} \right] 2.18 \frac{1}{\bar{p}} k_\infty^{-0.50225} \phi^{0.253} \right] \left[1 + \frac{4 \left[2.18 \frac{1}{\bar{p}} k_\infty^{-0.50225} \phi^{0.253} \right]}{1 + 2.18 \frac{1}{\bar{p}} k_\infty^{-0.50225} \phi^{0.253}} \right] = 0 \dots\dots\dots (D-11)$$

Eq. D-10 is an *implicit* relation where the k_∞ value is solved as a *root* of this relation. **Fig. D.1** presents the "pseudo-Knudsen" numbers obtained with Eq. D-6 and Eq. D-9 plotted against the reference "pseudo-Knudsen" numbers (recall that we defined the reference "pseudo-Knudsen" number as solution of Eq. D-

4). In **Fig. D.2** presents the equivalent liquid permeabilities computed with Eq. D-8 and Eq. D-10 plotted against the reference Klinkenberg-corrected permeability. **Figs. D.3** and **D.4** show the behavior of the following function of k_{∞} for a given data point (Sample 1-8, $k_a = 0.0012699$ md, $\bar{p} = 45.27$ psig, $\phi = 0.023$):

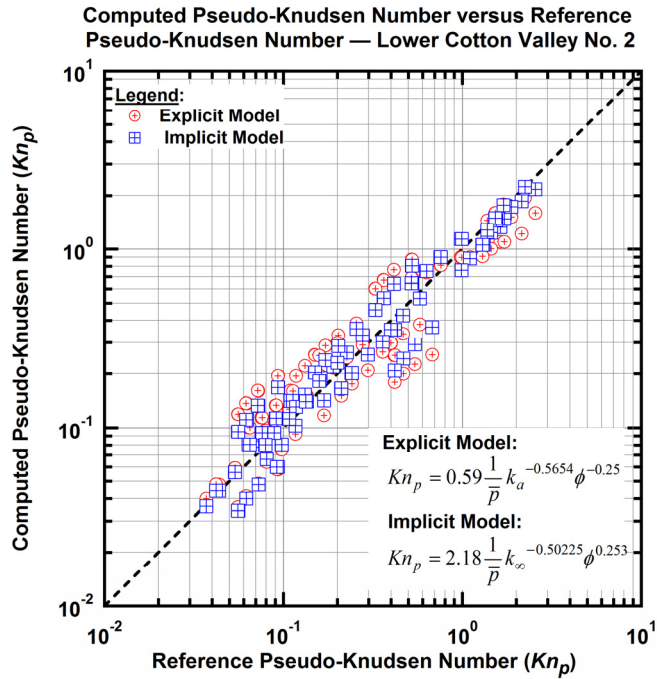


Figure D.1 — Correlated "pseudo-Knudsen" number (Eq. D-6 and Eq. D-9) versus reference "pseudo-Knudsen" number (solution of Eq. D-4) — the implicit model (Eq. D-9) achieves a better estimation of Kn_p than the explicit model (Eq. D-6).

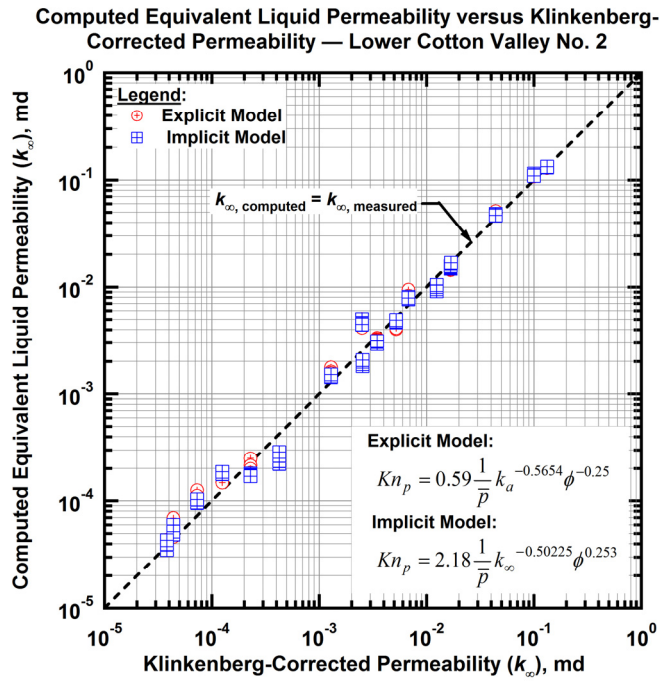


Figure D.2 — Computed equivalent liquid permeability versus the reference Klinkenberg-corrected permeability (extrapolated from a Klinkenberg plot (k_a versus reciprocal mean pressure)) — both models present reasonably good results.

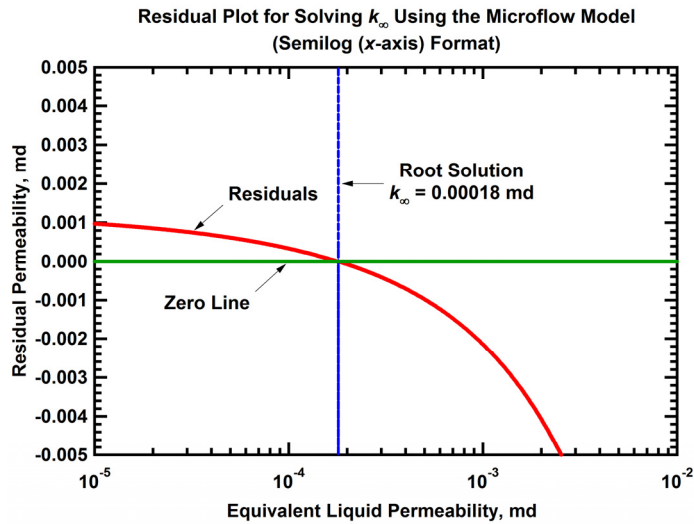


Figure D.3 — Plot of the residuals computed with Eq. D.11 against the equivalent liquid permeability (k_{ω}) for a particular point of our data set — Sample 1-8, $k_a = 0.0012699 \text{ md}$, $\bar{p} = 45.27 \text{ psig}$, $\phi = 0.023$. The Klinkenberg-corrected permeability for this sample is $k_{\infty} = 0.000125 \text{ md}$. The root solution for this case yields $k_{\omega} = 0.00018 \text{ md}$, which implies an absolute relative error of 30.56 percent (compared to the "Klinkenberg" permeability).

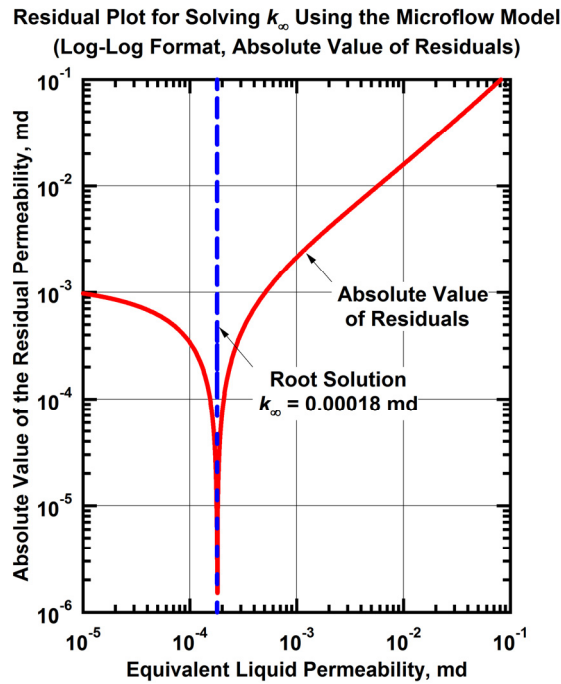


Figure D.4 — Plot of the absolute value of residuals computed with Eq. D.11 against the equivalent liquid permeability (k_{∞}) for a particular point of our data set — Sample 1-8, $k_a = 0.0012699$ md, $\bar{p} = 45.27$ psig, $\phi = 0.023$ (same point than **Fig D.3**). This plot gives a clearer view of the root solution.

We recognize that this correlation is only valid for this data set, but we hope that this formulation inspires others to utilize the generic form of Eq. D-4, coupled with a model for Kn_p (e.g., Eq. D-6 or Eq. D-9).

References

1. Karniadakis, G.E. and Beskok, A.: *Micro-flows, Fundamentals and Simulation*, Springer-Verlag, New-York (2002).
2. Loeb, L.B.: *The Kinetic Theory of Gases*, second edition, McGraw-Hill Co. Inc., New York (1934).
3. Klinkenberg, L.J.: "The Permeability of Porous Media to Liquid and Gases," paper presented at the API 11th Mid Year Meeting, Tulsa, Oklahoma (May 1941); in *API Drilling and Production Practice* (1941), 200-213
4. Sampath, K. and Keighin, C.W.: "Factors Affecting Gas Slippage in Tight Sandstones," paper SPE 9872 presented at the 1981 SPE/DOE Low Permeability Symposium, May 27-29, 1981, Denver, Colorado.
5. Jones, F.O. and Owens, W.W.: "A laboratory Study of Low Permeability Gas Sands," paper SPE 7551 presented at the 1979 SPE Symposium on Low-Permeability Gas Reservoirs, May 20-22, 1979, Denver, Colorado.
6. Data Source: Lower Cotton Valley, Vixen Field, Caldwell Parish, Louisiana Core Report, Anadarko Petroleum Corp., (2005).

APPENDIX E

COMPARISON OF ALL MODELS FOR STEADY-STATE MEASUREMENTS

The following section provides a summary and an overall comparison of the existing correlations as well as the "microflow" model (calibrated on data acquired by *steady-state method*) for the prediction of permeability from core experiments.

E.1 Direct Correlation between the Klinkenberg-Corrected Permeability and Porosity, Pressure and Permeability to Gas.

Using the datasets acquired under *steady-state conditions* (Lower Cotton Valley Nos. 1 and 2, see ref. 1 and 2, the data are presented in **Table E.1** below), it is possible to correlate the Klinkenberg-corrected permeability (k_{∞}) (see ref. 3) with the mean absolute core pressure (\bar{p}), the porosity (ϕ) and the measured gas permeability (k_a). This relation is expressed as:

$$k_{\infty} = c_0 (k_a)^{c_1} (\phi)^{c_2} (\bar{p})^{c_3} \dots\dots\dots (E-1)$$

For this case, we obtained by regression the following coefficients:

$$\begin{aligned} c_0 &= 0.05188 \\ c_1 &= 1.365 \\ c_2 &= -0.0099 \\ c_3 &= 00.83768 \end{aligned}$$

Fig. E.1 below represents the equivalent liquid permeability computed using Eq. E-1 computed against the reference Klinkenberg-corrected permeability (extrapolated by multipoint-Klinkenberg analysis)

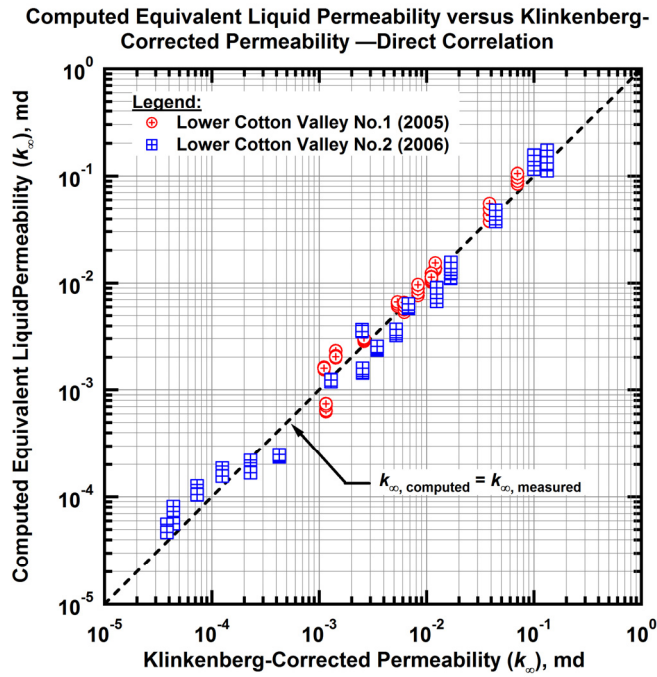


Figure E.1 — Equivalent liquid permeability computed using the direct correlation (Eq. E-1) versus Klinkenberg-corrected permeability — this correlation gives a very good fit.

Table E.1 — Data used in the comparison study — datasets from the Lower Cotton Valley Formation (refs. 1 and 2).

		\bar{p} , psia	k_a , md	$k_{e, \text{md}}$	b_K , psia	ϕ , fraction
Lower Cotton Valley No. 1	SAMPLE 1	56.05	8.51E-03	1.42E-03	278.0	0.089
		56.05	8.47E-03	1.42E-03	278.0	0.089
		81.4	6.25E-03	1.42E-03	278.0	0.089
		81.4	6.25E-03	1.42E-03	278.0	0.089
		105.95	5.13E-03	1.42E-03	278.0	0.089
		105.9	5.15E-03	1.42E-03	278.0	0.089
		131.55	4.57E-03	1.42E-03	278.0	0.089
	131.55	4.57E-03	1.42E-03	278.0	0.089	
	SAMPLE 2	54.05	1.87E-02	5.36E-03	133.8	0.08
		54.1	1.86E-02	5.36E-03	133.8	0.08
		79.3	1.40E-02	5.36E-03	133.8	0.08
		79.25	1.40E-02	5.36E-03	133.8	0.08
		103.55	1.23E-02	5.36E-03	133.8	0.08
		103.55	1.22E-02	5.36E-03	133.8	0.08
129.7		1.11E-02	5.36E-03	133.8	0.08	
129.65	1.11E-02	5.36E-03	133.8	0.08		

Table E.1 — Continued

		\bar{p} , psia	k_a , md	k_{cs} , md	b_K , psia	ϕ , fraction
		SAMPLE 3		60.35	9.82E-03	2.61E-03
60.35	9.83E-03			2.61E-03	166.8	0.067
77.85	8.02E-03			2.61E-03	166.8	0.067
77.7	8.07E-03			2.61E-03	166.8	0.067
105.4	6.71E-03			2.61E-03	166.8	0.067
105.35	6.74E-03			2.61E-03	166.8	0.067
137.1	5.84E-03			2.61E-03	166.8	0.067
137	5.97E-03			2.61E-03	166.8	0.067
SAMPLE 4		56.65	7.84E-03	1.10E-03	345.8	0.085
		56.65	7.85E-03	1.10E-03	345.8	0.085
		82.2	5.63E-03	1.10E-03	345.8	0.085
		82.25	5.64E-03	1.10E-03	345.8	0.085
		108.65	4.60E-03	1.10E-03	345.8	0.085
		108.5	4.62E-03	1.10E-03	345.8	0.085
		132	4.09E-03	1.10E-03	345.8	0.085
		132	4.09E-03	1.10E-03	345.8	0.085
SAMPLE 5		57	7.73E-02	3.84E-02	57.7	0.077
		57.15	7.74E-02	3.84E-02	57.7	0.077
		81.35	6.51E-02	3.84E-02	57.7	0.077
		81.3	6.52E-02	3.84E-02	57.7	0.077
		105.75	5.96E-02	3.84E-02	57.7	0.077
		105.7	5.96E-02	3.84E-02	57.7	0.077
		132.8	5.51E-02	3.84E-02	57.7	0.077
		132.8	5.51E-02	3.84E-02	57.7	0.077
SAMPLE 6		81.45	3.00E-03	1.16E-03	125.5	0.043
		81.45	2.94E-03	1.16E-03	125.5	0.043
		105.95	2.47E-03	1.16E-03	125.5	0.043
		105.9	2.48E-03	1.16E-03	125.5	0.043
		138.25	2.21E-03	1.16E-03	125.5	0.043
		138.2	2.21E-03	1.16E-03	125.5	0.043
		159.1	2.07E-03	1.16E-03	125.5	0.043
		159.1	2.07E-03	1.16E-03	125.5	0.043
SAMPLE 7		56.7	2.44E-02	8.30E-03	109.8	0.075
		56.7	2.44E-02	8.30E-03	109.8	0.075
		82.4	1.90E-02	8.30E-03	109.8	0.075
		82.4	1.90E-02	8.30E-03	109.8	0.075
		105	1.70E-02	8.30E-03	109.8	0.075
		105	1.70E-02	8.30E-03	109.8	0.075
		130.95	1.54E-02	8.30E-03	109.8	0.075
		130.95	1.55E-02	8.30E-03	109.8	0.075

Table E.1 — Continued

	\bar{p} , psia	k_a , md	k_{cs} , md	b_K , psia	ϕ , fraction	
Lower Cotton Valley No. 1	SAMPLE 8	48.1	1.64E-01	7.04E-02	63.6	0.101
		48.1	1.64E-01	7.04E-02	63.6	0.101
		56.15	1.49E-01	7.04E-02	63.6	0.101
		56.15	1.49E-01	7.04E-02	63.6	0.101
		67.35	1.37E-01	7.04E-02	63.6	0.101
		67.35	1.37E-01	7.04E-02	63.6	0.101
		78.7	1.29E-01	7.04E-02	63.6	0.101
		78.7	1.29E-01	7.04E-02	63.6	0.101
Lower Cotton Valley No. 1	SAMPLE 9	58	1.84E-02	6.17E-03	114.7	0.069
		58	1.84E-02	6.17E-03	114.7	0.069
		82.55	1.45E-02	6.17E-03	114.7	0.069
		82.55	1.45E-02	6.17E-03	114.7	0.069
		105.15	1.29E-02	6.17E-03	114.7	0.069
		105.15	1.29E-02	6.17E-03	114.7	0.069
		129.8	1.17E-02	6.17E-03	114.7	0.069
		129.8	1.18E-02	6.17E-03	114.7	0.069
Lower Cotton Valley No. 1	SAMPLE 10	56.75	3.65E-02	1.20E-02	115.6	0.087
		56.5	3.68E-02	1.20E-02	115.6	0.087
		80.1	2.87E-02	1.20E-02	115.6	0.087
		80.05	2.86E-02	1.20E-02	115.6	0.087
		105.6	2.52E-02	1.20E-02	115.6	0.087
		105.45	2.52E-02	1.20E-02	115.6	0.087
Lower Cotton Valley No. 2	SAMPLE 12	57.25	3.03E-02	1.11E-02	98.3	0.1
		57.7	2.97E-02	1.11E-02	98.3	0.1
		66.165	2.73E-02	1.11E-02	98.3	0.1
		65.9	2.78E-02	1.11E-02	98.3	0.1
		106.2	2.13E-02	1.11E-02	98.3	0.1
		106.2	2.13E-02	1.11E-02	98.3	0.1
		84.05	2.41E-02	1.11E-02	98.3	0.1
		84.05	2.38E-02	1.11E-02	98.3	0.1
Lower Cotton Valley No. 2	SAMPLE 1_8	59.97	1.27E-03	1.25E-04	565.3	0.023
		59.965	1.27E-03	1.25E-04	565.3	0.023
		75.405	1.03E-03	1.25E-04	565.3	0.023
		75.4	1.03E-03	1.25E-04	565.3	0.023
		90.095	8.77E-04	1.25E-04	565.3	0.023
		90.045	8.78E-04	1.25E-04	565.3	0.023
		104.885	7.95E-04	1.25E-04	565.3	0.023
		104.88	7.95E-04	1.25E-04	565.3	0.023

Table E.1 — Continued

	\bar{p} , psia	k_a , md	k_{cs} , md	b_K , psia	ϕ , fraction	
Lower Cotton Valley No.2	SAMPLE 2_10	39.56	1.80E-01	1.32E-01	14.2	0.063
		39.555	1.80E-01	1.32E-01	14.2	0.063
		54.92	1.66E-01	1.32E-01	14.2	0.063
		54.915	1.66E-01	1.32E-01	14.2	0.063
		69.745	1.59E-01	1.32E-01	14.2	0.063
		69.74	1.58E-01	1.32E-01	14.2	0.063
		84.72	1.55E-01	1.32E-01	14.2	0.063
		84.72	1.55E-01	1.32E-01	14.2	0.063
	SAMPLE 2_22	59.69	2.57E-02	1.68E-02	32.5	0.056
		59.665	2.60E-02	1.68E-02	32.5	0.056
		74.57	2.41E-02	1.68E-02	32.5	0.056
		74.505	2.41E-02	1.68E-02	32.5	0.056
		89.94	2.28E-02	1.68E-02	32.5	0.056
		89.885	2.29E-02	1.68E-02	32.5	0.056
		104.785	2.19E-02	1.68E-02	32.5	0.056
		104.74	2.20E-02	1.68E-02	32.5	0.056
	SAMPLE 3_8	39.54	8.05E-02	4.40E-02	32.8	0.078
		39.54	8.05E-02	4.40E-02	32.8	0.078
		54.785	6.89E-02	4.40E-02	32.8	0.078
		54.785	6.89E-02	4.40E-02	32.8	0.078
		69.79	6.47E-02	4.40E-02	32.8	0.078
		69.785	6.48E-02	4.40E-02	32.8	0.078
		84.755	6.10E-02	4.40E-02	32.8	0.078
		84.755	6.09E-02	4.40E-02	32.8	0.078
	SAMPLE 3_48	59.61	8.28E-03	3.45E-03	83.6	0.07
		59.605	8.27E-03	3.45E-03	83.6	0.07
		74.73	7.35E-03	3.45E-03	83.6	0.07
		74.725	7.35E-03	3.45E-03	83.6	0.07
89.98		6.69E-03	3.45E-03	83.6	0.07	
89.98		6.69E-03	3.45E-03	83.6	0.07	
104.745		6.19E-03	3.45E-03	83.6	0.07	
104.745		6.19E-03	3.45E-03	83.6	0.07	
SAMPLE 1_1	59.23	9.71E-04	7.29E-05	753.5	0.029	
	59.22	9.71E-04	7.29E-05	753.5	0.029	
	74.565	7.80E-04	7.29E-05	753.5	0.029	
	74.52	7.80E-04	7.29E-05	753.5	0.029	
	89.335	6.61E-04	7.29E-05	753.5	0.029	
	89.335	6.62E-04	7.29E-05	753.5	0.029	
	104.415	5.95E-04	7.29E-05	753.5	0.029	
	104.405	5.97E-04	7.29E-05	753.5	0.029	

Table E.1 — Continued

	\bar{p} , psia	k_a , md	k_{cs} , md	b_K , psia	ϕ , fraction	
Lower Cotton Valley No.2	SAMPLE 1_5	59.9	6.95E-04	4.37E-05	801.0	0.02
		59.9	6.94E-04	4.37E-05	801.0	0.02
		75.06	5.10E-04	4.37E-05	801.0	0.02
		75.06	5.11E-04	4.37E-05	801.0	0.02
		89.71	4.22E-04	4.37E-05	801.0	0.02
		89.705	4.23E-04	4.37E-05	801.0	0.02
		104.58	3.79E-04	4.37E-05	801.0	0.02
		104.57	3.78E-04	4.37E-05	801.0	0.02
	SAMPLE 1_7	59.76	5.28E-04	3.80E-05	771.0	0.017
		59.76	5.28E-04	3.80E-05	771.0	0.017
		75.965	4.03E-04	3.80E-05	771.0	0.017
		75.965	4.03E-04	3.80E-05	771.0	0.017
		89.87	3.63E-04	3.80E-05	771.0	0.017
		89.865	3.64E-04	3.80E-05	771.0	0.017
		104.77	3.30E-04	3.80E-05	771.0	0.017
		104.76	3.30E-04	3.80E-05	771.0	0.017
	SAMPLE 2_2	59.605	1.57E-03	4.24E-04	165.1	0.036
		59.585	1.58E-03	4.24E-04	165.1	0.036
		75.01	1.32E-03	4.24E-04	165.1	0.036
		75	1.33E-03	4.24E-04	165.1	0.036
		90.09	1.21E-03	4.24E-04	165.1	0.036
		90.085	1.21E-03	4.24E-04	165.1	0.036
		104.785	1.12E-03	4.24E-04	165.1	0.036
		104.785	1.12E-03	4.24E-04	165.1	0.036
	SAMPLE 2_7	59.51	1.80E-02	1.24E-02	26.8	0.06
		59.505	1.80E-02	1.24E-02	26.8	0.06
		74.955	1.67E-02	1.24E-02	26.8	0.06
		74.95	1.67E-02	1.24E-02	26.8	0.06
89.915		1.61E-02	1.24E-02	26.8	0.06	
89.915		1.60E-02	1.24E-02	26.8	0.06	
104.77		1.57E-02	1.24E-02	26.8	0.06	
104.77		1.57E-02	1.24E-02	26.8	0.06	
SAMPLE 2_8	59.51	5.76E-03	2.53E-03	77.1	0.051	
	59.505	5.76E-03	2.53E-03	77.1	0.051	
	74.68	5.06E-03	2.53E-03	77.1	0.051	
	74.675	5.06E-03	2.53E-03	77.1	0.051	
	89.68	4.67E-03	2.53E-03	77.1	0.051	
	89.68	4.67E-03	2.53E-03	77.1	0.051	
	104.815	4.38E-03	2.53E-03	77.1	0.051	
	104.815	4.39E-03	2.53E-03	77.1	0.051	

Table E.1 — Continued

	\bar{p} , psia	k_a , md	k_{cs} , md	b_K , psia	ϕ , fraction	
Lower Cotton Valley No.2	SAMPLE 2_12	59.665	1.15E-02	2.50E-03	215.1	0.055
		59.665	1.15E-02	2.50E-03	215.1	0.055
		74.66	9.58E-03	2.50E-03	215.1	0.055
		74.645	9.57E-03	2.50E-03	215.1	0.055
		89.845	8.55E-03	2.50E-03	215.1	0.055
		89.845	8.55E-03	2.50E-03	215.1	0.055
		104.875	7.87E-03	2.50E-03	215.1	0.055
		104.865	7.88E-03	2.50E-03	215.1	0.055
	SAMPLE 2_28	59.66	1.03E-02	5.19E-03	58.6	0.037
		59.66	1.03E-02	5.19E-03	58.6	0.037
		75.32	9.24E-03	5.19E-03	58.6	0.037
		75.315	9.23E-03	5.19E-03	58.6	0.037
		89.78	8.52E-03	5.19E-03	58.6	0.037
		89.77	8.53E-03	5.19E-03	58.6	0.037
		104.95	8.15E-03	5.19E-03	58.6	0.037
		104.945	8.14E-03	5.19E-03	58.6	0.037
	SAMPLE 3_4	59.1	1.44E-03	2.28E-04	303.1	0.04
		59.055	1.46E-03	2.28E-04	303.1	0.04
		74.675	1.14E-03	2.28E-04	303.1	0.04
		74.675	1.15E-03	2.28E-04	303.1	0.04
		89.42	9.80E-04	2.28E-04	303.1	0.04
		89.41	9.86E-04	2.28E-04	303.1	0.04
		104.51	8.52E-04	2.28E-04	303.1	0.04
		104.51	8.45E-04	2.28E-04	303.1	0.04
	SAMPLE 3_6	59.76	1.45E-01	9.99E-02	26.4	0.066
		59.76	1.44E-01	9.99E-02	26.4	0.066
		74.78	1.35E-01	9.99E-02	26.4	0.066
		74.775	1.34E-01	9.99E-02	26.4	0.066
89.755		1.29E-01	9.99E-02	26.4	0.066	
89.75		1.29E-01	9.99E-02	26.4	0.066	
104.51		1.26E-01	9.99E-02	26.4	0.066	
104.515		1.26E-01	9.99E-02	26.4	0.066	
SAMPLE 3_10	39.645	2.13E-02	6.78E-03	84.8	0.071	
	39.61	2.14E-02	6.78E-03	84.8	0.071	
	54.99	1.69E-02	6.78E-03	84.8	0.071	
	54.985	1.69E-02	6.78E-03	84.8	0.071	
	69.86	1.49E-02	6.78E-03	84.8	0.071	
	69.86	1.50E-02	6.78E-03	84.8	0.071	
	84.83	1.39E-02	6.78E-03	84.8	0.071	
	84.825	1.39E-02	6.78E-03	84.8	0.071	

Table E.1 — Continued

	\bar{p} , psia	k_a , md	k_{∞} , md	b_K , psia	ϕ , fraction	
Lower Cotton Valley No.2	SAMPLE 3_36	60.345	2.80E-02	1.68E-02	39.2	0.057
		60.33	2.78E-02	1.68E-02	39.2	0.057
		75.365	2.55E-02	1.68E-02	39.2	0.057
		75.35	2.56E-02	1.68E-02	39.2	0.057
		90.27	2.40E-02	1.68E-02	39.2	0.057
		90.26	2.40E-02	1.68E-02	39.2	0.057
		105.115	2.32E-02	1.68E-02	39.2	0.057
		105.105	2.33E-02	1.68E-02	39.2	0.057
	SAMPLE 3_55	60.14	5.18E-03	1.28E-03	183.7	0.066
		60.125	5.18E-03	1.28E-03	183.7	0.066
		74.84	4.37E-03	1.28E-03	183.7	0.066
		74.835	4.38E-03	1.28E-03	183.7	0.066
		90.09	3.91E-03	1.28E-03	183.7	0.066
		90.09	3.91E-03	1.28E-03	183.7	0.066
		105.24	3.63E-03	1.28E-03	183.7	0.066
		105.245	3.63E-03	1.28E-03	183.7	0.066

E.2 Existing Correlations for Use in Single-Point Steady-State Measurement.

The existing correlations are based on the Klinkenberg model,³ relating the measured gas permeability (k_a) to the reciprocal mean pressure (\bar{p}) by the following equation:

$$k_a = k_{\infty} \left[1 + \frac{b_K}{\bar{p}} \right] \dots\dots\dots (E-2)$$

The existing correlations relate the gas slippage factor (b_K) with the available petrophysical data such as Klinkenberg-corrected permeability (k_{∞}) and porosity (ϕ). The correlations are presented in **Table E.2** for clarity:

Table E.2 — Summary of the " b_K versus petrophysical data" correlations used in the comparison study.

Models	Relations	Eq.
Heid <i>et al</i> ⁴	$k_a = k_\infty \left[1 + \frac{b_K}{\bar{p}} \right]$, with $b_K = 11.419(k_\infty)^{-0.39}$	(E-2) (E-3)
Jones-Owens ⁵	$k_a = k_\infty \left[1 + \frac{b_K}{\bar{p}} \right]$, with $b_K = 12.639(k_\infty)^{-0.33}$	(E-2) (E-4)
Sampath-Keighin ⁶	$k_a = k_\infty \left[1 + \frac{b_K}{\bar{p}} \right]$, with $b_K = 13.851 \left[\frac{k_\infty}{\phi} \right]^{-0.53}$	(E-2) (E-5)
Square-root	$k_a = k_\infty \left[1 + \frac{b_K}{\bar{p}} \right]$, with $b_K = \beta \left[\frac{k_\infty}{\phi} \right]^{-0.5}$ (the β -term depends on the nature of the gas used for the core flow experiments, in the case of nitrogen, $\beta = 43.345$)	(E-2) (E-6)
Direct correlation	$k_\infty = c_0 (k_a)^{c_1} (\phi)^{c_2} (\bar{p})^{c_3}$, with: $c_0 = 0.05188$ $c_1 = 1.365$ $c_2 = -0.0099$ $c_3 = 00.83768$	(E-1)

E.2 Microflow Model — Theoretical Formulation.

The different microflow models developed in the following are derived from the work of Karniadakis and Beskok.⁷ The following correlations are based on the microflow model, relating the measured gas permeability (k_a) to the Knudsen (or pseudo Knudsen) number by the following equation:

$$k_a = k_\infty \left[1 + \left[\frac{128}{15\pi^2} \tan^{-1} \left[4 Kn^{0.4} \right] \right] Kn \right] \left[1 + \frac{4Kn}{1+Kn} \right] \dots\dots\dots (E-7)$$

In Eq. E-7, the Knudsen number (Kn) is defined by:

$$Kn = \frac{\bar{\lambda}}{l_{char}} \dots\dots\dots (E-8)$$

Where $\bar{\lambda}$ is the mean free path of the gas molecules (*i.e.*, the average distance (length) between 2 consecutive molecular interactions at the mean pressure (\bar{p})) is defined by:³

$$\bar{\lambda}(p, T) = \sqrt{\pi/2} \frac{1}{\bar{p}} \mu \sqrt{\frac{RT}{M}} \quad [\mu \equiv \mu(\bar{p}, T)] \dots\dots\dots (E-9)$$

It is possible to give a theoretical formulation of Kn as a function of the mean pressure (\bar{p}), the porosity (ϕ) and the Klinkenberg-corrected permeability (k_∞) for the particular case where nitrogen is the flowing gas during the core flow experiments, This formulation is given as follows:

$$Kn = 10.836 \frac{1}{p} \left[\frac{k_\infty}{\phi} \right]^{-0.5} \dots\dots\dots (E-10)$$

E.3 Microflow Model — Explicit and Implicit Formulations

The Knudsen number (Kn) cannot be *measured by direct laboratory measurements*, however we can define the "pseudo" Knudsen number (Kn_p) as the solution of the following equation for a given pair of values of (k_a, k_∞):

$$k_a - k_\infty \left[1 + \left[\frac{128}{15\pi^2} \tan^{-1} \left[4 Kn_p^{0.4} \right] \right] Kn_p \right] \left[1 + \frac{4Kn_p}{1 + Kn_p} \right] = 0 \dots\dots\dots (E-11)$$

The "pseudo" Knudsen numbers (Kn_p) can be then correlated with the available data (\bar{p} , ϕ , and k_a or k_∞); two types of correlations can be obtained from this process:

- "Implicit" correlations, using the following form: $Kn_p = a_0 k_\infty^{a_1} \phi^{a_2} / \bar{p}$. In the preceding formulation, the coefficients (a_0, a_1, a_2) depend on the dataset/combination of datasets used for the calibration of the model.
- "Explicit" correlations, using the following form: $Kn_p = b_0 k_a^{b_1} \phi^{b_2} / \bar{p}$. In the preceding formulation, the coefficients (b_0, b_1, b_2) depend on the dataset/combination of datasets used for the calibration of the model.

The table below (**Table E.3**) presents the different sets of coefficient obtained by considering the datasets individually or as a combination for the calibration of the model:

Figs E.2 to E.30 present the absolute relative error profiles using the equivalent liquid permeabilities computed for each sample using the models presented in Table E.2 and Table E.3.

Table E.3 — Detail of the different explicit and implicit microflow models, based on various calibrations.

Datasets Used for Calibration	Correlations	Eq.
Lower Cotton Valley No. 1	Explicit: $Kn_p = 113.86 \frac{1}{\bar{p}} k_a^{-0.5916} \phi^{1.609}$	(E-12)
	Implicit: $Kn_p = 32.07 \frac{1}{\bar{p}} k_\infty^{-0.4667} \phi^{1.0825}$	(E-13)
Lower Cotton Valley No. 2	Explicit: $Kn_p = 0.5904 \frac{1}{\bar{p}} k_a^{-0.5654} \phi^{-0.25}$	(E-14)
	Implicit: $Kn_p = 2.18 \frac{1}{\bar{p}} k_\infty^{-0.5023} \phi^{0.253}$	(E-15)
Lower Cotton Valley Nos. 1 and 2	Explicit: $Kn_p = 4.278 \frac{1}{\bar{p}} k_a^{-0.6434} \phi^{0.4822}$	(E-16)
	Implicit: $Kn_p = 7.0697 \frac{1}{\bar{p}} k_\infty^{-0.5425} \phi^{0.6830}$	(E-17)

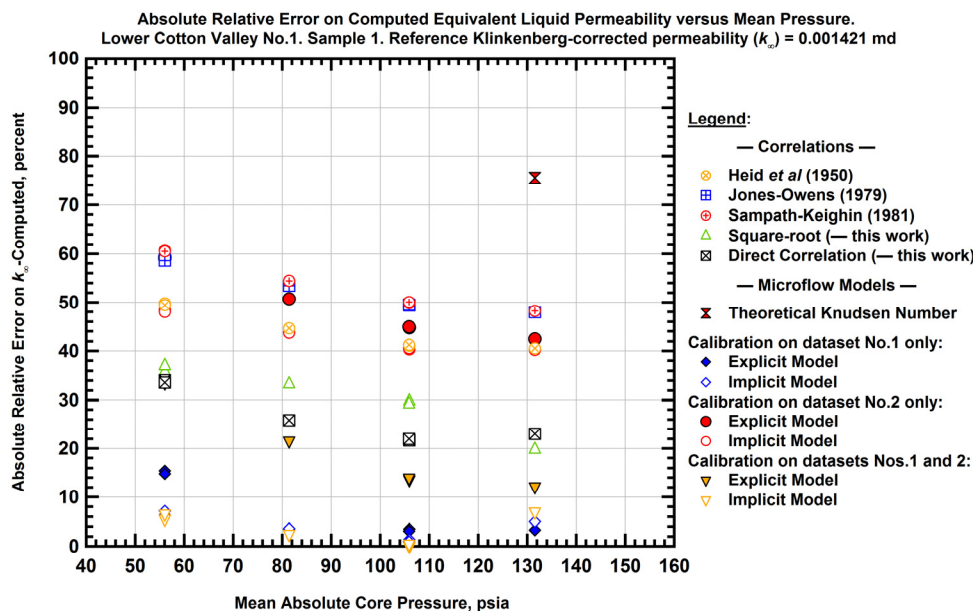


Figure E.2 — Comparison of the absolute relative errors for the computed equivalent liquid permeabilities versus mean pressure — Lower Cotton Valley No.1 Sample 1.

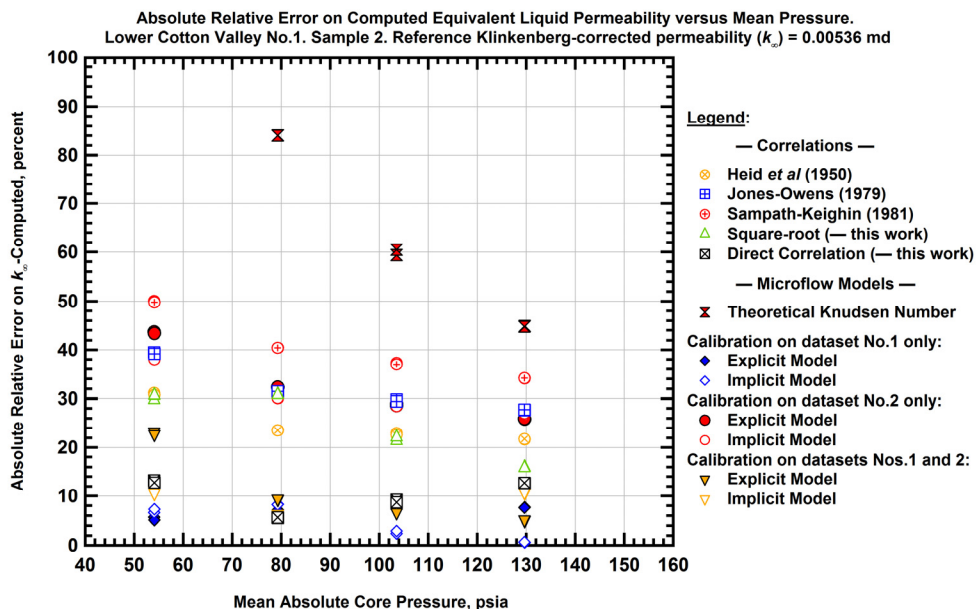


Figure E.3 — Comparison of the absolute relative errors for the computed equivalent liquid permeabilities versus mean pressure — Lower Cotton Valley No.1 Sample 2

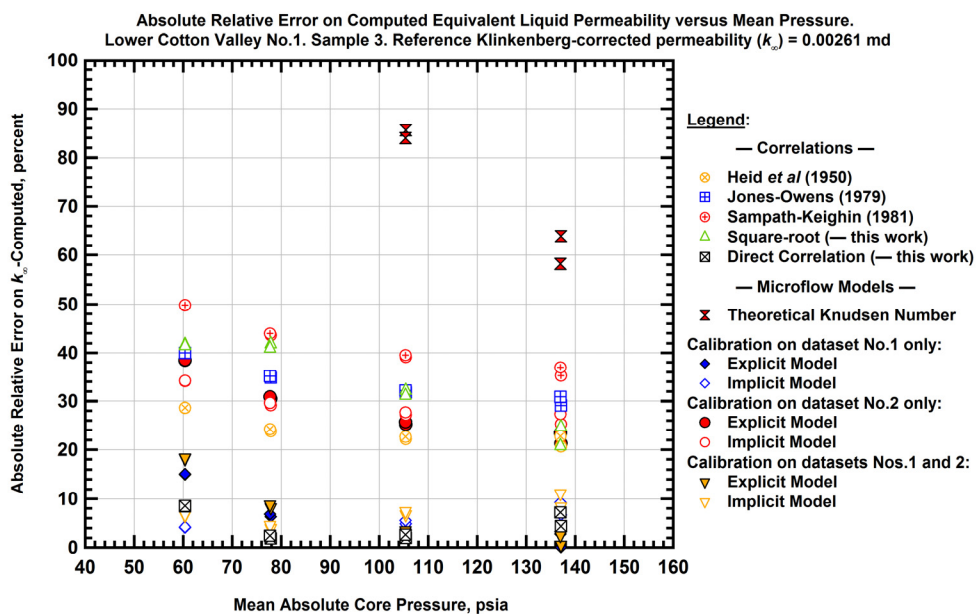


Figure E.4 — Comparison of the absolute relative errors for the computed equivalent liquid permeabilities versus mean pressure — Lower Cotton Valley No.1 Sample 3

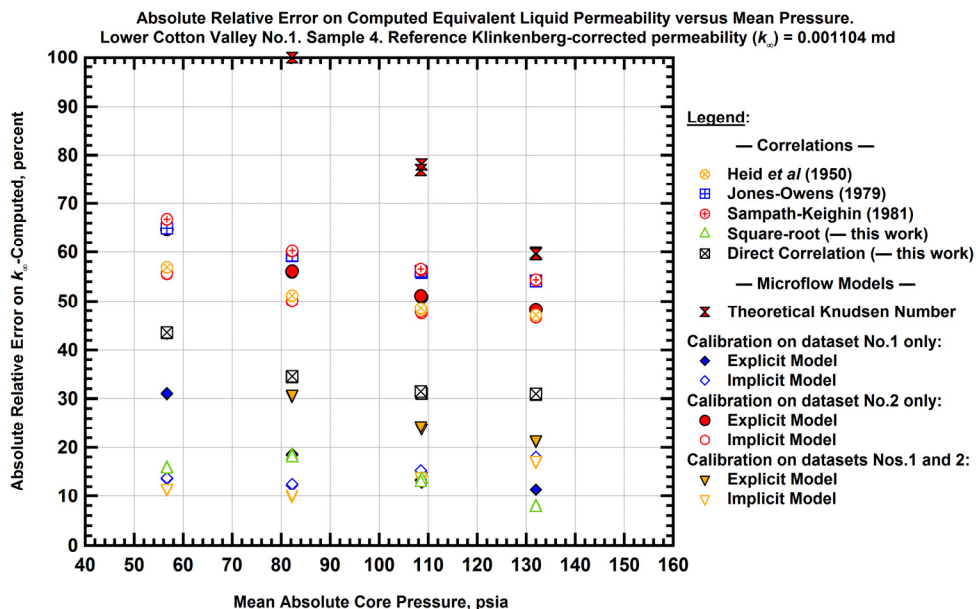


Figure E.5 — Comparison of the absolute relative errors for the computed equivalent liquid permeabilities versus mean pressure — Lower Cotton Valley No.1 Sample 4

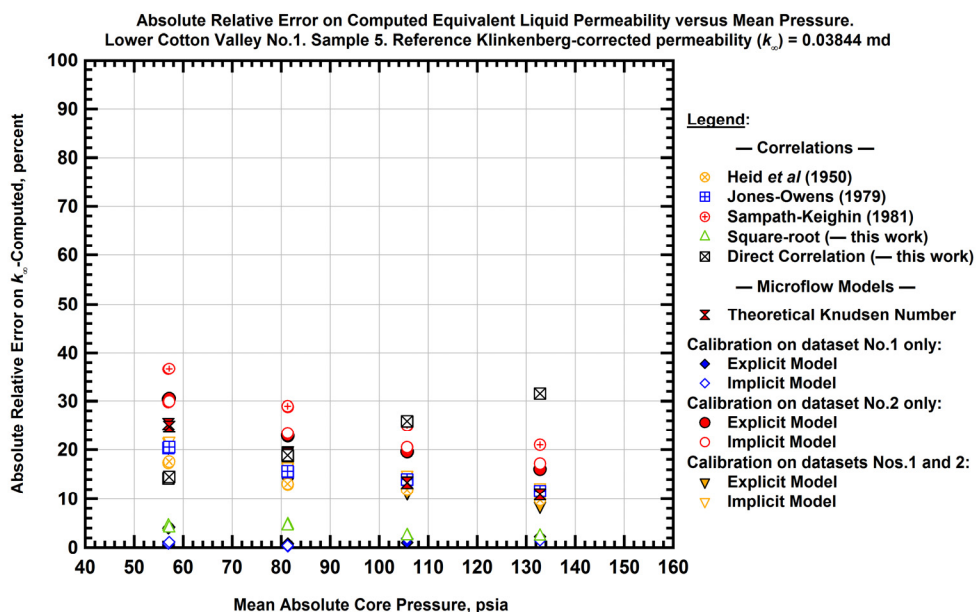


Figure E.6 — Comparison of the absolute relative errors for the computed equivalent liquid permeabilities versus mean pressure — Lower Cotton Valley No.1 Sample 5

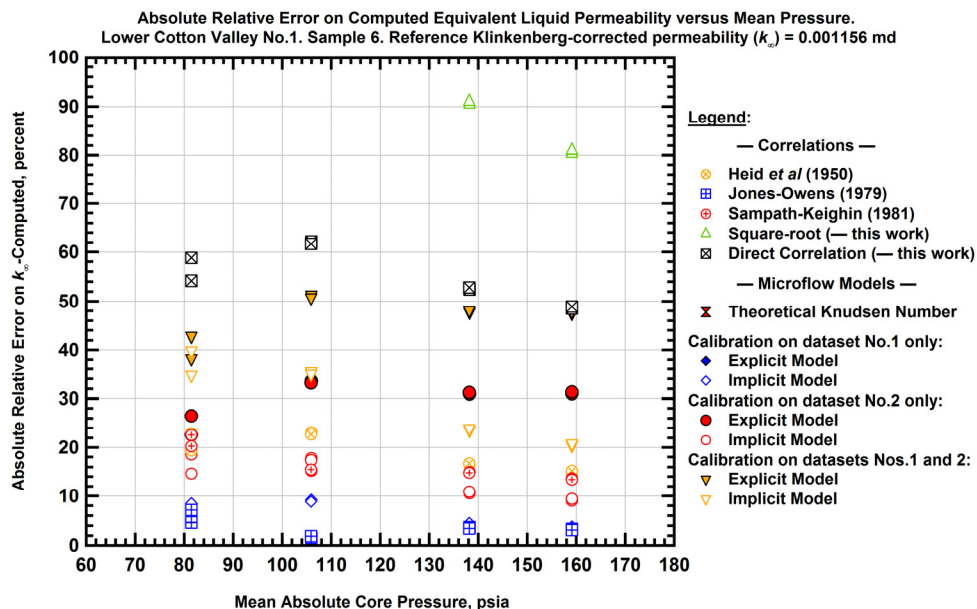


Figure E.7 — Comparison of the absolute relative errors for the computed equivalent liquid permeabilities versus mean pressure — Lower Cotton Valley No.1 Sample 6

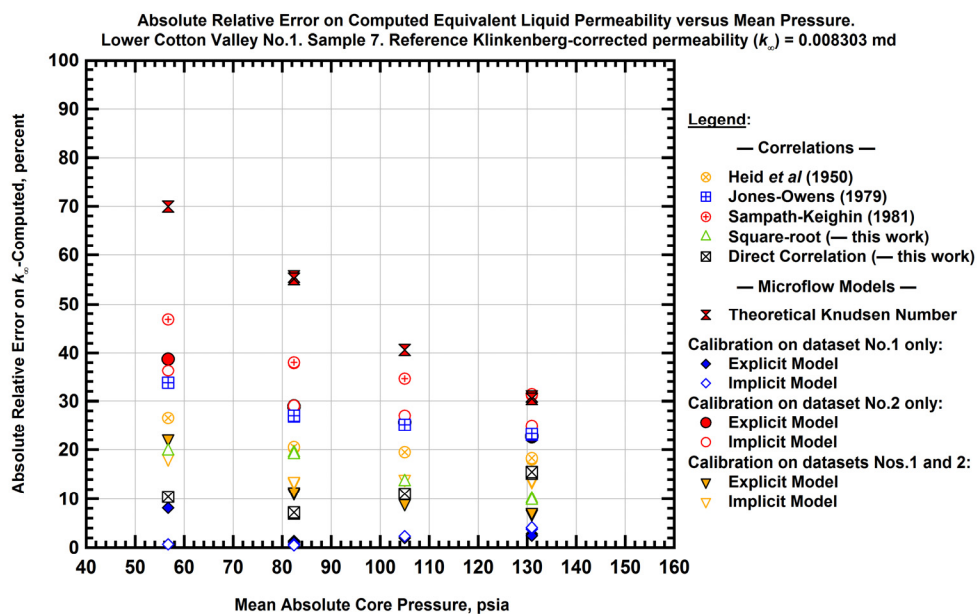


Figure E.8 — Comparison of the absolute relative errors for the computed equivalent liquid permeabilities versus mean pressure — Lower Cotton Valley No.1 Sample 7

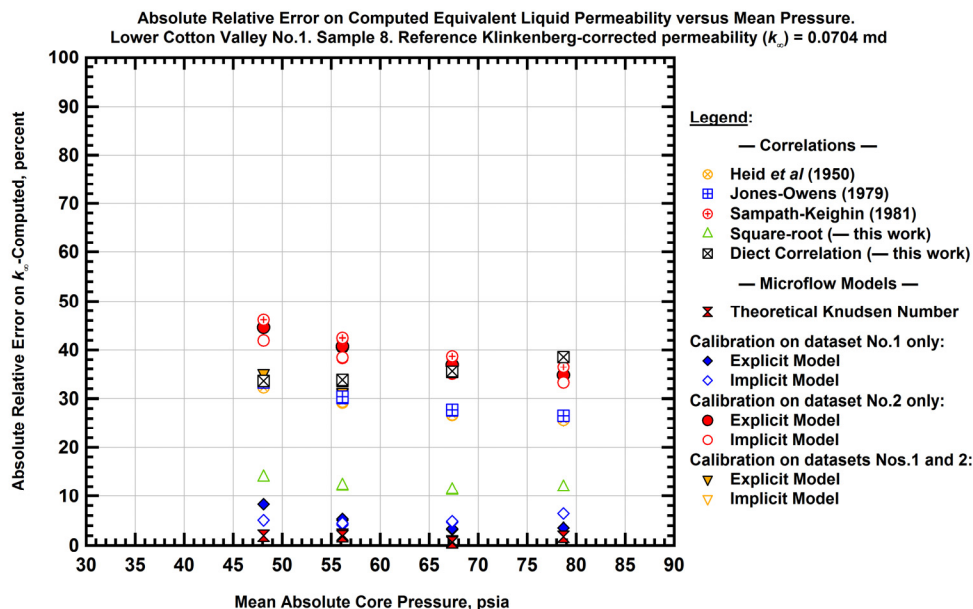


Figure E.9 — Comparison of the absolute relative errors for the computed equivalent liquid permeabilities versus mean pressure — Lower Cotton Valley No.1 Sample 8

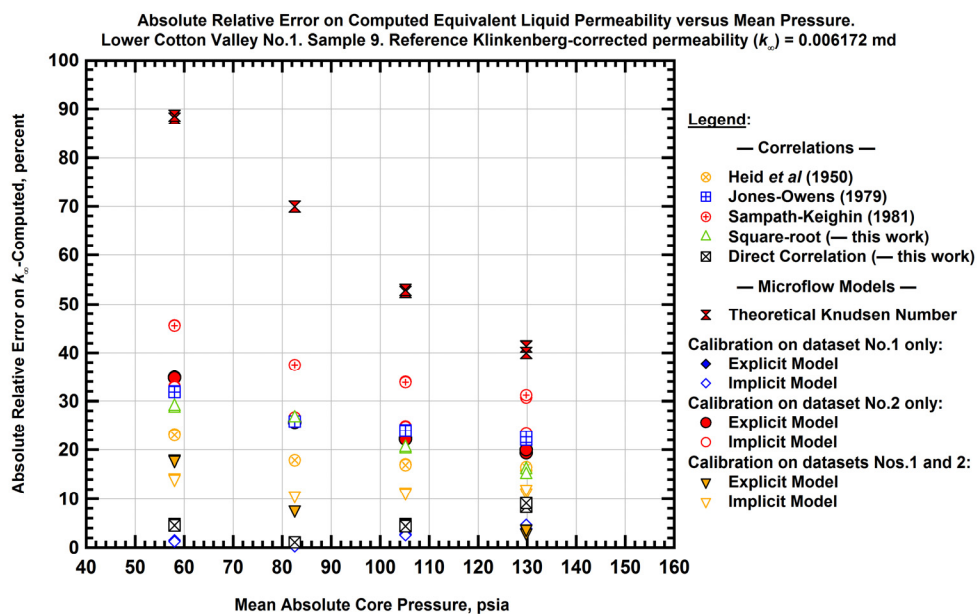


Figure E.10 — Comparison of the absolute relative errors for the computed equivalent liquid permeabilities versus mean pressure — Lower Cotton Valley No.1 Sample 9

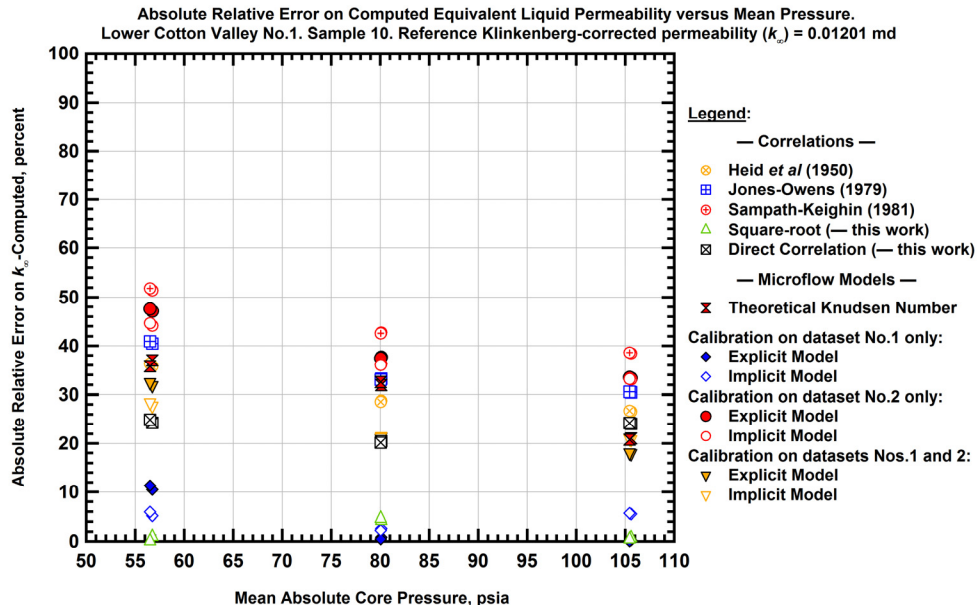


Figure E.11 — Comparison of the absolute relative errors for the computed equivalent liquid permeabilities versus mean pressure — Lower Cotton Valley No.1 Sample 10

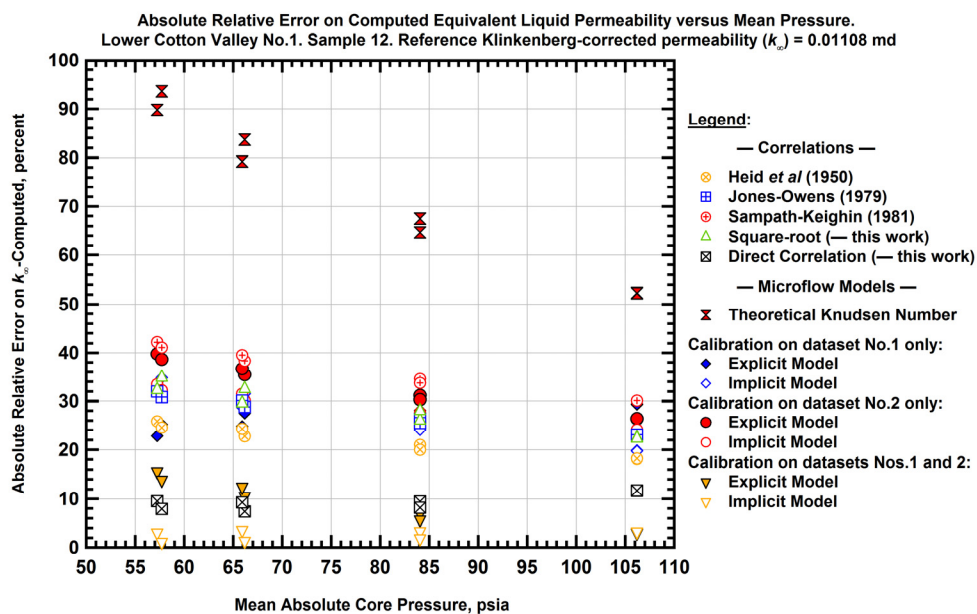


Figure E.12 — Comparison of the absolute relative errors for the computed equivalent liquid permeabilities versus mean pressure — Lower Cotton Valley No.1 Sample 12

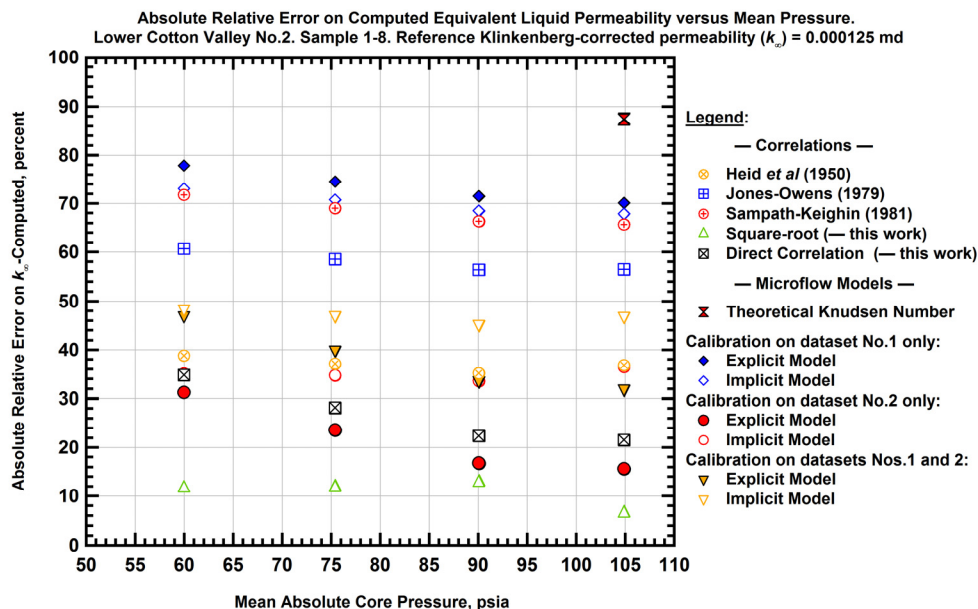


Figure E.13 — Comparison of the absolute relative errors for the computed equivalent liquid permeabilities versus mean pressure — Lower Cotton Valley No.2 Sample 1-8

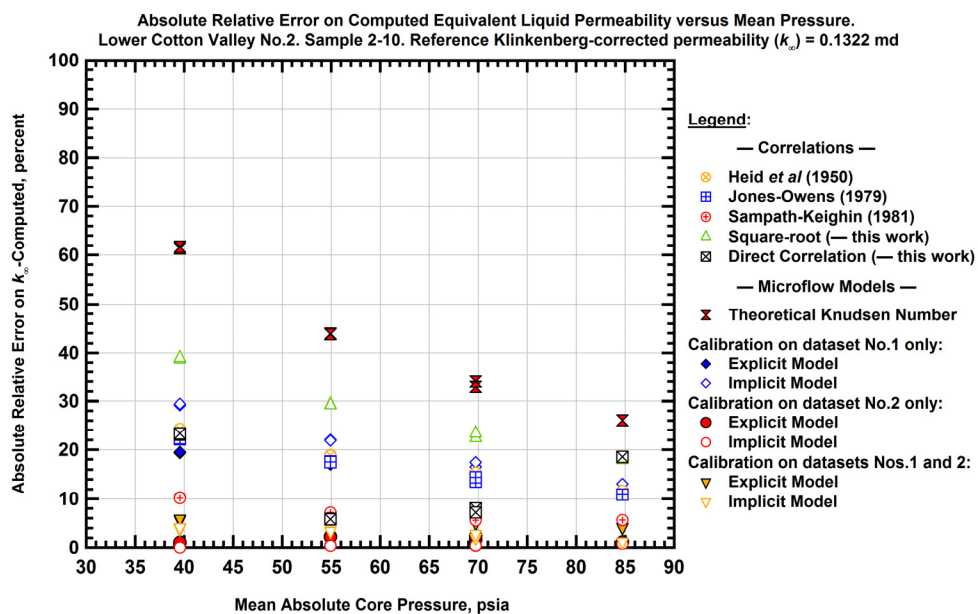


Figure E.14 — Comparison of the absolute relative errors for the computed equivalent liquid permeabilities versus mean pressure — Lower Cotton Valley No.2 Sample 2-10

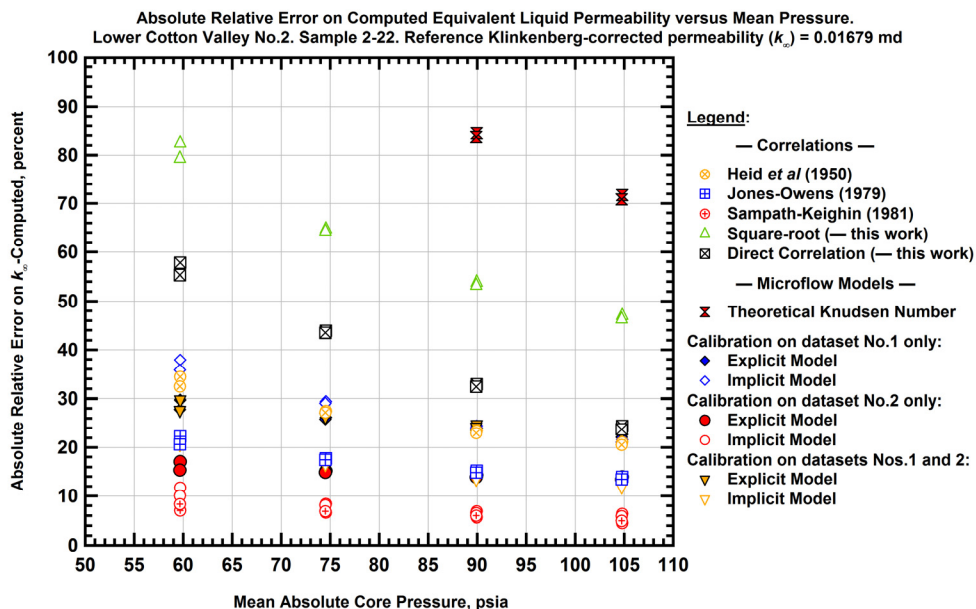


Figure E.15 — Comparison of the absolute relative errors for the computed equivalent liquid permeabilities versus mean pressure — Lower Cotton Valley No.2 Sample 2-22

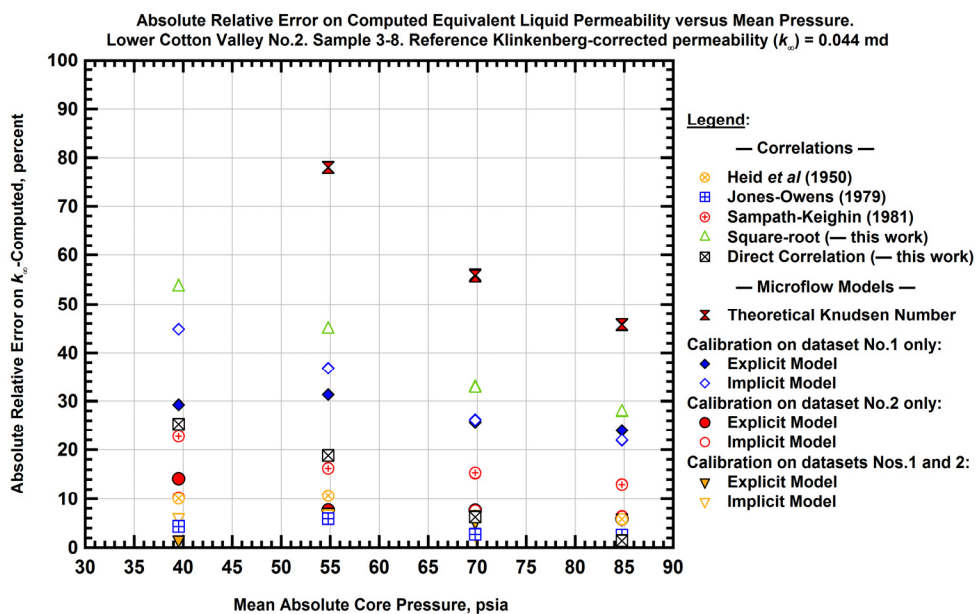


Figure E.16 — Comparison of the absolute relative errors for the computed equivalent liquid permeabilities versus mean pressure — Lower Cotton Valley No.2 Sample 3-8

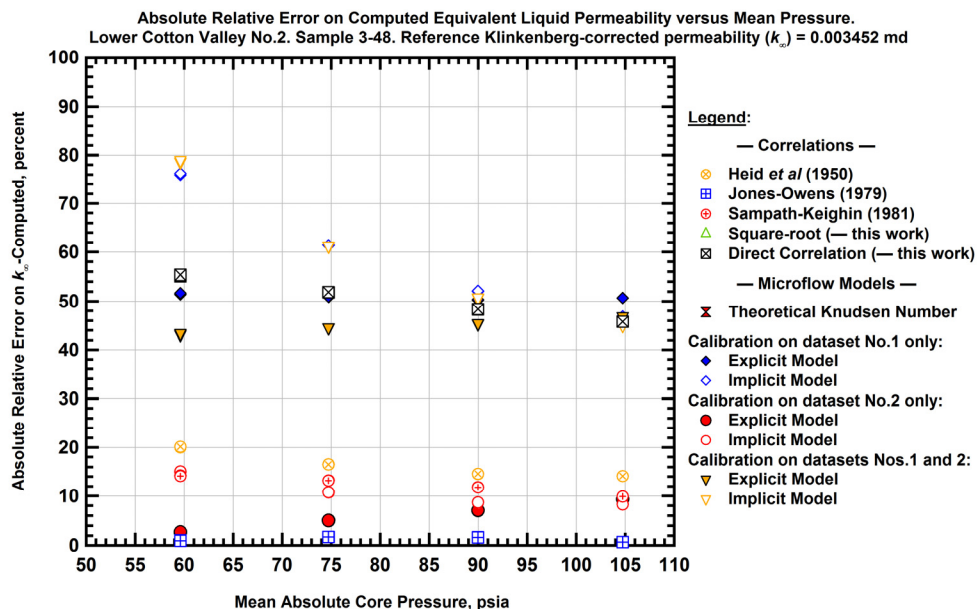


Figure E.17 — Comparison of the absolute relative errors for the computed equivalent liquid permeabilities versus mean pressure — Lower Cotton Valley No.2 Sample 3-48

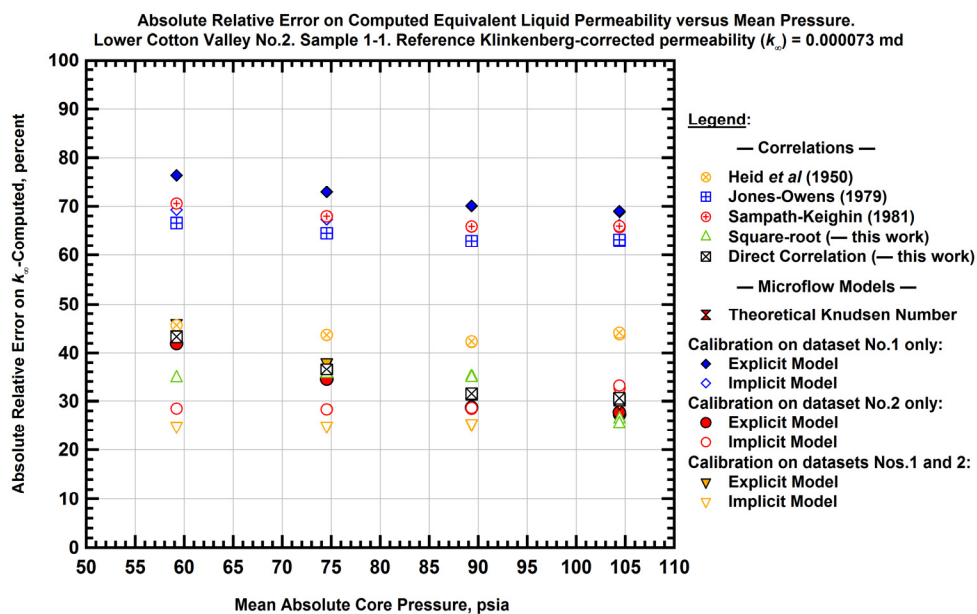


Figure E.18 — Comparison of the absolute relative errors for the computed equivalent liquid permeabilities versus mean pressure — Lower Cotton Valley No.2 Sample 1-1

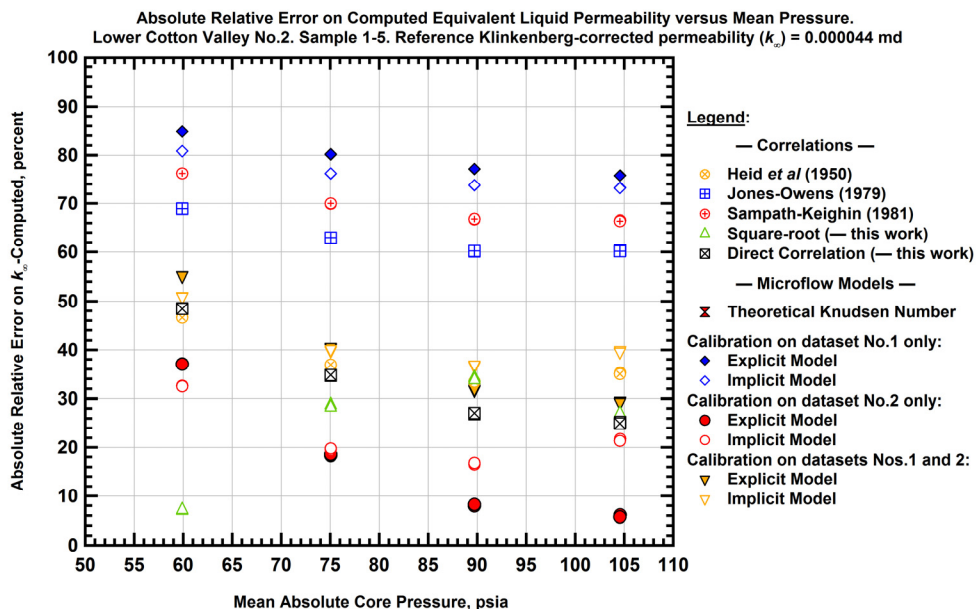


Figure E.19 — Comparison of the absolute relative errors for the computed equivalent liquid permeabilities versus mean pressure — Lower Cotton Valley No.2 Sample 1-5

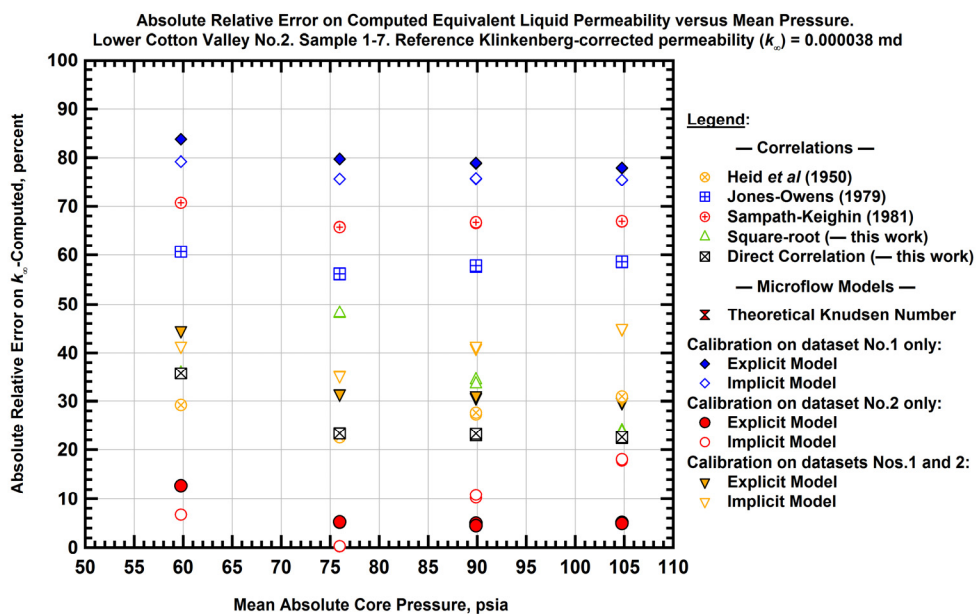


Figure E.20 — Comparison of the absolute relative errors for the computed equivalent liquid permeabilities versus mean pressure — Lower Cotton Valley No.2 Sample 1-7

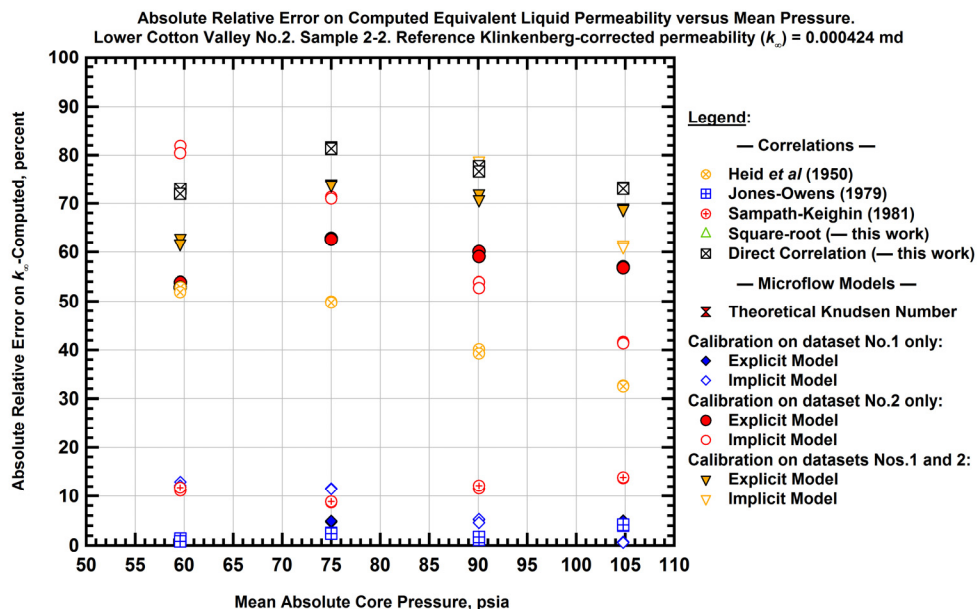


Figure E.21 — Comparison of the absolute relative errors for the computed equivalent liquid permeabilities versus mean pressure — Lower Cotton Valley No.2 Sample 2-2

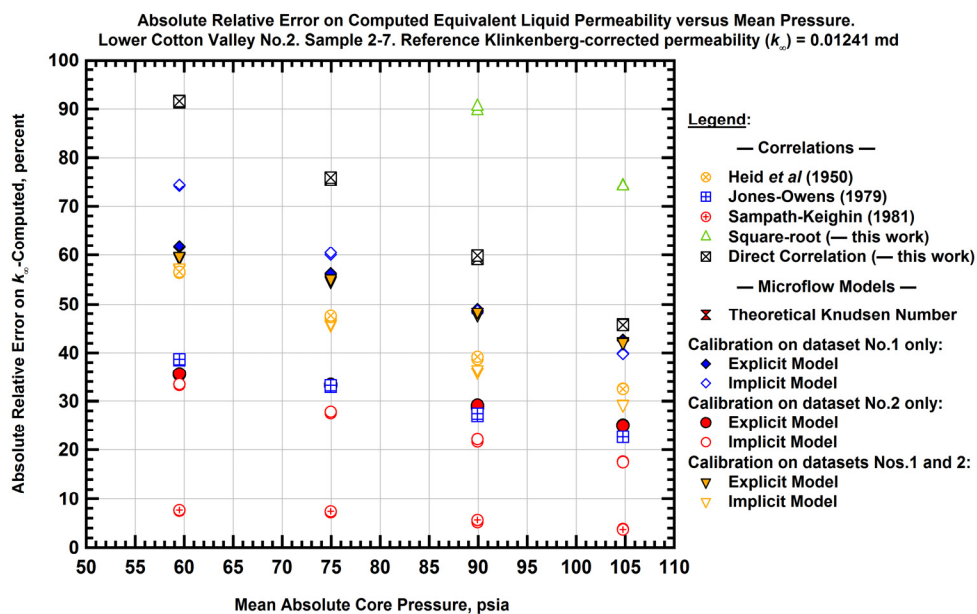


Figure E.22 — Comparison of the absolute relative errors for the computed equivalent liquid permeabilities versus mean pressure — Lower Cotton Valley No.2 Sample 2-7

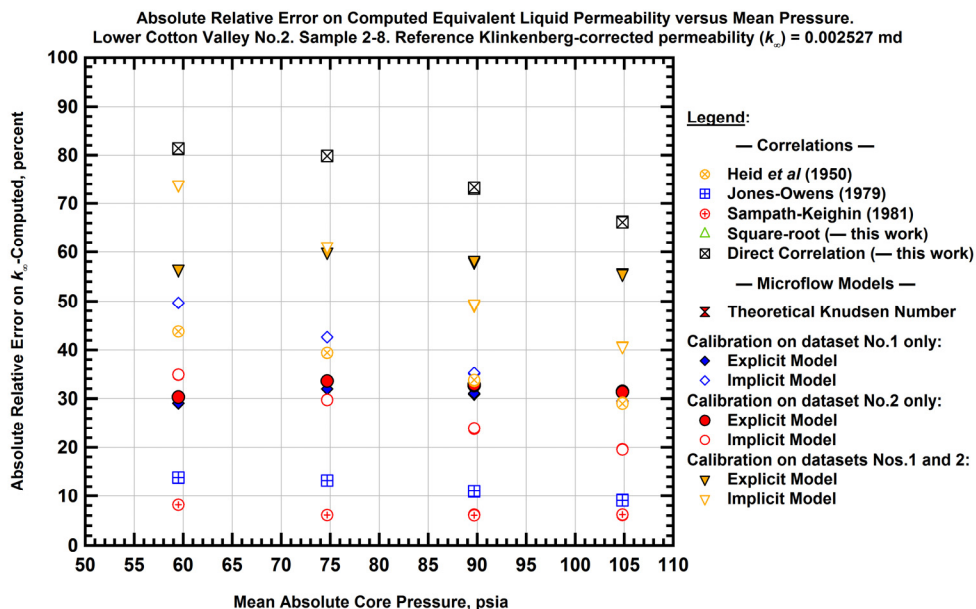


Figure E.23 — Comparison of the absolute relative errors for the computed equivalent liquid permeabilities versus mean pressure — Lower Cotton Valley No.2 Sample 2-8

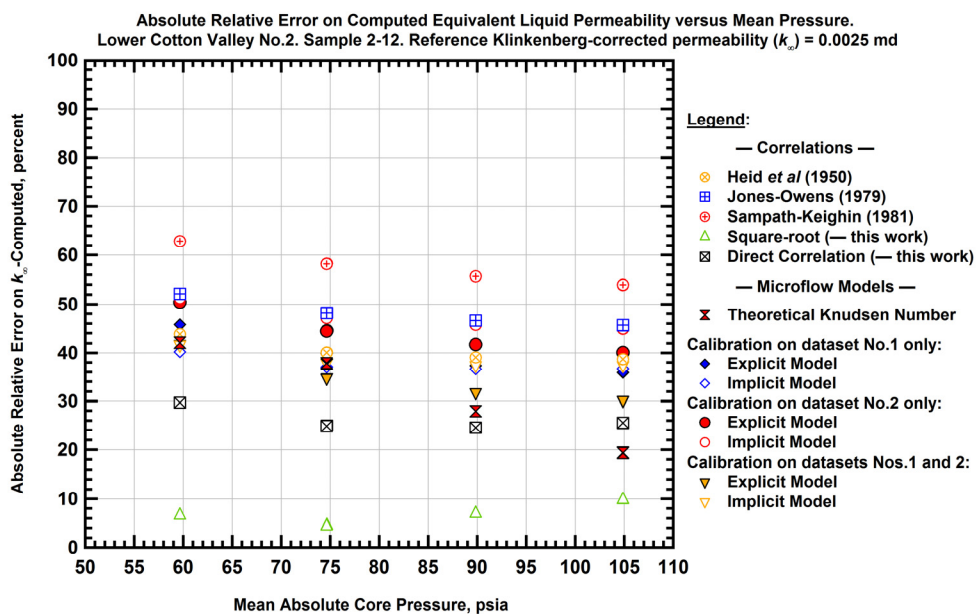


Figure E.24 — Comparison of the absolute relative errors for the computed equivalent liquid permeabilities versus mean pressure — Lower Cotton Valley No.2 Sample 2-12

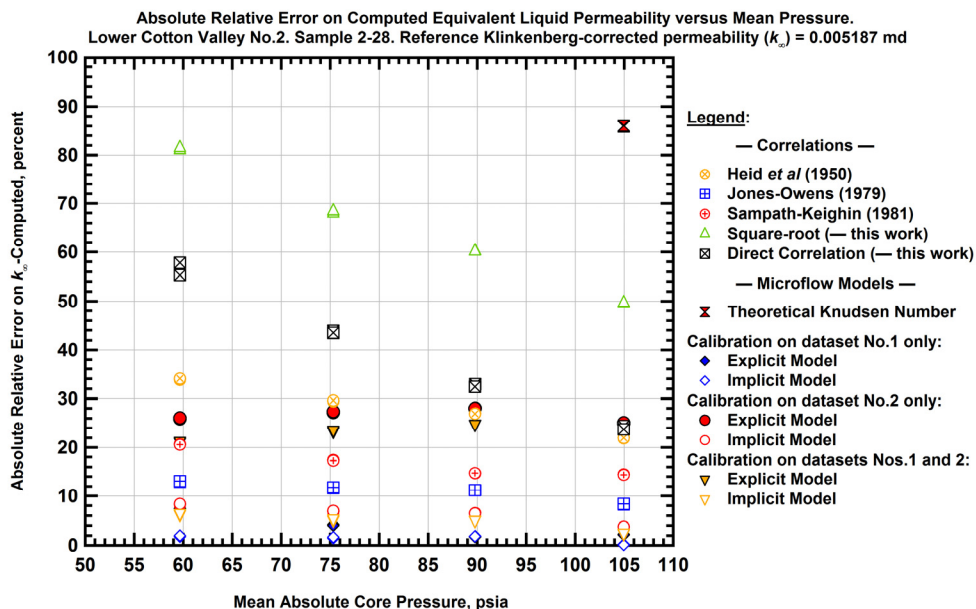


Figure E.25 — Comparison of the absolute relative errors for the computed equivalent liquid permeabilities versus mean pressure — Lower Cotton Valley No.2 Sample 2-28

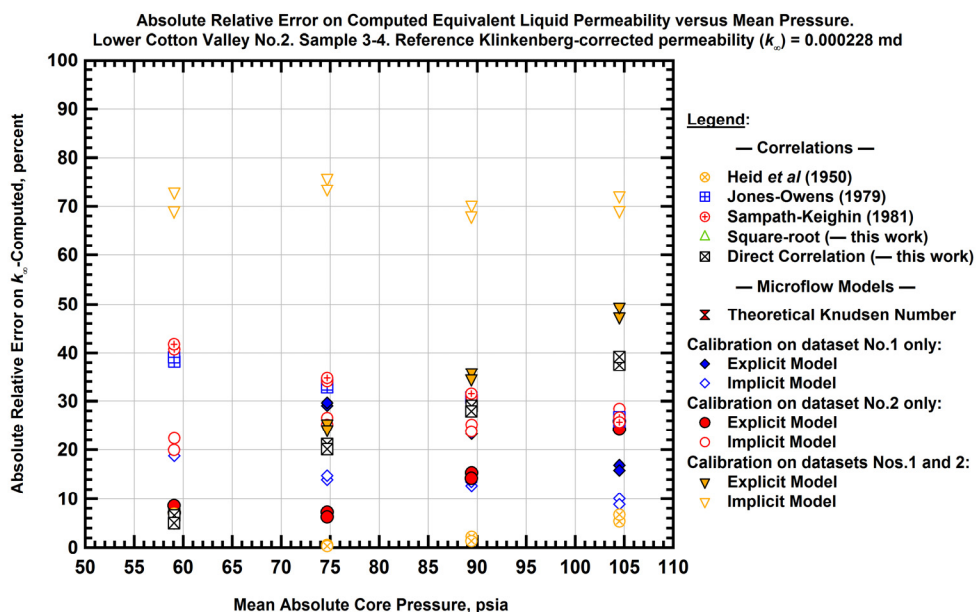


Figure E.26 — Comparison of the absolute relative errors for the computed equivalent liquid permeabilities versus mean pressure — Lower Cotton Valley No.2 Sample 3-4

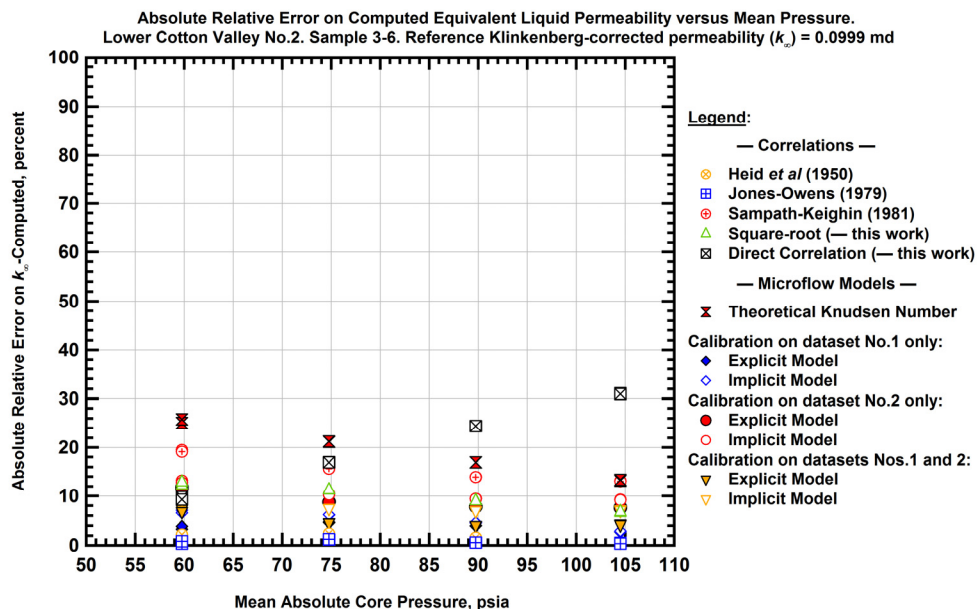


Figure E.27 — Comparison of the absolute relative errors for the computed equivalent liquid permeabilities versus mean pressure — Lower Cotton Valley No.2 Sample 3-6

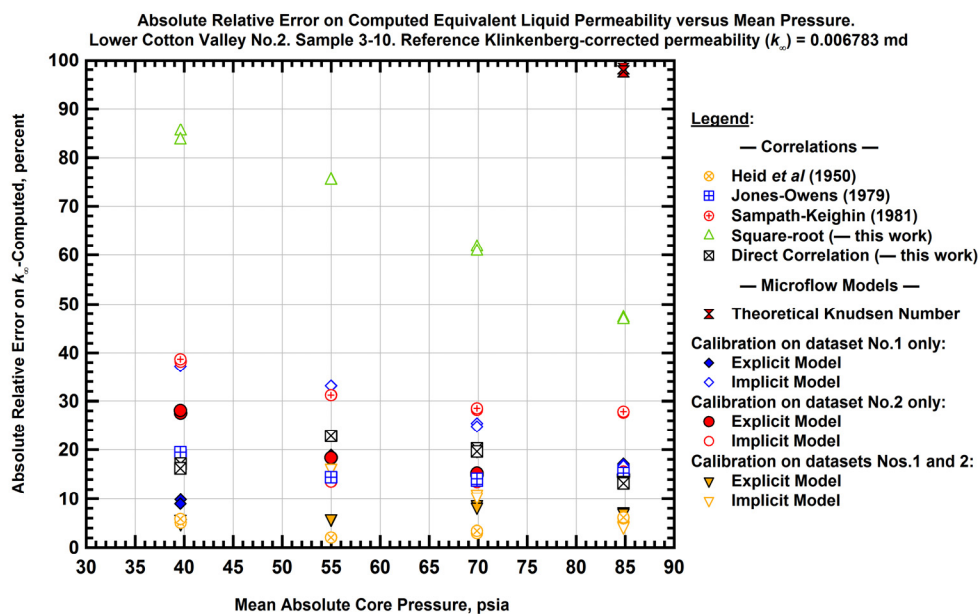


Figure E.28 — Comparison of the absolute relative errors for the computed equivalent liquid permeabilities versus mean pressure — Lower Cotton Valley No.2 Sample 3-10

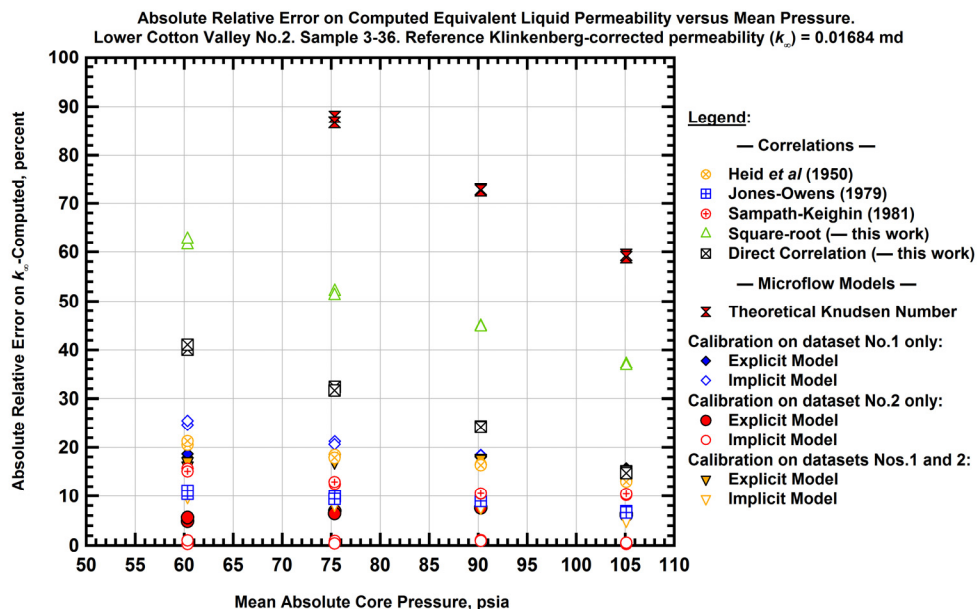


Figure E.29 — Comparison of the absolute relative errors for the computed equivalent liquid permeabilities versus mean pressure — Lower Cotton Valley No.2 Sample 3-36

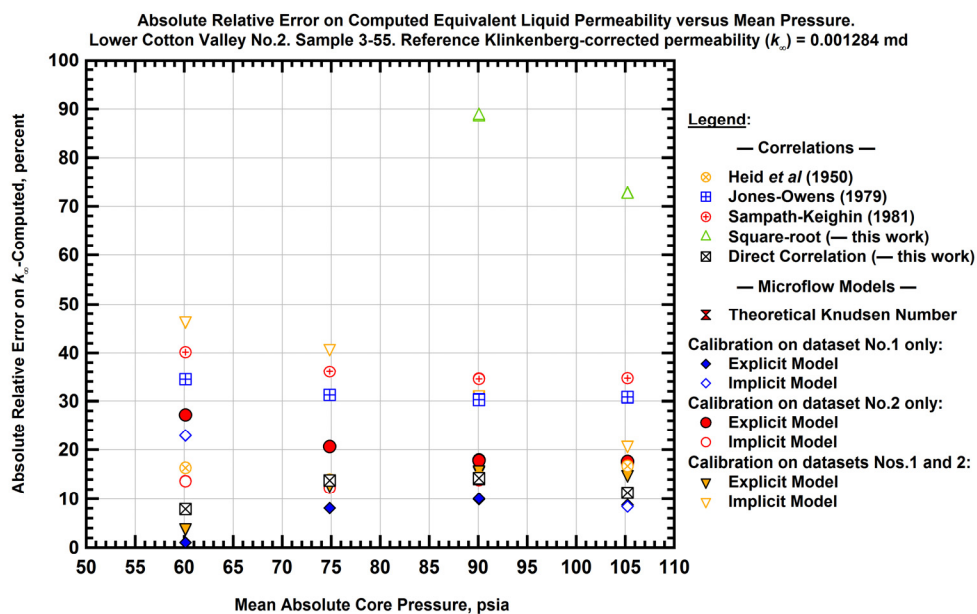


Figure E.30 — Comparison of the absolute relative errors for the computed equivalent liquid permeabilities versus mean pressure — Lower Cotton Valley No.2 Sample 3-55

References

1. Data Source: *Lower Cotton Valley Formation Core Report* — Anadarko Petroleum Corp., (2005)
2. Data Source: Lower Cotton Valley, Vixen Field, Caldwell Parish, Louisiana Core Report, Anadarko Petroleum Corp., (2006).
3. Klinkenberg, L.J.: "The Permeability of Porous Media to Liquid and Gases," paper presented at the API 11th Mid Year Meeting, Tulsa, Oklahoma (May 1941); in *API Drilling and Production Practice* (1941), 200-213
4. Heid, J.G., McMahon, J.J., Nielsen, R.F. and Yuster, S.T.: "Study of the Permeability of Rocks to Homogeneous Fluids," paper presented at the Spring Meeting of the Southwestern District, Division of Production, Dallas, Texas (March 1950); in *API Drilling and Production Practice* (1950), 230-246
5. Jones, F.O. and Owens, W.W.: "A laboratory Study of Low Permeability Gas Sands," paper SPE 7551 presented at the 1979 SPE Symposium on Low-Permeability Gas Reservoirs, May 20-22, 1979, Denver, Colorado.
6. Sampath, K. and Keighin, C.W.: "Factors Affecting Gas Slippage in Tight Sandstones," paper SPE 9872 presented at the 1981 SPE/DOE Low Permeability Symposium, May 27-29, 1981, Denver, Colorado.
7. Karniadakis, G.E. and Beskok, A.: *Micro-flows, Fundamentals and Simulation*, Springer-Verlag, New-York (2002).

VITA

Name: François-André Florence

Permanent Address: 131, rue de la santé
75013 PARIS
France

E-mail Address: francois-a.florence@mines-saint-etienne.org

Education: Texas A&M University, College Station, Texas, USA
Master of Science Degree in Petroleum Engineering
May 2007

Ecole Nationale Supérieure des Mines, Saint Etienne, France
Diplôme d'Ingénieur Civil des Mines
September 2004

Affiliations: Society of Petroleum Engineers